STRUCTURAL SYSTEMS
RESEARCH PROJECT

Report No.
SSRP – 2000/13

FLEXURAL BEHAVIOR OF CIRCULAR HOLLOW COLUMNS WITH A SINGLE LAYER OF REINFORCEMENT UNDER SEISMIC LOADING

by

JUN-ICHI HOSHIKUMA
M.J.N. PRIESTLEY

Final Research Report for Caltrans under Contract No. 59A0051

November 2000

Department of Structural Engineering
University of California, San Diego
La Jolla, California 92093-0085

University of California, San Diego
Department of Structural Engineering
Structural Systems Research Project

Report No. SSRP – 2000/13

Flexural Behavior Of Circular Hollow Columns With A Single Layer Of Reinforcement Under Seismic Loading

by

Jun-ichi Hoshikuma
Visiting Scholar

M.J.N. Priestley
Professor of Structural Engineering

Final Research Report for Caltrans under Contract No. 59A0051

Department of Structural Engineering
University of California, San Diego
La Jolla, California 92093-0085

November 2000

Technical Report Documentation Page

1. Report No.	2. Government Accession No.	3. Recipient's Catalog No.
SSRP 2000/13		

4. Title and Subtitle	5. Report Date
"Flexural Behavior Of A Circular Hollow Columns With A Single Layer Of Reinforcement"	
	6. Performing Organization Code

7. Author(s)	8. Performing Organization Report No.
Hoshikuma, J., and Priestley, M.J.N.	UCSD / SSRP-2000/13

9. Performing Organization Name and Address	10. Work Unit No. (TRAIS)
Department of Structural Engineering School of Engineering University of California, San Diego La Jolla, California 92093-0085	11. Contract or Grant No. 59A0051

12. Sponsoring Agency Name and Address	13. Type of Report and Period Covered
California Department of Transportation Engineering Service Center 1801 30th St., West Building MS-9 Sacramento, California 95807	Final Report - 14. Sponsoring Agency Code

15. Supplementary Notes

Prepared in cooperation with the State of California Department of Transportation.

16. Abstract

Hollow sections are often used for tall bridge columns to reduce their mass, reduce seismic inertia forces, and reduce foundation forces. However, the seismic performance of hollow columns is still not fully understood although a few experimental works were conducted previously. There are several interesting areas which must be investigated for the hollow columns, i.e., ductility capacity, shear strength, effect of diagonal loading in rectangular section, retrofit measures et al. This report presents the flexural ductility capacity of the hollow circular columns with one layer of longitudinal and transverse reinforcement placed near the outside face of the section.

The behavior of two flexure-dominant circular hollow reinforced concrete columns, with different longitudinal reinforcement ratios, under cyclic loading is investigated through a discussion of experimental studies. It should be noted that column proportions and reinforcement details of the test units are modeled on typical of those that might be used for major bridges in California and differ significantly from those in previous researches.

Test results showed that the columns failed suddenly when concrete on the inside face of the wall was crushed. It was also found that confinement-induced transverse strain at the plastic hinge region did not reach the yield strain before failure. These facts suggest that the limited lateral pressure is induced in the concrete shell and thus the inside face concrete is subjected to poor confinement even though sufficient transverse reinforcement is placed near the outside face of the hollow columns.

Moment-curvature analyses were carried out for the test units, to evaluate the lateral force-displacement response. The stress-strain curve of the confined concrete was calculated with an assumption that the maximum effective lateral pressure occurred when the spiral strain reached a maximum useful confinement-induced strain of 0.001. As a result, the theoretical force-displacement relation showed a good agreement with the experimental response.

17. Key Words	18. Distribution Statement
	Unlimited

19. Security Classification (of this report)	20. Security Classification (of this page)	21. No. of Pages	22. Price
Unclassified	Unclassified	~84	

Form DOT F 1700.7 (8-72) Reproc

DISCLAIMER

The contents of this report reflect the views of the authors who are responsible for the facts and accuracy of the data presented herein. The contents do not necessarily reflect the official views or policies of the State of California or the Federal Highway Administration. This report does not constitute a standard, specification or regulation.

TABLE OF CONTENTS

LIST OF SYMBOLS

A_b = area of transverse steel

A_g = gross section area

d_{bl} = nominal diameter of longitudinal bar

d_{bs} = nominal diameter of transverse steel

D = diameter of hollow column

E_s = modulus of elasticity of steel

f_c' = compressive strength of unconfined concrete

f_{cc}' = compressive strength of confined concrete

f_h = confinement-induced transverse steel stress

f_l' = effective lateral confining stress in equivalent solid section

f_{l2}' = effective lateral confining stress in circumferential direction

f_y = yield strength of longitudinal bar

f_u = ultimate strength of longitudinal bar

F_H = lateral force

H = concrete wall thickness

k_e = confinement effectiveness coefficient

L = column height

L_p = plastic hinge length

P = axial compressive force

s = spacing of transverse steel

t = concrete wall thickness

Δ = structural displacement

ρ_{bl} = longitudinal reinforcement ratio

ρ_s = transverse steel volumetric ratio

ϕ = curvature

LIST OF FIGURES

LIST OF TABLES

ACKNOWLEDGMENTS

The research described in this report was funded by the California Department of Transportation (Caltrans) under Caltrans Contract number 59A0051. Conclusions and recommendations in this report are those of the authors and should not be construed to imply endorsement by Caltrans.

The authors greatly appreciate Giulio Ranzo for his useful comments on test results presented in this report and technical advice on construction of test units. They would like to thank the technicians at the Charles Lee Powell Structures Laboratories for their help during construction and testing of the test units, namely Charlie Stearns, Alex Sherman, Frank Ho, Bob Parks, Chris Latham, and Larry Berman.

ABSTRACT

Hollow sections are often used for tall bridge columns to reduce their mass, reduce seismic inertia forces, and reduce foundation forces. However, the seismic performance of hollow columns is still not fully understood although a few experimental works were conducted previously. There are several interesting areas which must be investigated for the hollow columns, i.e., ductility capacity, shear strength, effect of diagonal loading in rectangular section, retrofit measures et al. This report presents the flexural ductility capacity of the hollow circular columns with one layer of longitudinal and transverse reinforcement placed near the outside face of the section.

The behavior of two flexure-dominant circular hollow reinforced concrete columns, with different longitudinal reinforcement ratios, under cyclic loading is investigated through a discussion of experimental studies. It should be noted that column proportions and reinforcement details of the test units are modeled on columns typical of those that might be used for major bridges in California and differ significantly from those in previous researches.

Test results showed that the columns failed suddenly when concrete on the inside face of the wall was crushed. It was also found that confinement-induced transverse strain at the plastic hinge region did not reach the yield strain before failure. These facts suggest that the limited lateral pressure is induced in the concrete shell and thus the inside face concrete is subjected to poor confinement even though sufficient transverse reinforcement is placed near the outside face of the hollow columns.

Moment-curvature analyses were carried out for the test units, to evaluate the lateral force-displacement response. The stress-strain curve of the confined concrete was calculated with an assumption that the maximum effective lateral pressure occurred when the spiral strain reached a maximum useful confinement-induced strain of 0.001. As a result, the theoretical force-displacement relation showed a good agreement with the experimental response.

CHAPTER 1

1 INTRODUCTION

1.1 Introduction

A hollow concrete section is often used for column design, particularly for very tall bridge columns in seismic areas including California, New Zealand, Japan and Italy et al., for reducing the mass and therefore minimizing the self-weight contribution to the inertial mode of vibration during an earthquake. The hollow columns also enable to reduce foundation dimensions and thus save the construction cost substantially. Therefore, these advantages have promoted the use of hollow columns instead of similar solid members. On the other hand, the seismic behavior of the hollow columns has been controversial due to a lack of understanding.

The effect of the hollow section should be adequately assessed in the seismic design, because the structural response of the hollow column under seismic loading may be significantly different from that of solid column due to existence of a void section. However, there are several unknown areas which must be understood, that is, assessment of ductility capacity and shear strength, retrofit measures et al.

The research described in this report deals with the flexural ductility capacity of the hollow circular columns with one layer of longitudinal and transverse reinforcement placed near the outside face of the section. In the past, hollow section columns, of both rectangular and circular section, have been reinforced by two layers of reinforcement. However, with circular sections the inner circumferential bar has a tendency to pull through the inner cover concrete, because of the bursting stress and requires large amounts of cross linking to ensure adequate radial confinement (see Fig. 1.1a). In other words, the inner layer is likely to be detrimental, rather than beneficial, to confinement requirements. On the other hand, if a single layer of reinforcement is used close to the outer face of the hollow column, the core inside the outer hoop is subjected to radial confining pressure reducing from

$$fr = \frac{A_h f_h}{R.s} \tag{1.1}$$

at the level of the hoop to zero on the inside surface where $A_h f_h$ and s are the hoop bar area stress and spacing, respectively, and R is the radius of the hoops or spiral. In the circumferential direction a higher confining stress of

$$f_h = \frac{A_h f_h}{t.s} = f_r \frac{R}{t} \tag{1.2}$$

is developed, where t is the wall thickness. The wall is thus subjected to biaxial confinement conditions, with the ratio of radial and hoop confining stresses varying through the wall thickness. Although the average effective confining stress will be larger than for a solid circular column, the low effective confining stress on the inside surface would indicate a probability of early crushing at low longitudinal strain.

The above considerations would lead to expectations for low displacement ductility capacity when wall thickness t is small compared to radius R. However, since hollow columns are typically only used for very high bridges, yield displacements are also high, and ductility demand is typically low. For example, consider a circular cantilever hollow column with outside diameter D=8m, height H=30m, wall thickness t=0.6m, reinforced longitudinally with reinforcement of yield strength 455MPa. The effective yield curvature can be approximated as

$$\phi_y = \frac{2.2\varepsilon_y}{D} \tag{1.3}$$

where $\varepsilon_y = 455/200{,}000 = 0.00278$.

The effective yield displacement is

$$\Delta_y = \phi_y \frac{H^2}{3} \tag{1.4}$$

$$= \frac{2.2\ x 0.00278 x\ 30^2}{8\ x\ 3}$$

$$= \underline{0.23\text{m}}$$

Such a column would respond to the Sylmar record of the 1994 Northridge earthquake with a peak displacement ductility demand of less than μ_Δ=2, regardless of period.

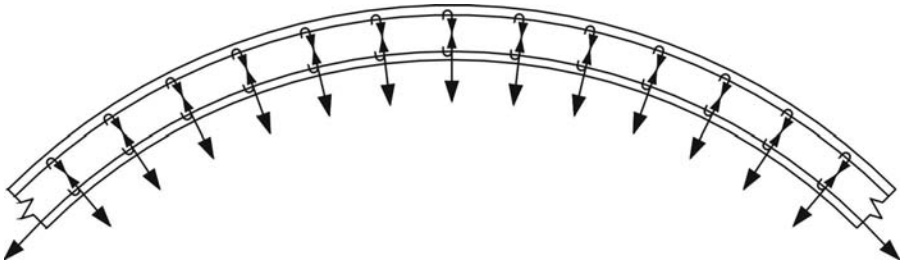

(a) Bursting Forces From Inside Hoop Bar In Two-Layer Design

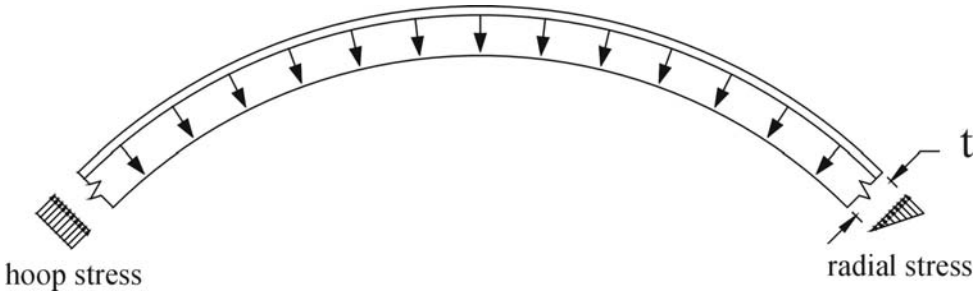

(b) Radial And Hoop Stresses Induced In Wall From A Single Layer Hoop Design

Fig. 1.1 Alternative Design for Hollow Circular Sections

In order to investigate the inelastic behavior, and ductility capacity of hollow circular columns, cyclic loading tests were conducted for two large-scaled flexural columns with different longitudinal reinforcement ratios. Furthermore, moment-curvature analyses were carried out for the test units. An analytical model was discussed for consideration of confinement effectiveness due to existence of the void section. Analytical results were compared with the experimental response in terms of the strain and the lateral force-displacement relation.

1.2 Overview of Previous Research

The flexural performance of hollow columns has been previously investigated experimentally by a number of researchers. It was found from the previous research works [2-3] that hollow reinforced concrete columns, with two layers of longitudinal and transverse reinforcement placed near in-/outside faces and cross ties through the wall thickness, can exhibit a ductile behavior. On the other hand, few experimental researches on the flexural performance of the hollow circular columns with one layer of reinforcement have been conducted. Zahn et al. [4] made cyclic loading tests for six hollow circular columns with different wall thickness ratio to outside diameter of the section (0.14 to 0.24) and different axial load ratio (0.08 to 0.40). The outside diameter of the columns was 400mm and aspect ratio was 4.5. The longitudinal reinforcement ratios to gross concrete section including the void were 2.56% in all test units. In other words, the longitudinal reinforcement ratios to net concrete section varied from 3.67% to 5.40%. Test results showed that the ductility capacity of the hollow columns significantly depended on the position of the neutral axis at the flexural strength. If the neutral axis crossed the void section with some distance from the inside face, the column exhibited low ductile behavior due to early vertical splitting and crushing of the inside face concrete. A value of 0.008 was proposed for the longitudinal compression strain of the inside face concrete at crushing based on theoretical and experimental approaches.

Kawashima et al. [5] tested two pairs of circular hollow columns with the longitudinal reinforcement ratio to net concrete section of 1.35% and 2.19%, respectively. The column

outside diameter was 800mm and the inside diameter was 518mm, resulting in a 141mm wall thickness. The wall thickness ratio to outside diameter is calculated as 0.18. The transverse hoops were 9mm diameter plain round bars and these were placed with the spacing of 200mm. Lateral load was applied in single bending to give the aspect ratio of 3.1, but no axial force was applied. Experimental results showed that crushing of the inside face concrete caused the deterioration of the shear strength, particularly in the column with high longitudinal reinforcement ratio. They also pointed out that the confinement effect induced in the hollow section was significantly less than in the solid section due to the premature crushing of inside face concrete.

1.3 Research Objective

The final goal of the research is to develop design recommendations for the ductility capacity of the hollow circular columns. As part of the research, cyclic loading tests were conducted for two large-scaled hollow circular columns. As described in previous section, a few tests have already been carried out for the hollow circular columns with one layer of reinforcement. However, it can be suggested that the wall thickness ratio in the previous columns seems to be larger than of the hollow columns designed actually in California. Because the wall thickness ratio is one of the most important factors to control the flexural ductility capacity of the hollow columns, new loading tests have been required for the Californian hollow columns to investigate the flexural performance under seismic loading. Table 1 compares the test unit dimensions and an axial load ratio between the previous researchers' columns and the authors' (see Chapter 2 for details). As shown, the wall thickness ratio of the authors' columns is significantly smaller than the previous columns.

An objective of the research described in this report is to investigate the flexural performance of the hollow circular columns with thin concrete wall through the loading tests and discuss the confinement effect in the hollow section based on test results. Shear strength of the hollow circular columns under seismic loading has been investigated in a companion research project. Details of the study may be seen reported elsewhere [6].

Table 1-1 Test Unit Details in Previous Experiments and Authors'

Researcher	Zahn et al [4]	Kawashima [5]	Authors
T / D	0.14-0.24	0.18	0.092
L / D	4.5	3.1	4.3
d_{bl} (mm)	16	10-13	13-19
$\rho_{l\,n}$ (%)	3.67-5.40	1.35-2.19	1.45-3.18
d_{bs} (mm)	10-12	9	6
S (mm)	75-90	200	35
ρ_s (%)	1.13-1.36	0.18	0.22
$P / f_c' A_g$	0.08-0.40	0	0.13

CHAPTER 2

2 DETAILS OF LOADING TESTS

2.1 Test Unit Dimensions

Two hollow circular columns with different longitudinal reinforcement ratio, called herein HF1 and HF2, were constructed and tested in this research. Dimensions of the columns are shown in Fig. 2.1. Since geometry of the section in actual hollow bridge columns constructed or planned by Caltrans is modeled as realistic as possible, and also prototypes are typically 3-6m diameter or sometimes more with longitudinal reinforcement of #11 or larger, the scale ratio was targeted to 1:4 in this test program for which the scale effects would be minimal. It should be noted that the test unit below mid-height section was constructed by reinforced concrete with hollow section and a loading steel tube was connected to the column top for the extension of the height, which made on-site-construction at the Structural Components Laboratory, UCSD be speedy and efficient.

The outer diameter of the hollow section was 1524mm and the inner diameter 1244mm, resulting in 140mm wall thickness or the wall thickness ratio of 0.092. The height of the hollow reinforced concrete section was 3480 mm, sufficient to observe the flexural performance at the plastic hinge region. A total column height from the base to loading point is 6528mm, tested in single bending to give the aspect ratio of 4.28.

Details of steel arrangement are depicted in Fig. 2.2. The test column had 34 bundles of 2 #4 bars (HF1) or 2 #6 bars (HF2) in one layer distributed evenly with a constant cover of 19mm (HF1) or 16mm (HF2). The longitudinal reinforcement ratios to the net area of the concrete were 1.45% and 3.18%, respectively. The transverse reinforcement was a W5 wire (6.35mm diameter) placed with 35mm spiral pitch in the range of plastic end region [7] and column top region, and 70mm spiral pitch in the other region. The footing was reinforced with 24 #8 O bars and 8 #8 Z bars in loading direction. Fig. 2.3 is a photo of the reinforcement cage.

The loading steel tube was connected to the column top through 34 #7 high strength thread rods which were spliced to longitudinal reinforcements with the development length of 838mm, as shown in Fig. 2.4. The thread rods were placed in precise position by using a template. The loading steel tube was fabricated with 25mm thickness base plate, 1219mm inside-to-inside diameter/19mm thickness steel tube, and a loading stub, and was designed based on overstrength moment of the hollow reinforced concrete section so that it remained elastic at the maximum feasible column base moment during testing. A layer of hydrostone was placed between the hollow column top and the base plate of the loading steel tube to ensure a smooth bearing surface.

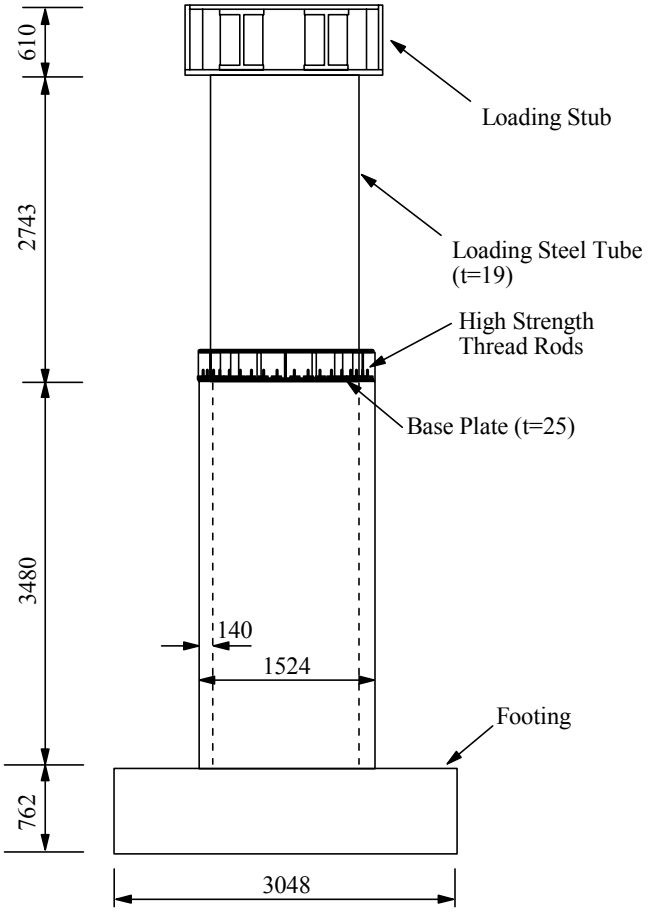

Fig. 2.1 Geometry of Test Unit

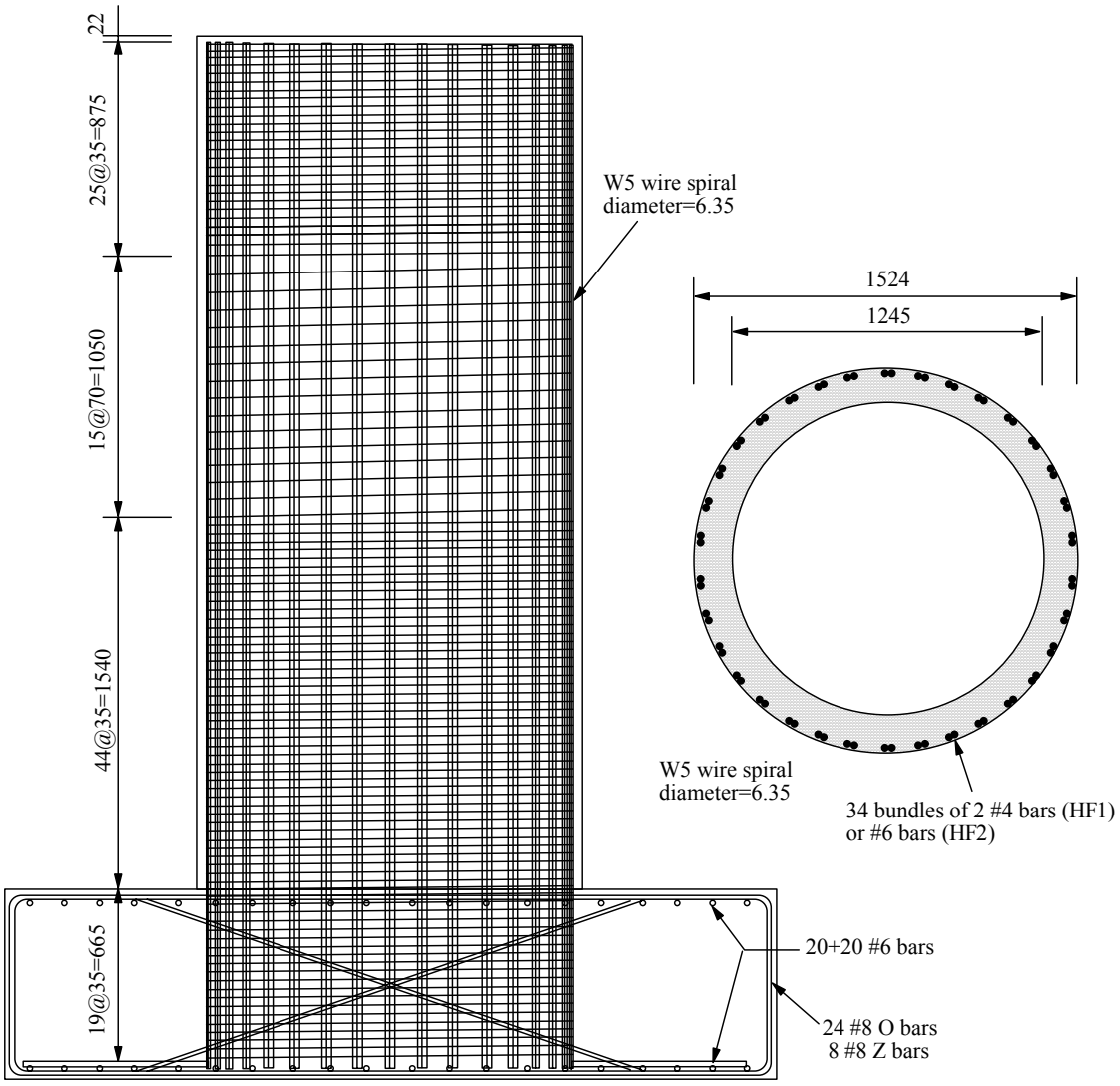

Fig. 2.2 Details of Reinforcement

Structural details of the loading steel tube are depicted in Fig. 2.5. The tube has an inside-to-inside diameter of 1219mm with a steel plate thickness of 19mm. The base plate (t=25mm) was welded to the steel tube bottom with 34 stiffeners and a ring plate. There are 34 drilled holes on the base plate for connection to the hollow column through the thread rods. The loading stub was fabricated with the stiffened W-beams and the steel plates, and it was welded on the top of the steel tube.

Fig. 2.3 Reinforcement Cage

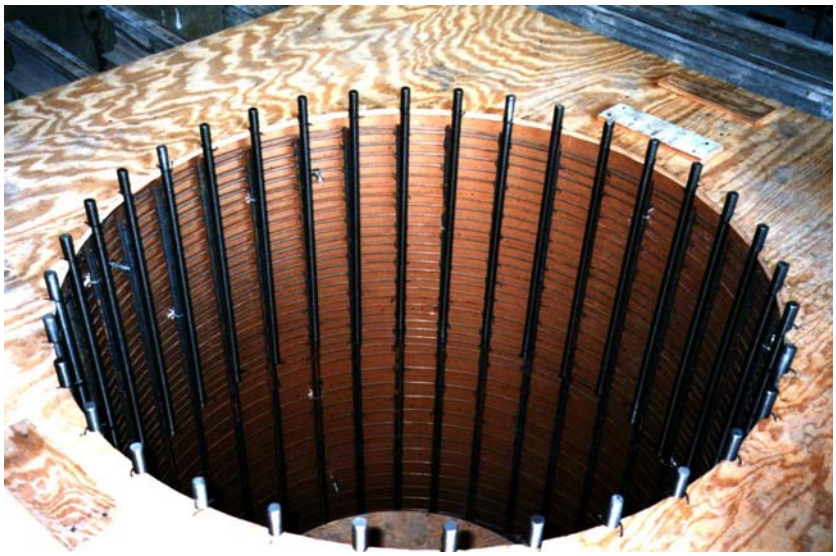

Fig. 2.4 Thread Rods Spliced to Longitudinal Reinforcement Bars

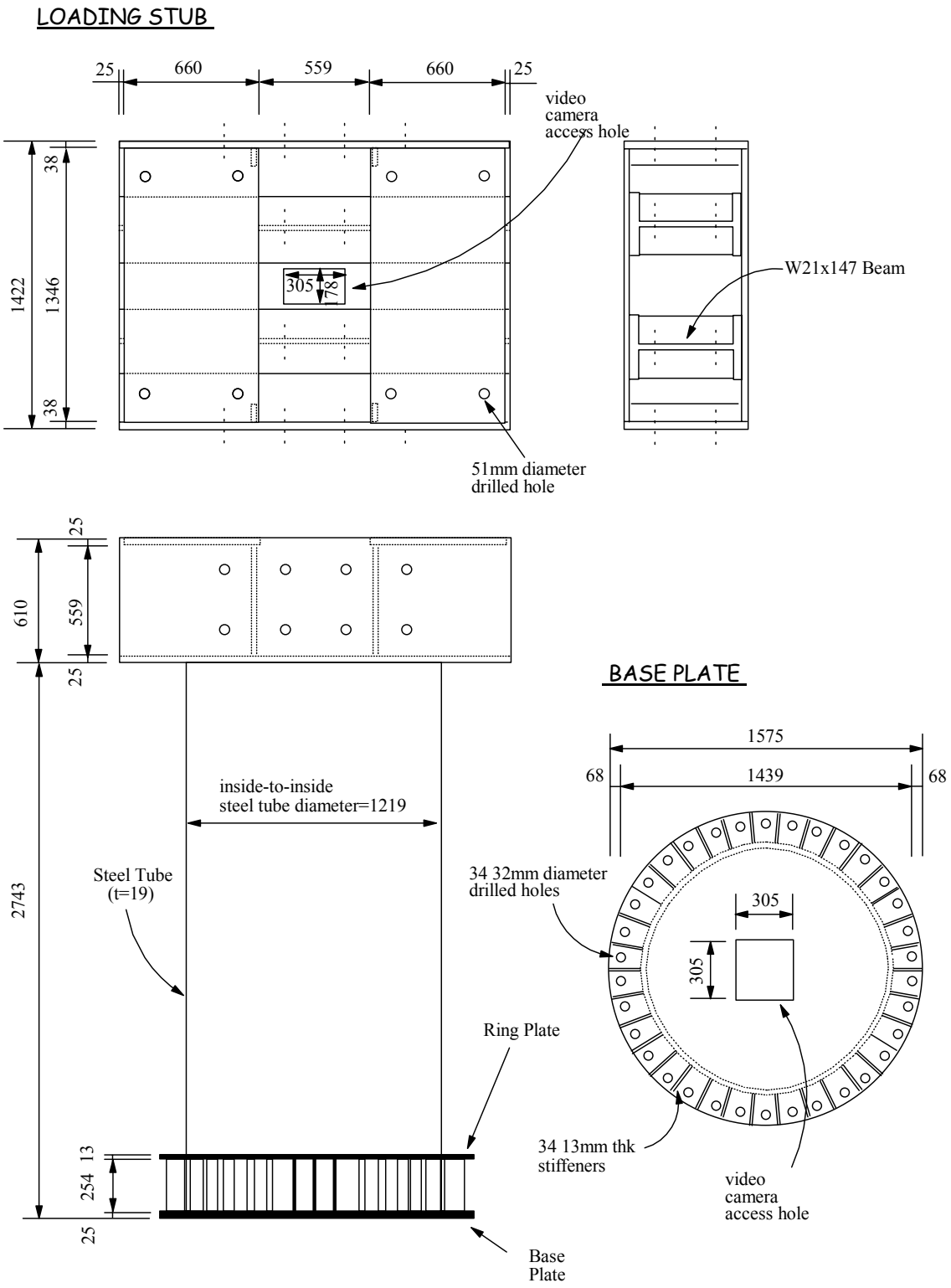

Fig. 2.5 Details of Loading Steel Tube

2.2 Material Properties

Table 2.1 shows the results of the standard cylinder compression tests for the concrete used in the test units. Samples of utilized longitudinal and transverse steel bars were tested to determine their yield strengths and elastic moduli. The values obtained are given in Table 2.2.

Table 2-1 Concrete Strength on Date of Testing (MPa)

Test Unit	Footing	Column
HF1	43.1	37.4
HF2	40.2	38.5

Table 2-2 Steel Material Properties

Steel Type	f_y (MPa)	f_u (MPa)	E_s (GPa)
Longitudinal (#4)	427	700	185
Longitudinal (#6)	444	738	192
Spirals	625	820	175

2.3 Test Setup

The overall test setup is illustrated in Fig. 2.6. The tests were carried out at the Structural Components Laboratory, UCSD. The test units were supported by the footing clamped to the strong floor by 16 post-tensioned dywidag high strength bars. In order to strengthen the footing and prevent cracking, horizontal prestress of 5340kN (HF1) and 7120kN (HF2) were given to the footing in the loading direction through 8 post-tensioned dywidag high strength bars. A lateral load was provided by a TJ Vicker hydraulic actuator (+2513/-1397kN load capacity with a maximum stroke of +/-0.46m). The actuator was mounted to the reaction wall with a mounting plate and aligned with the centerline of the loading stub. Fig. 2.7 is a photo of the test setup.

A vertical load was applied to the units through the use of four 46mm diameter dywidag high strength bars (Grade 150 (f_y =1030MPa)) and two rocker beam assemblies developed for an earlier research project at UCSD [8]. A total vertical load of 2913kN (HF1) or 2997kN (HF2), corresponding to the axial load ratios ($P / f_c'A_g$) of nearly 0.13, was applied and maintained throughout the test.

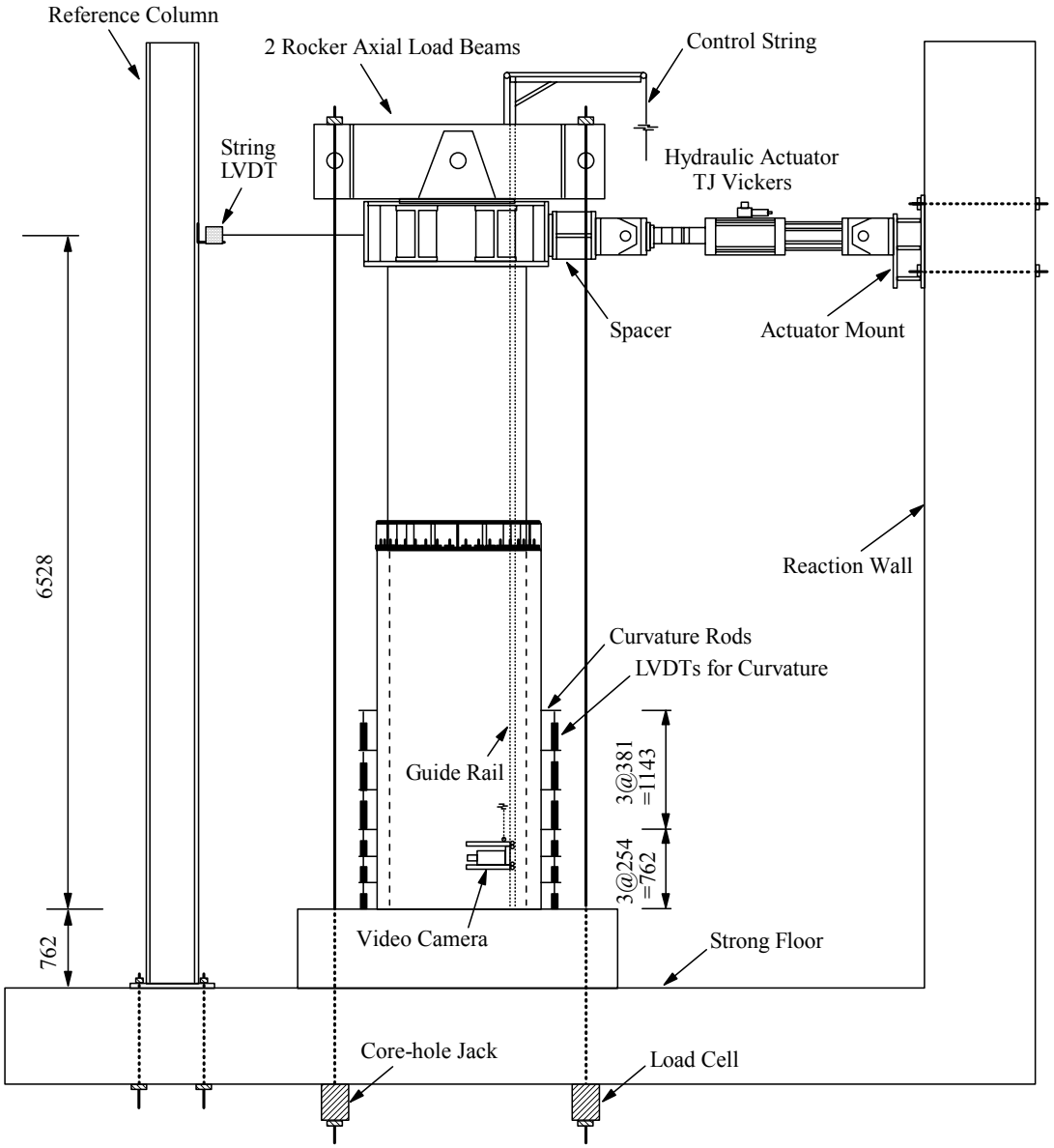

Fig. 2.6 Test Setup

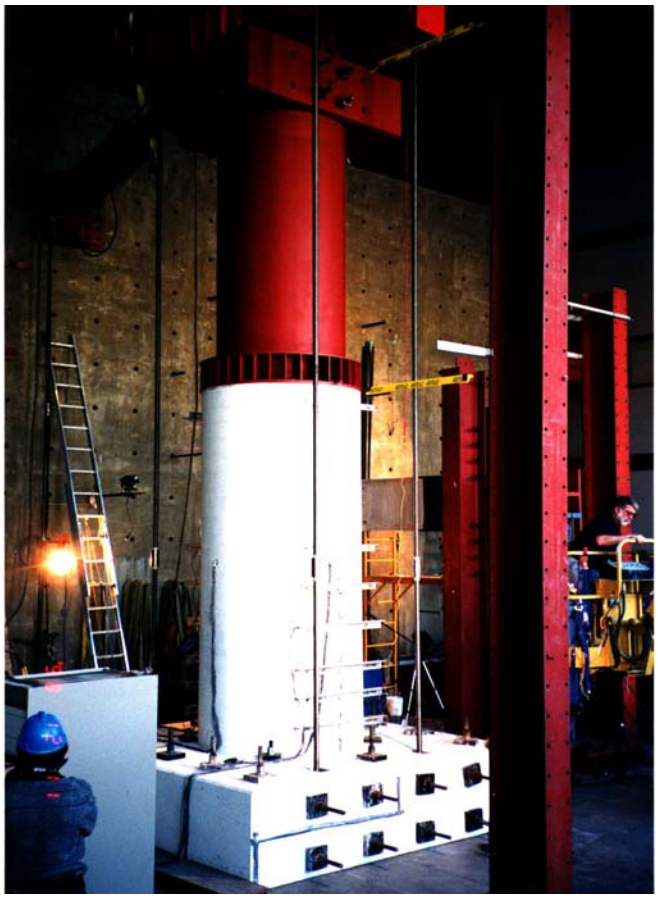

Fig. 2.7 Test Setup

2.4 Instrumentation

Linear-variable-displacement-transducers (LVDTs) and strain gauges were employed for the measurement of displacement, curvature and steel strain. A layout of the LDVTs is depicted in Fig. 2.6. Lateral displacement at the loading point was measured by a string LVDT attached to the reference column through an aluminum bracket. Six LVDTs were mounted each on the north and south faces for the curvature measurement at the plastic end region.

The LVDT brackets were connected to aluminum angles which were supported by 10mm diameter thread curvature rods anchored to either side of the column core. Shear deformation was not measured in the tests because the flexural deformation was expected to dominate the column behavior.

Fourteen strain gauges were put on each longitudinal bar placed at the cardinal points. Transverse bars were instrumented with the strain gauges at twelve levels in the plastic end region. The strain gauges employed in the tests were electric resistance 5mm long ones. The gauge layout for longitudinal and transverse bars is shown in Fig. 2.8.

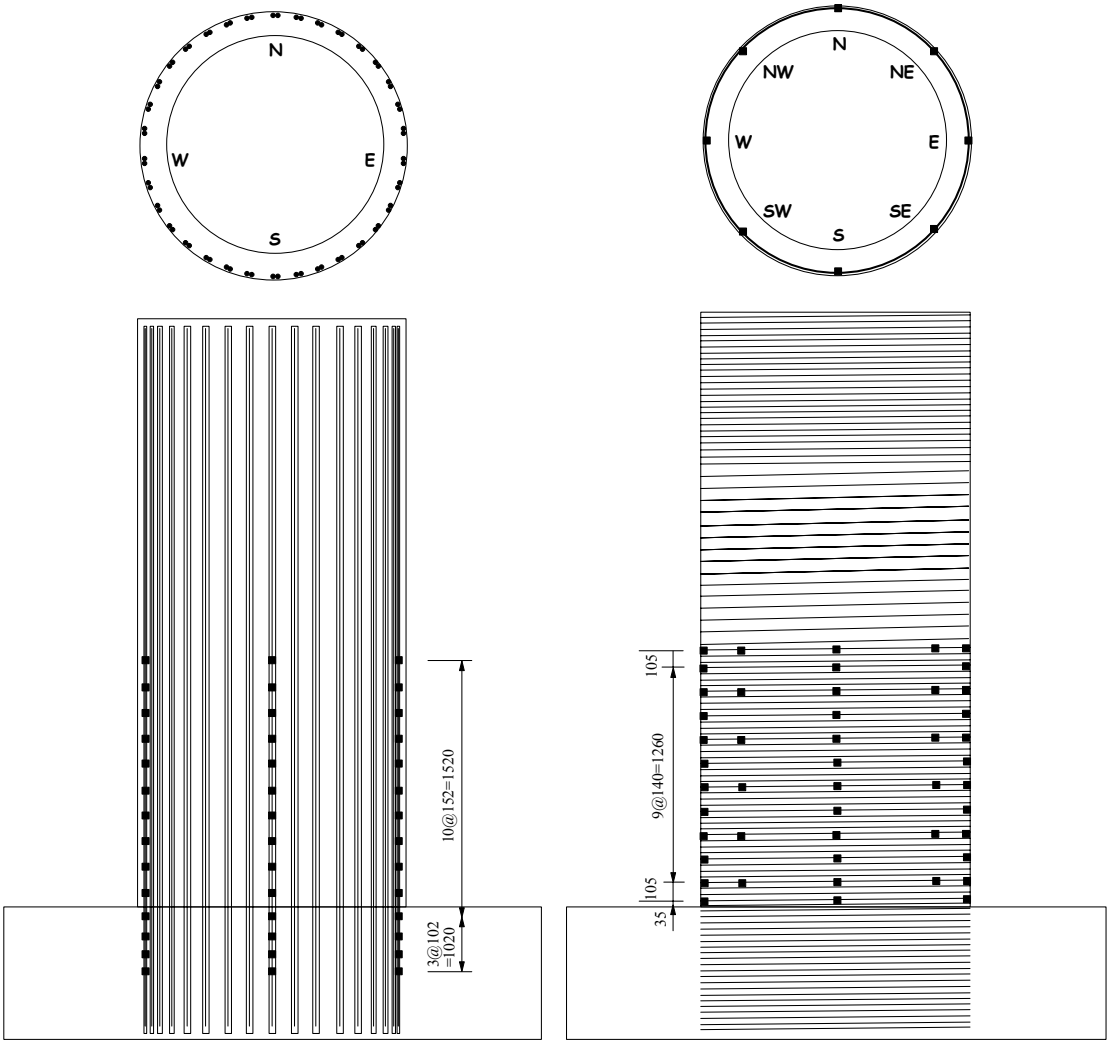

(a) Longitudinal Bars (b) Transverse Bars

Fig. 2.8 Strain Gauges Layout

A movable video camera was placed in the void section to observe damage developed on inside face concrete during testing. The video camera was supported by a guide rail set up near the south inside face as shown in Fig. 2.6 and 2.9. The system provided a panoramic view of the inside except the south face.

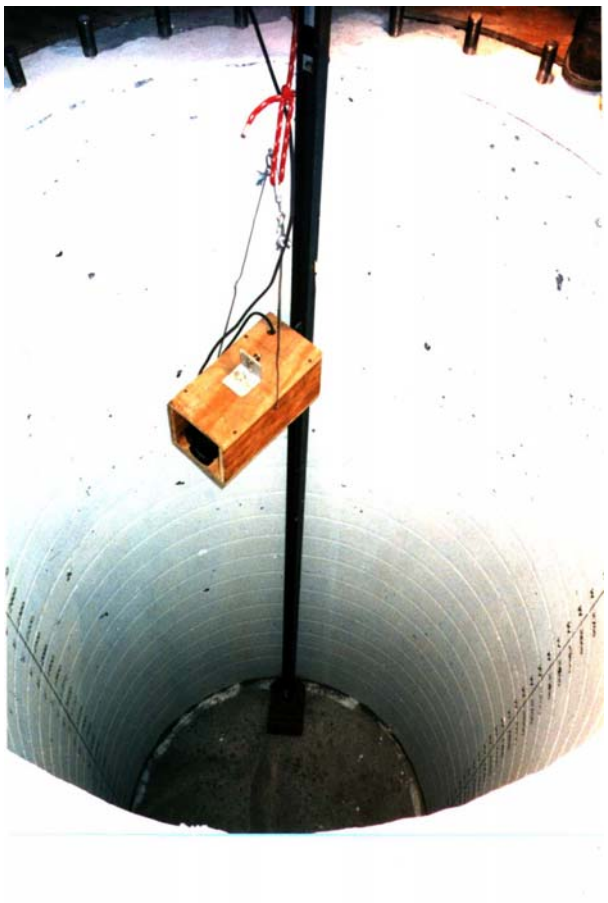

Fig. 2.9 Movable Video Camera Placed Inside

2.5 Loading Procedure

The columns were loaded quasi-statically and subjected to cycles of force reversals under force control until theoretical first yield of the extreme longitudinal reinforcement, and subsequently to cycles in displacement control to prescribed ductility levels. The test sequence consisted of single cycles at 25%, 50%, 75% and 100% of the first yield force and

three cycles at ductility levels of 1.0, 1.5, 2.0, 3.0 and 4.0, respectively unless failure occurred earlier. The complete loading pattern is shown in Fig. 2.10.

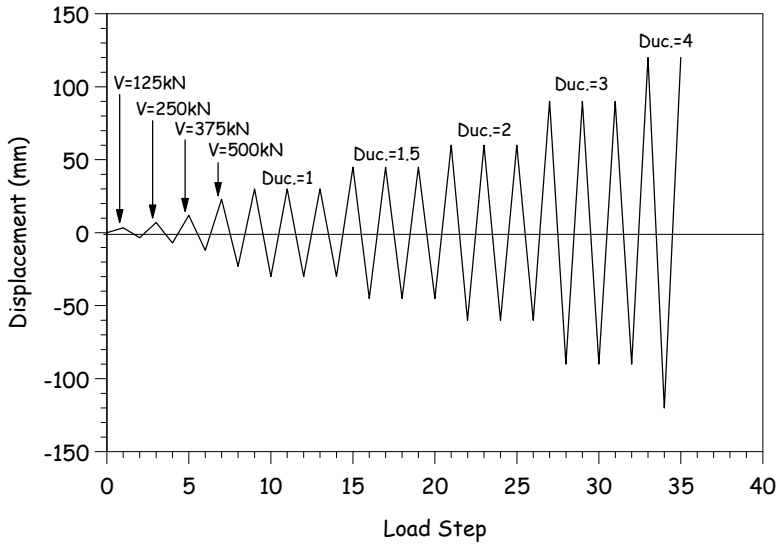

(a) HF1 Unit

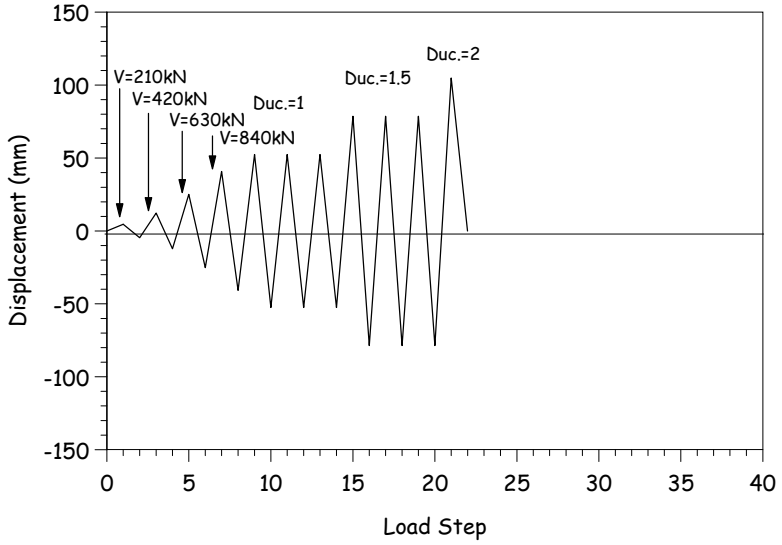

(b) HF2 Unit

Fig. 2.10 Loading Pattern

The theoretical lateral force at first yield of the longitudinal reinforcement was calculated based on a section analysis, and the displacement corresponding to the first yield was determined as the average of the values in the push and pull loading directions measured at this force during the tests. The first yield displacement was extrapolated to the ideal flexural strength based on the section analysis, corresponding to an exteme fiber concrete stain of ε_c=0.004, using measured material strengths, and a strain-hardening model for the reinforcing steel. The amplified displacement found from linear extrapolation of first yield displacement from yield force to ideal flexural strength was defined as the true yield displacement corresponding to a displacement ductility of $\mu_\Delta = 1$.

CHAPTER 3

3 EXPERIMENTAL RESULTS OF TEST UNIT HF1

3.1 Test Observations

Test observations noted during testing of HF1 are described as follows. It is noted that some vertical cracks were recognized before testing at the column top region where the thread rods were spliced to the longitudinal reinforcement as shown in Fig. 3.1. These cracks were developed when the post-tensioning was provided to the thread rods for connection of the loading steel tube. However, the crack width was very small (less than 0.1mm) and did not extend during lateral loading. Therefore, it can be said that these initial cracks did not affect the column behavior.

1) Up to First Yield (500kN)

No damage was apparent up to 1/2 of the first yield force. The first visible flexural cracks formed at 375kN (3/4 of first yield force) located over the bottom 800mm. Some horizontal cracks were also observed on the inside face concrete by video camera located in the void section. At the first yield force, many new horizontal cracks were developed on north and south faces from column base up to a height of 2650mm. These cracks were well-distributed with an average spacing of 120mm.

2) Ductility 1.0

The existing flexural cracks widened to approximately 0.2mm in width and extended onto east and west faces and inclined at approximately 60 degree to the column axis as shown in Fig. 3.2. Major horizontal cracks were found on north inside face concrete at 350mm, 800mm, 1000mm and 1400mm height from column base.

3) Ductility 1.5

New flexural cracks formed over the whole height of the concrete section. Fig. 3.3 shows the flexural cracks developed on the north face and shear cracks developed on east face at the ductility 1.5. The crack widths of the major flexural and shear cracks were 0.35mm and 0.2mm, respectively. It was noted that new vertical splitting cracks developed on north inside face over a height of 800mm from the base as shown in Fig. 3.4.

4) Ductility 2.0

The crack pattern at the ductility of 2.0 is shown in Fig. 3.5. The flexural cracks widened to nearly 1.0mm on north and south face. The shear cracks continued to extend onto section from column base up to 1.5m (about column diameter) and widened to about 0.4mm in width.

5) Ductility 3.0

Incipient crushing of the cover concrete was found at the column base as shown in Fig. 3.6. At this level, some flexural and shear cracks widened to nearly 2mm and 0.7mm, respectively. Fig. 3.7 shows the horizontal cracks and diagonal cracks appeared on the north and east inside face, respectively. It is noted that no concrete crushing was observed on inside face at the ductility 3.0.

6) Ductility 4.0

In the first push cycle to ductility 4.0, no longitudinal reinforcement buckled as shown in Fig. 3.8, while the inside face concrete was crushed over a height of 600mm from the base as visible in Fig. 3.9. Subsequently, the lateral force significantly dropped at the displacement of 104mm, corresponding to the ductility 3.5. On the first return cycle, the lateral force degraded at the displacement of 96mm (ductility = 3.3) due to failure of the inside face concrete.

In the second push cycle, the plastic hinge region continued to spall-off both the cover concrete and the inside face concrete and lost a significant amount of concrete.

Subsequently, the concrete shell was crushed by the axial load and the longitudinal reinforcements buckled on not only north and south faces but west. Several layers of spiral bars fractured due to the significant buckling of the longitudinal reinforcement.

After testing and dismounting the loading steel tube, the damage developed inside was investigated. Fig. 3.10 shows a panoramic view of the inside damage. The inside face concrete spalled off at the section between 300mm and 600mm height from column base. A thickness of the biggest spalled concrete block was nearly 75mm as proved in Fig. 3.11, which corresponds to 54% of the wall thickness.

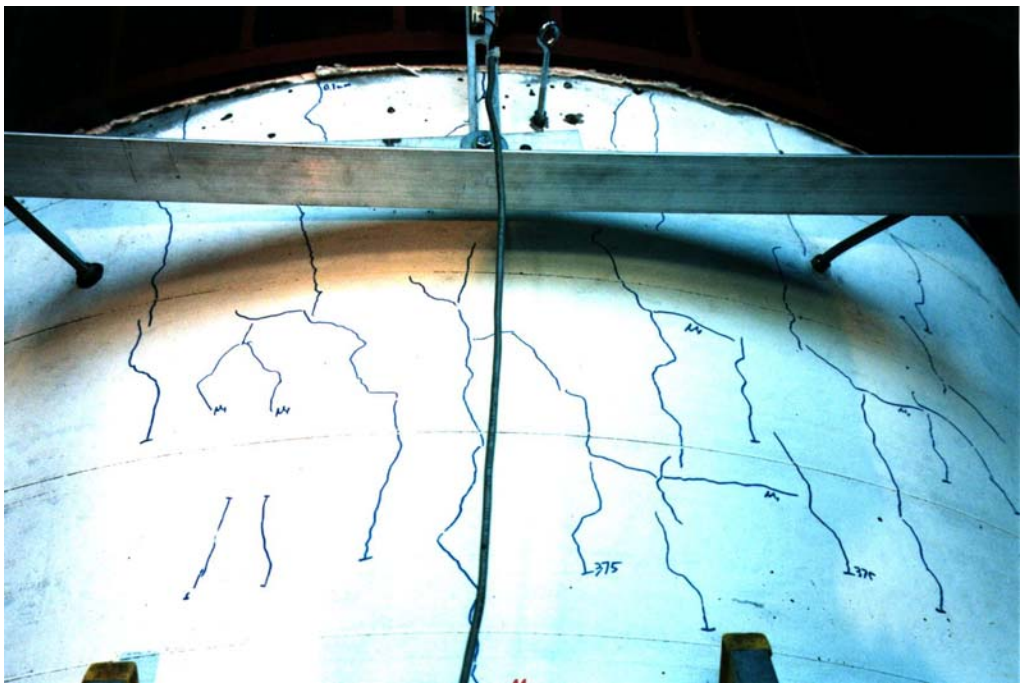

Fig. 3.1 Initial Minor Cracks Developed at Column Top Region

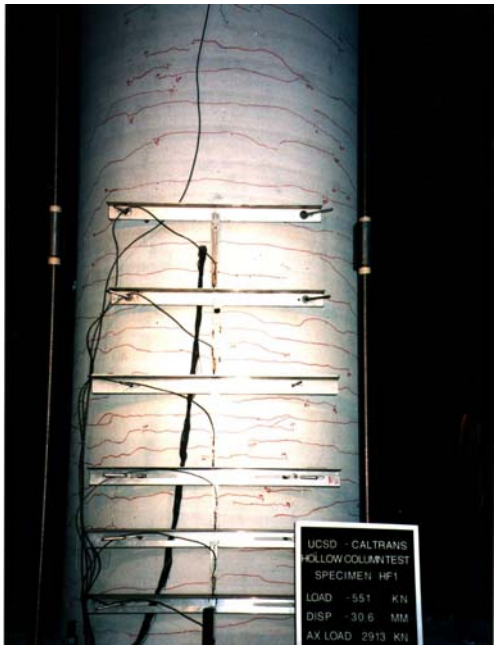

(a) Horizontal Cracks (North Face)

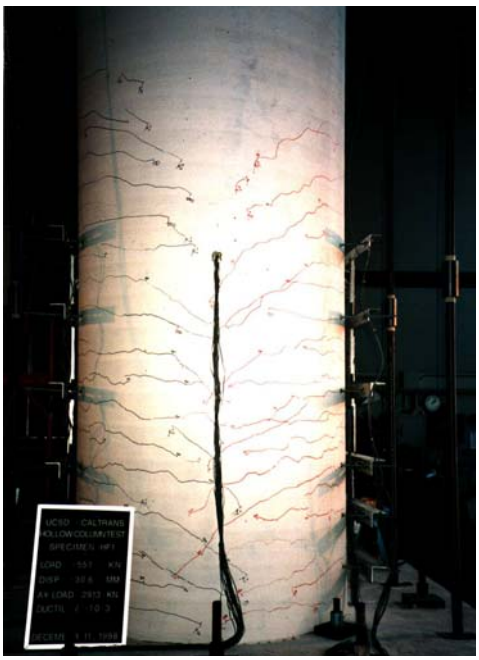

(b) Diagonal Cracks (East Face)

Fig. 3.2 Crack Pattern at Ductility 1.0

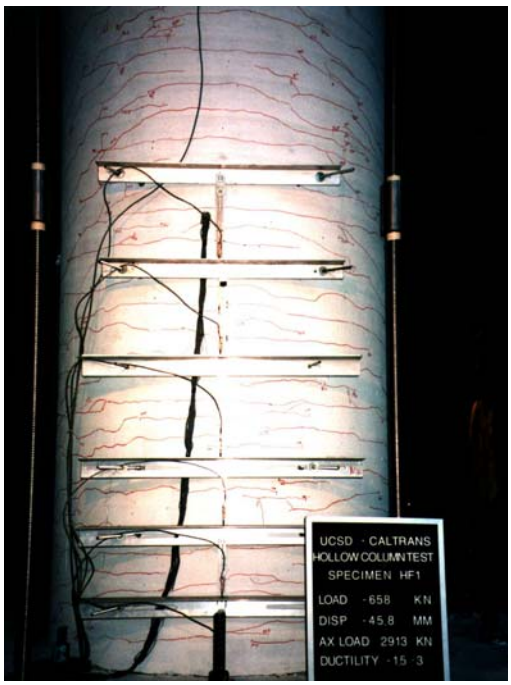

(a) Horizontal Cracks (North Face)

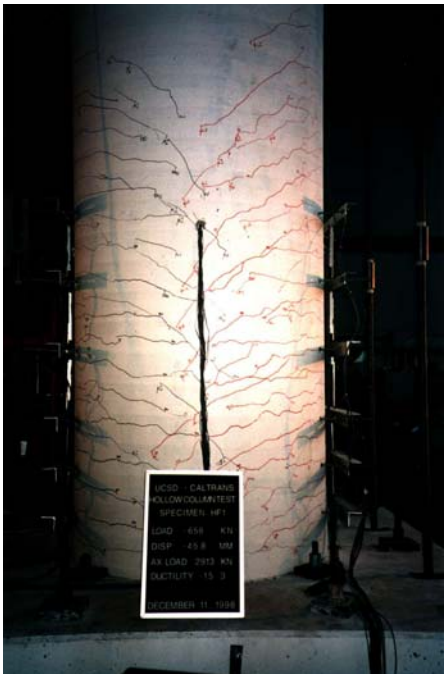

(b) Diagonal Cracks (East Face)

Fig. 3.3 Crack Pattern at Ductility 1.5

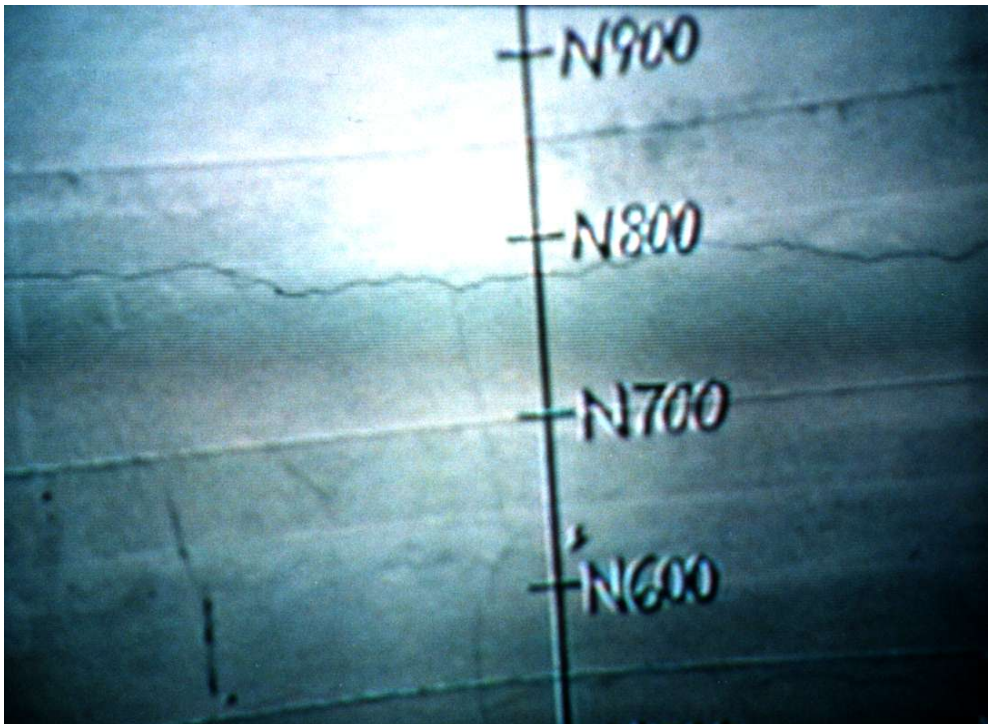

Fig. 3.4 Cracks Observed Inside at Ductility 1.5 (North Face)

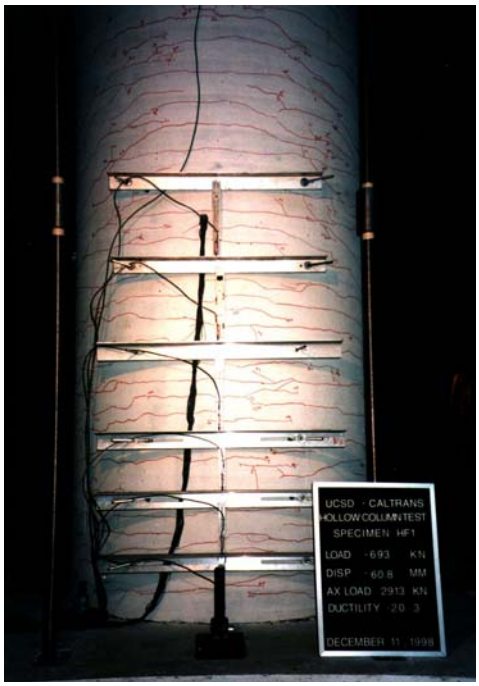

(a) Horizontal Cracks (North Face)

(b) Diagonal Cracks (East Face)

Fig. 3.5 Crack Pattern at Ductility 2.0

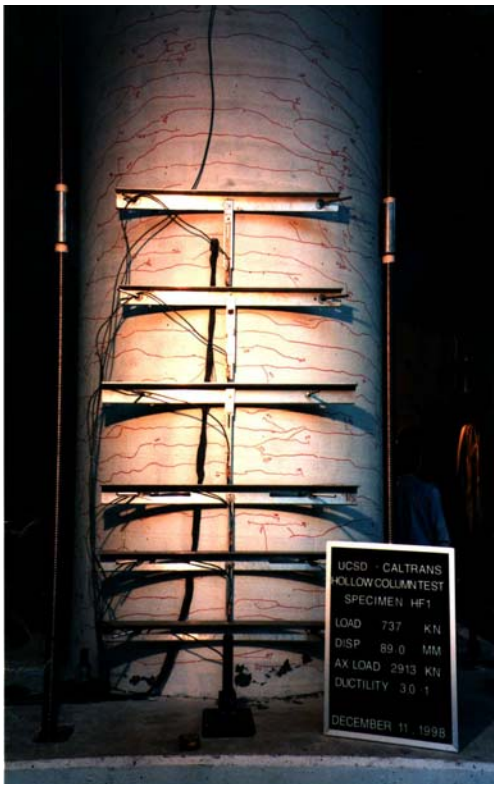

(a) Damage of North Face Concrete

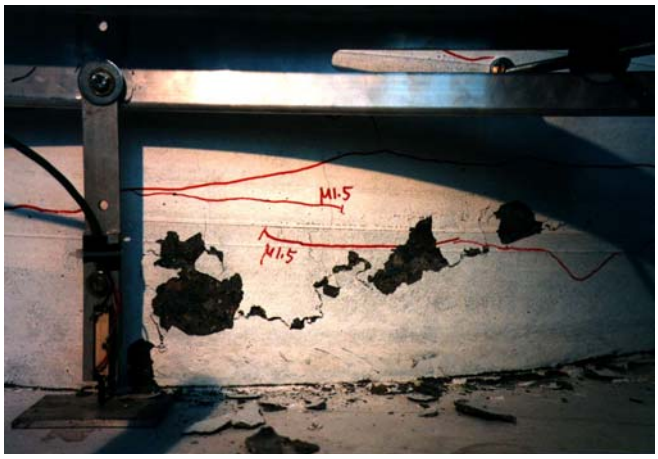

(b) Close-up

Fig. 3.6 Crushing of Cover Concrete at Ductility 3.0

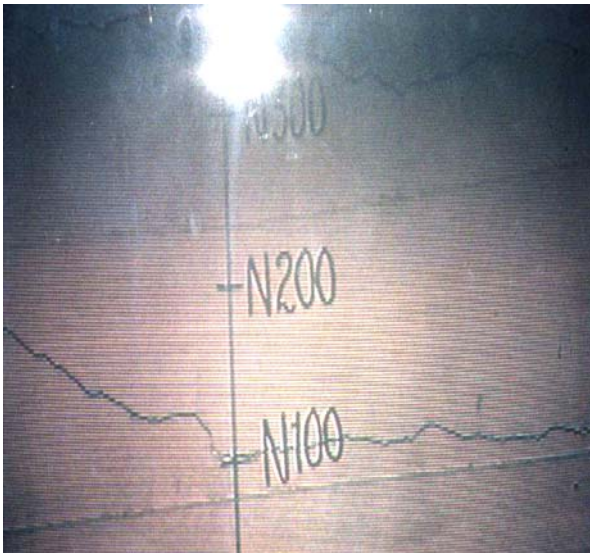

(a) Horizontal Cracks (North Face)

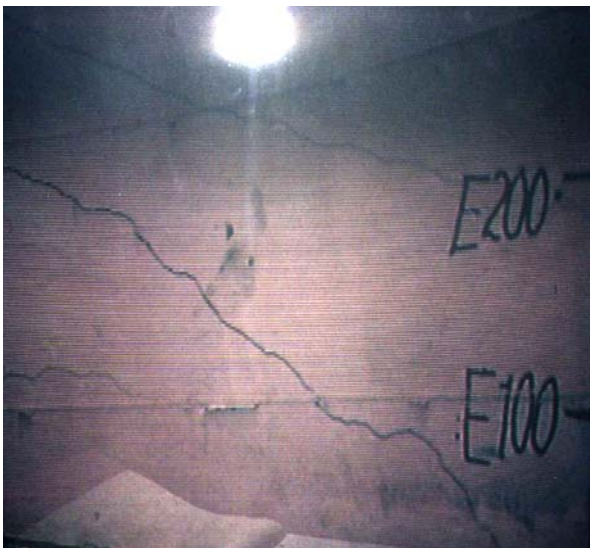

(b) Diagonal Cracks (East Face)

Fig. 3.7 Cracks Observed Inside at Ductility 3.0

(a) Damage of North Face Concrete (b) Close-up

Fig. 3.8 Failure of Column Base at Ductility 4.0

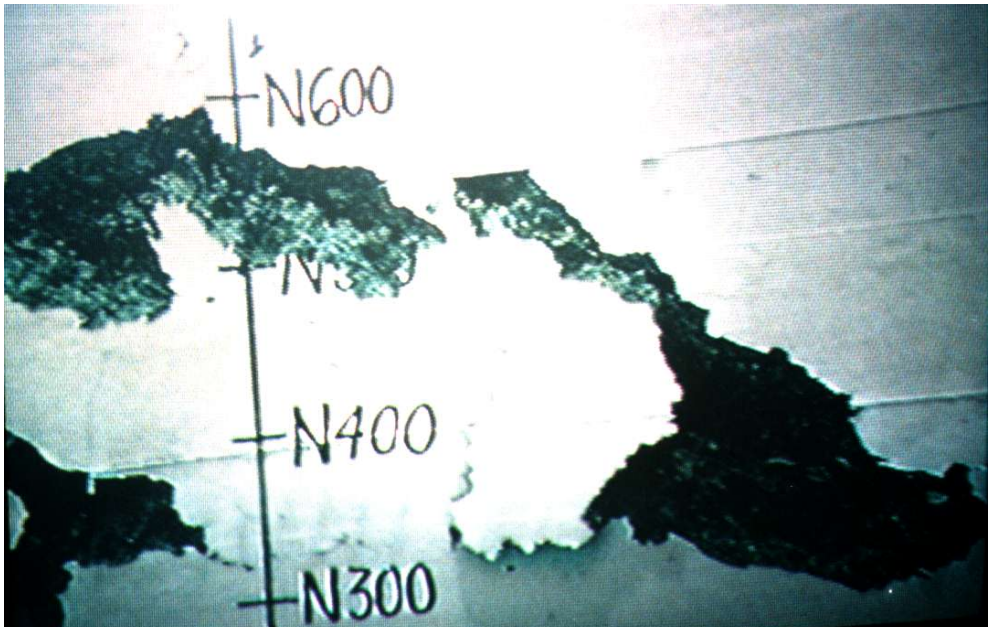

Fig. 3.9 Failure of Inside Face Concrete at Ductility 4.0

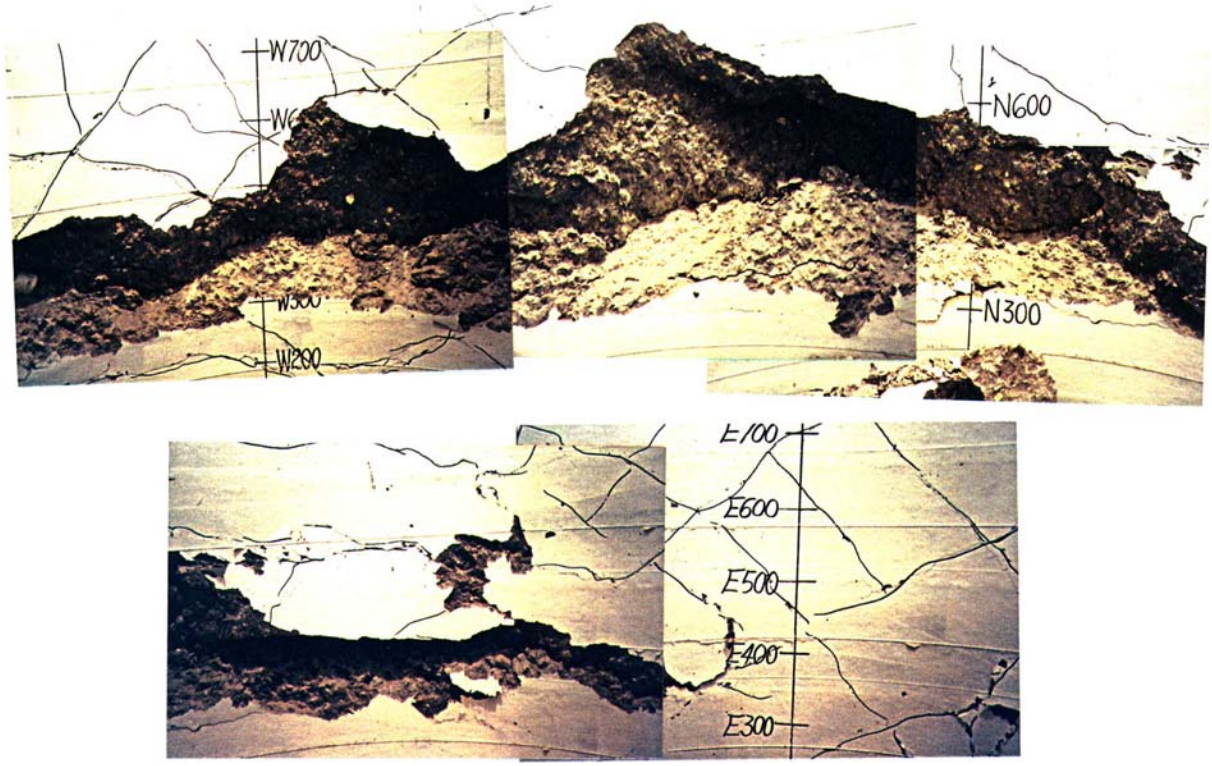

Fig. 3.10 Panoramic View of Inside Face Concrete after Testing (E-N-W)

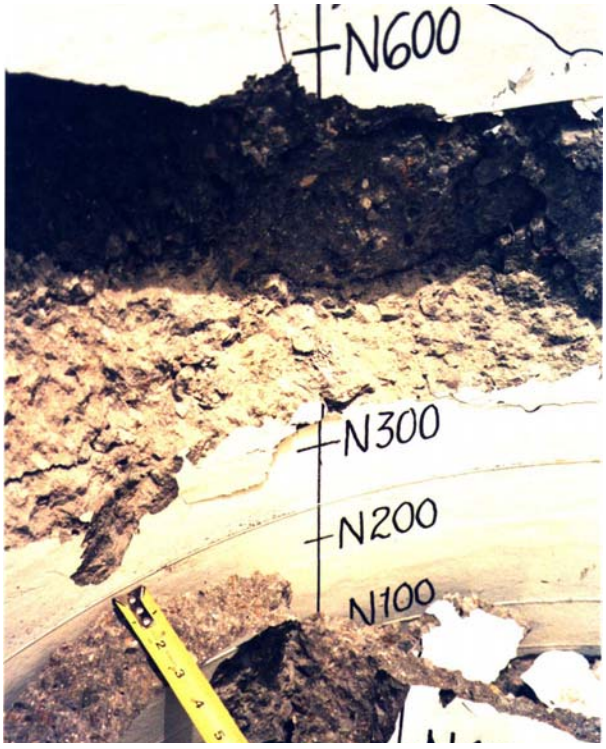

Fig. 3.11 Spalled-off Concrete Block with 75mm (3inch) Thickness

3.2 Hysteretic Response

The overall lateral force-displacement response is depicted in Fig. 3.12. It is obviously found that the hysteretic response exhibits pinched loop shape, as a consequence of the moderately high axial load. The experimental envelope of the hysteretic response exhibits a rounded shape or gradual stiffness degradation, but very stable response at each level of cycling up to $\mu_\Delta = 3$.

The lateral force reached nearly peak value at the ductility 2.0 and significantly dropped at the ductility 3.5 in push direction, corresponding to the lateral displacement of 104mm where the inside concrete was crushed on the north face. For the pull direction, deterioration of the lateral force was observed at the ductility of 3.3. Judging from test observations and experimental hysteretic response it is obvious that the failure of inside face concrete severely degraded the response. Ultimate ductility capacity can be determined as 3.3, with a safe design limit of 2.2, providing a 50% reserve of displacement capacity.

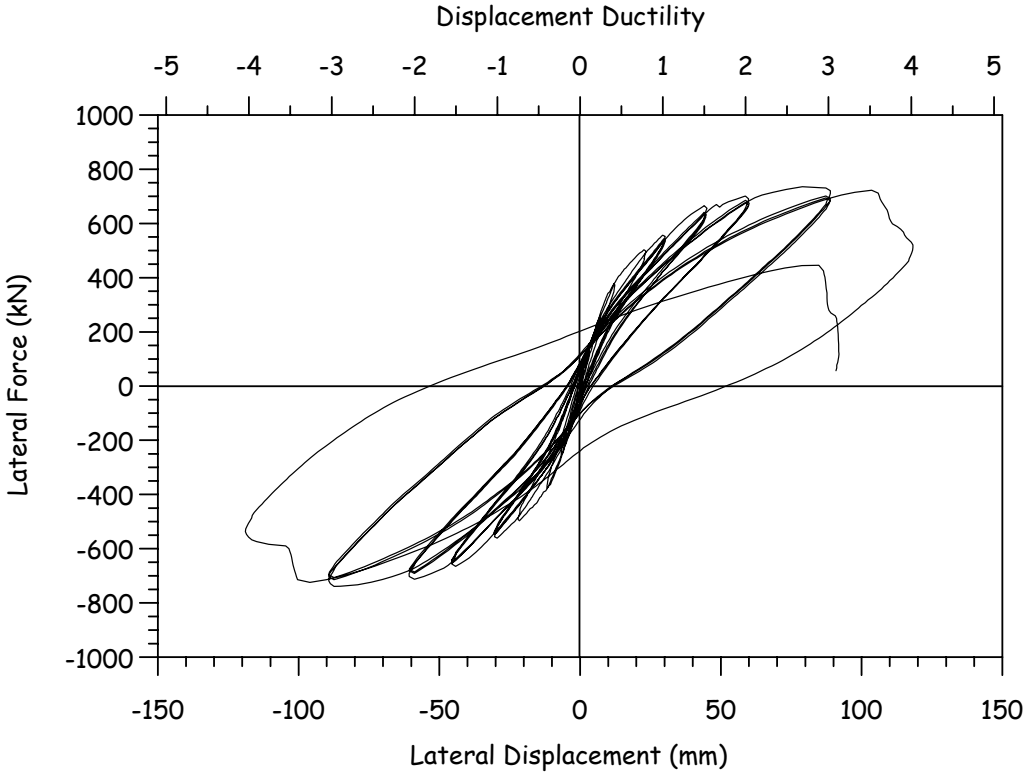

Fig. 3.12 Lateral Force-Displacement Hysteretic Response for Unit HF1

3.3 Curvature Profiles

Curvature profiles up the column height are plotted in Fig. 3.13 for six different stages of testing. Each curvature was calculated by the measured displacements of a pair of LVDTs placed on the north and south faces of the column. At each location, the curvature is reported at the center of the cell and is the average curvature over the cell height. It is noted that curvature at column bottom has been calculated taking into account strain penetration into the footing, by increasing the effective cell height by $\ell_{sp} = 0.022 f_y d_{b\ell}$, where f_y = yield stress (MPa) and $d_{b\ell}$ = longitudinal bar diameter.

The observed curvature at ideal yield (ductility=1.0) in the bottom cell was very similar to the theoretical yield curvature (=0.003 m^{-1}) based on a section analysis. The curvatures in the first and second cells from the bottom significantly increased with each increasing of ductility level as compared with those in the other cells, indicating that the inelastic deformation was largely concentrated over the first and second cells whose reference length in total is 540mm. The first major increase in curvatures was observed at ductility 3.0, where the onset of crushing of concrete was noted.

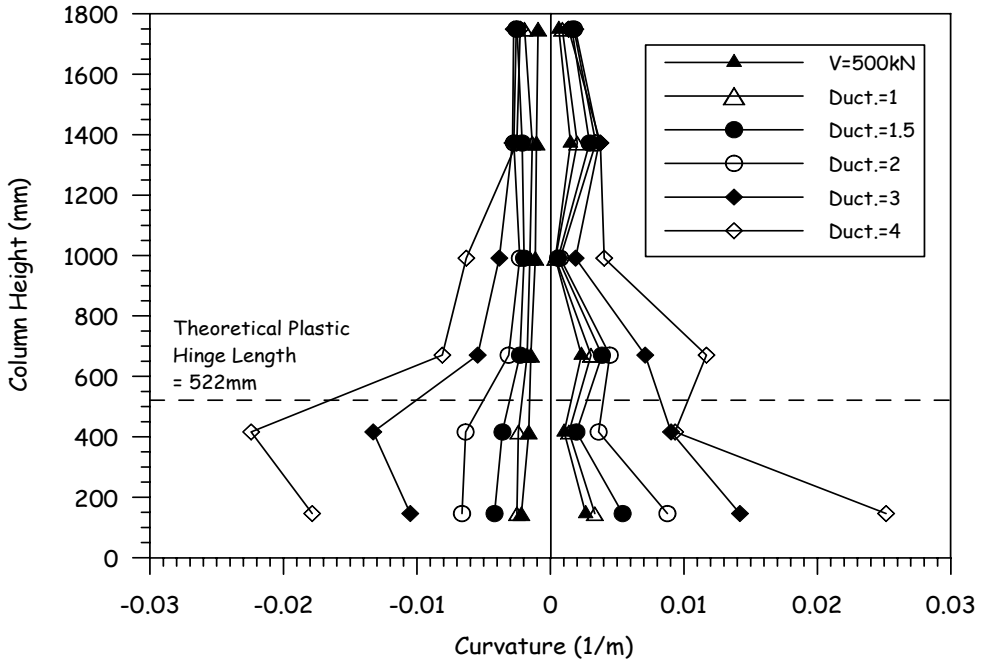

Fig. 3.13 Curvature Profiles

The position of the top of the theoretical plastic hinge length 0.08L=522mm [7] is noted in Fig. 3.13, where the rotation at the critical section resulting from strain penetration of the longitudinal reinforcement into the footing is excluded from the estimation of the theoretical plastic hinge length. As compared with the curvature profile, it can be said that the theoretical plastic hinge length given by a standard equation seems to be reasonable.

3.4 Longitudinal Strain Profiles

Longitudinal reinforcement strain profiles measured on north and south bars are plotted in Fig. 3.14. Due to the failure of some strain gauges during construction, some data points within the profiles have been omitted. The significant increase of strains occurred up to a height of approximately 1000mm between ductility 2.0 and 3.0. Strain penetration to a depth of more than 200mm into the footing was observed, which agrees well with a theoretical strain penetration depth of 0.022 f_y d_{bl} = 122mm [7]. Since curvatures are assumed constant over the theoretical strain penetration length, strain increases should occur over a length equal to approximately $2\ell_{sp}$.

Figs. 3.15 and 3.16 show plane-sectional longitudinal strain profiles at heights of 146mm and 419mm from the column base, respectively. The longitudinal strains were directly calculated from vertical LVDTs and strain gauges placed on vertical reinforcements at the cardinal points. Because the vertical LDVTs give average longitudinal strains over the reference length, the average of two of longitudinal reinforcement strains measured in the reference length were plotted. Up to a displacement ductility of 2.0, sections remained reasonably plane. The neutral axis depth at the ductility 2.0 is nearly 330mm, which is close to the theoretical position calculated by the moment-curvature analysis.

Although the section does not remain plane at the critical ductility levels of 3.5 in the push direction or 3.3 in the pull direction, the strain of inside face concrete at the plastic hinge region seems to be less than 5000 microstrains, indicating that the compressive strain at crushing on the inside face of the test unit is at most 5000 microstrains, averaged over the

experimental gauge length. Higher strains may, however, have occurred close to the base of the column. At high levels of ductility, strains indicated by strain gauges were less than those corresponding to the LVDTs. This is probably due to slip of reinforcing steel near the critical section with strain penetration into the base or up into the column.

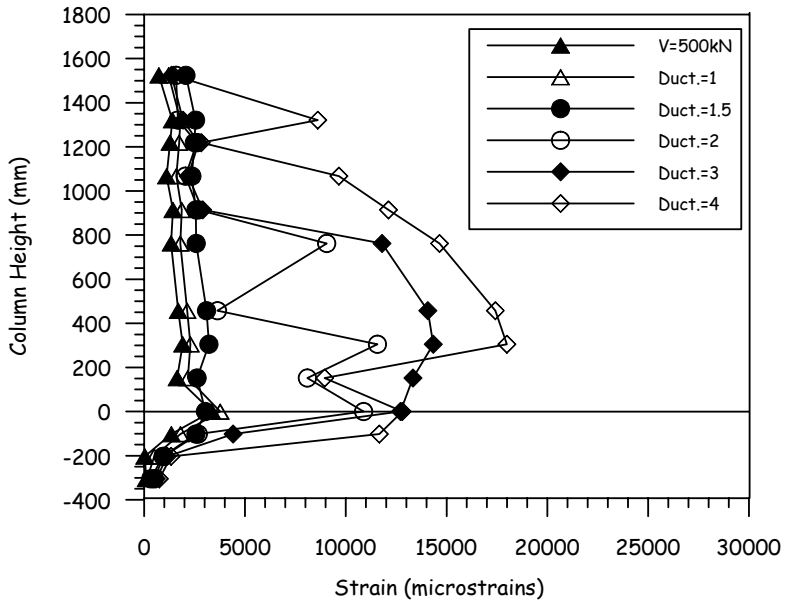

(a) North Bar

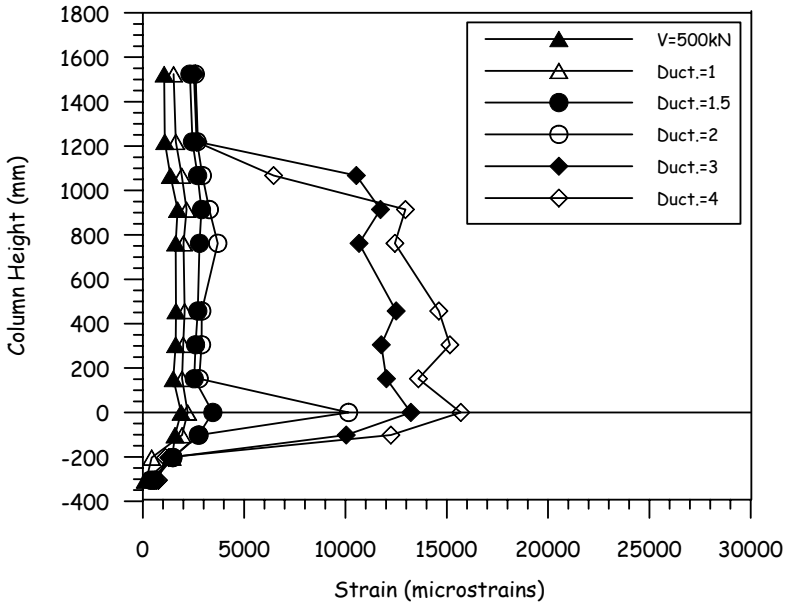

(b) South Bar

Fig. 3.14 Longitudinal Reinforcement Strain Profiles

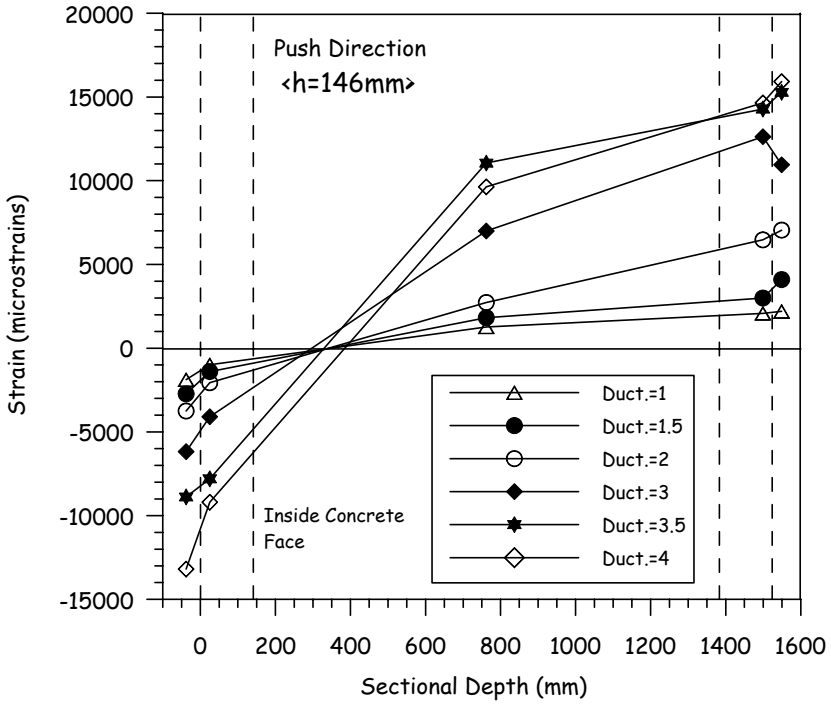

(a) Push Direction

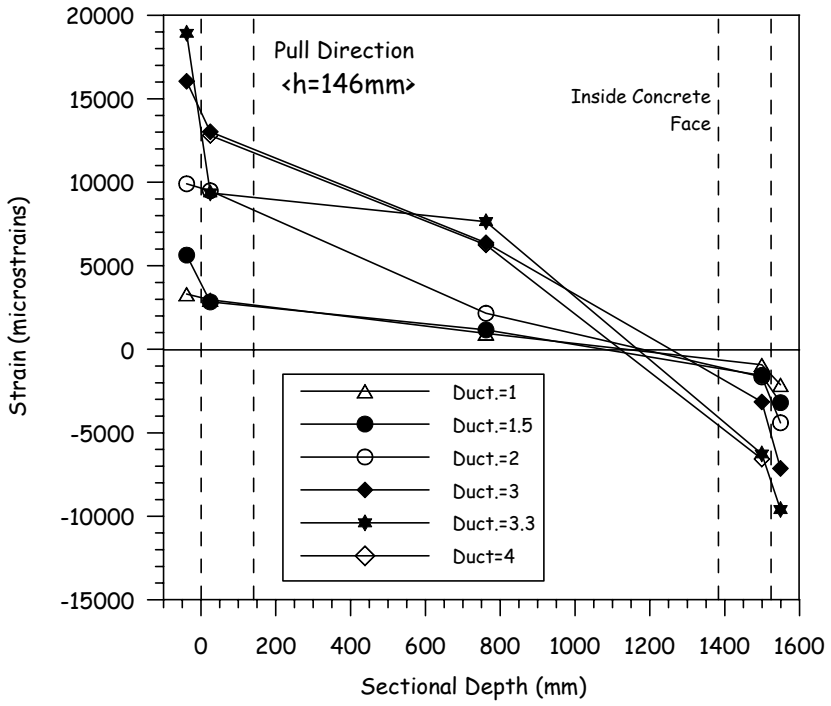

(b) Pull Direction

Fig. 3.15 Longitudinal Strain Profiles at Section of 146mm Height

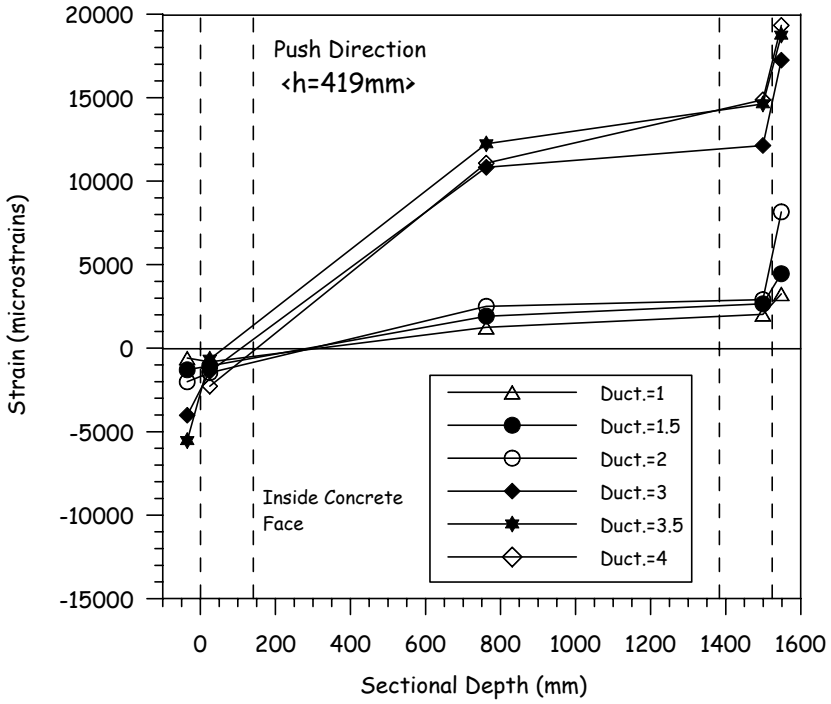

(a) Push Direction

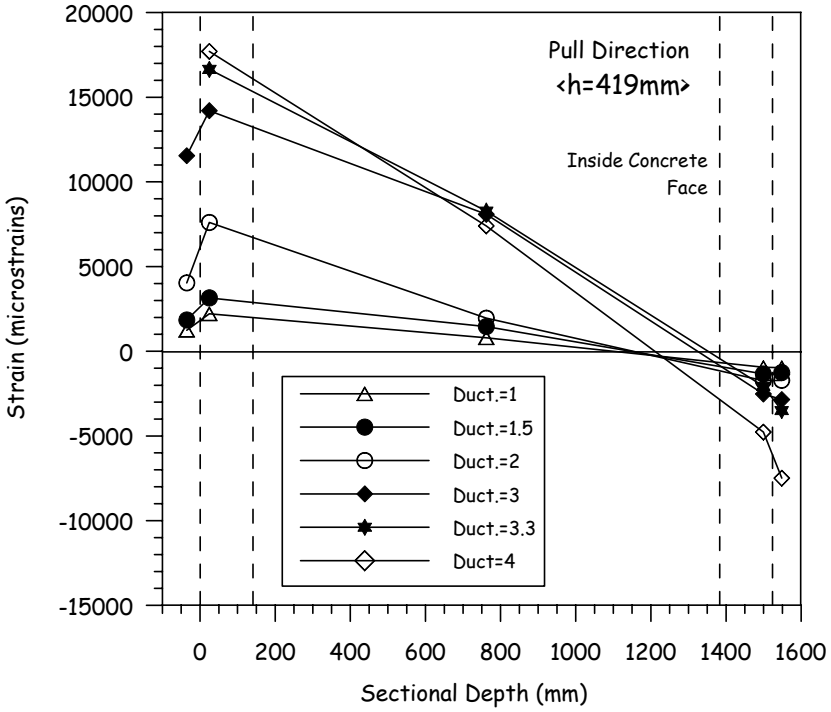

(b) Pull Direction

Fig. 3.16 Longitudinal Strain Profiles at Section of 419mm Height

3.5 Confinement-Induced Transverse Strain at Plastic Hinge Region

The strain profiles in the north and south gauges on the spiral at the maximum useful ductility of 3.5 and 3.3, respectively, are depicted in Fig. 3.17. Because the lateral force was applied in the north-south direction, the north or south face is in compression at the column bottom and confinement is provided by the spiral. Therefore, the strains measured on north gauges in the push direction and south gauges in pull direction were induced by only confinement. It should be noted that the confinement-induced strains at the plastic end region in a moment of spalling-off of the inside face concrete are at most 1780 microstrains that is nearly 50% of the yield strain of the spiral.

The theoretical plastic hinge length (522mm) described in Section 3.3 is compared with the strain profile in Fig. 3.17. It seems that the reasonable plastic hinge length is estimated by the standard equation proposed based on solid column test results.

Figs. 3.18 to 3.24 show the strain hysteresis responses of the spiral at the north face. The spiral strain at a level of 280mm height (where is nearly mid-height of the theoretical plastic hinge length) has reached about 1380 microstrains at the maximum useful ductility 3.5 and the spiral has yielded immediately after crushing of the inside face concrete. Similar strain behavior was also observed on the spiral at levels of 140mm, 420mm and 560mm height where the inside face concrete spalled off as proved in Fig. 3.10. Therefore, it can be said that the maximum effective lateral pressure that occurs when the spirals are stressed to their yield strength was not induced to the concrete shell in the plastic hinge region before failure, and that yield strain was only induced by the buckling of the longitudinal bars, other than by concrete confinement. At the sections of 700mm and 840mm height, the strain responses showed almost elastic behavior and indicated peak strains (approximately 1000 microstrains) in a moment of crushing of the inside face concrete. A dramatic increase in strain after concrete failure was not noted at these sections since the longitudinal bars buckled up to 550mm height from the column base as shown in Fig. 3.8.

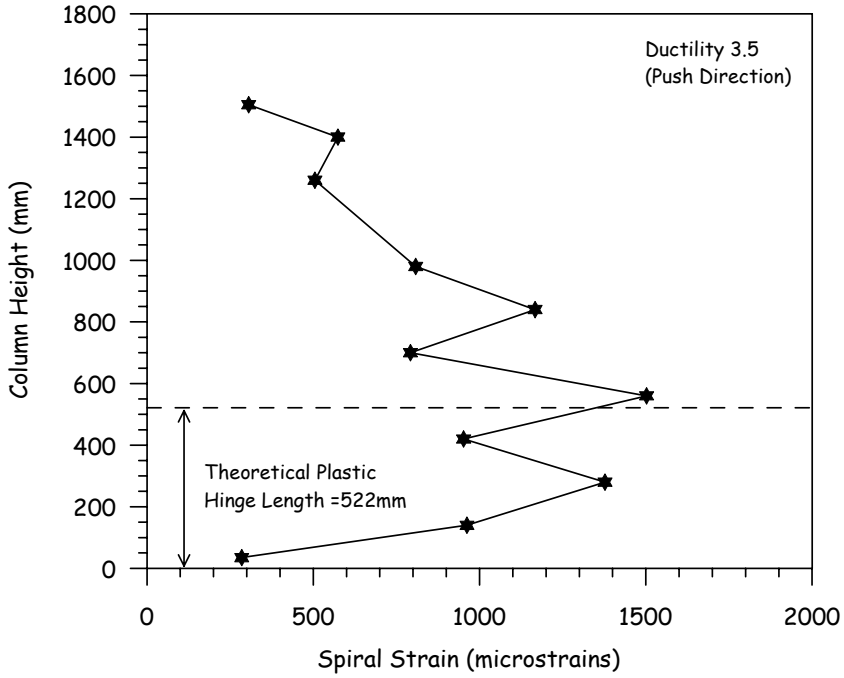

(a) North Face

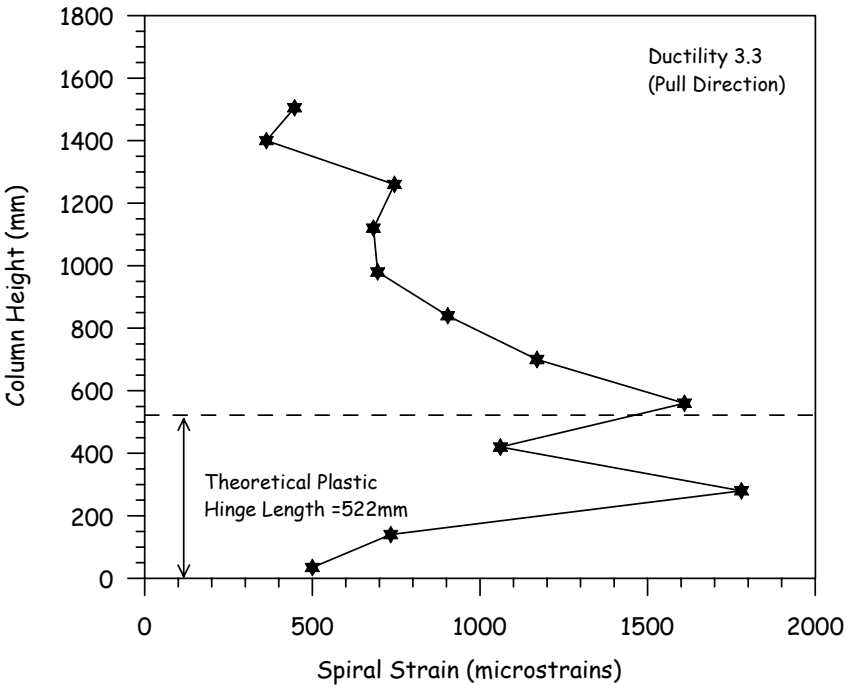

(b) South Face

Fig. 3.17 Spiral Strain Profiles

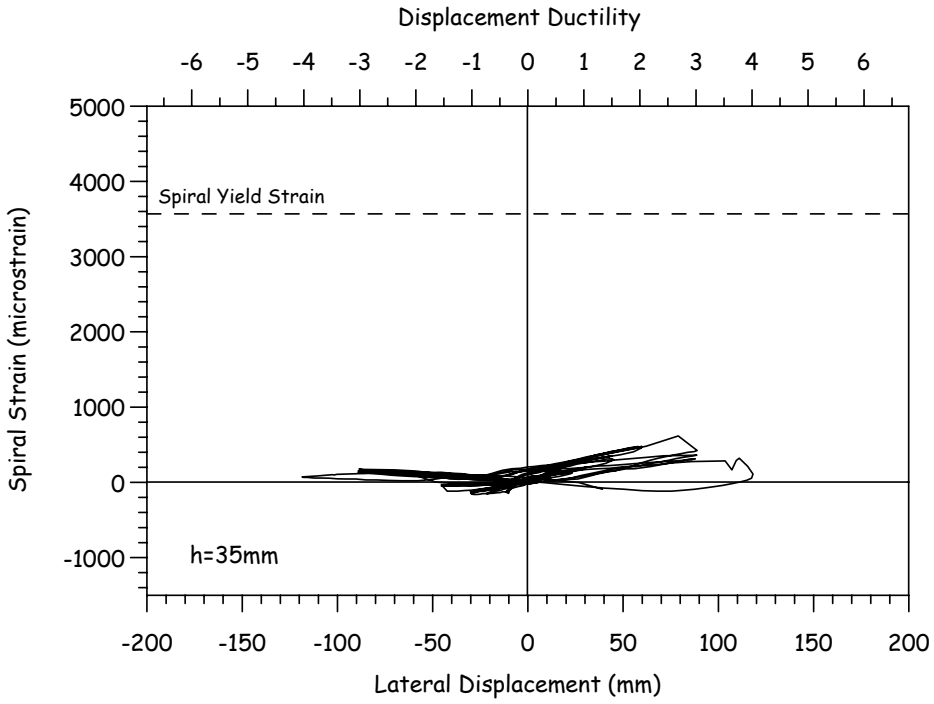

Fig. 3.18 Strain Hysteresis: 35mm Height

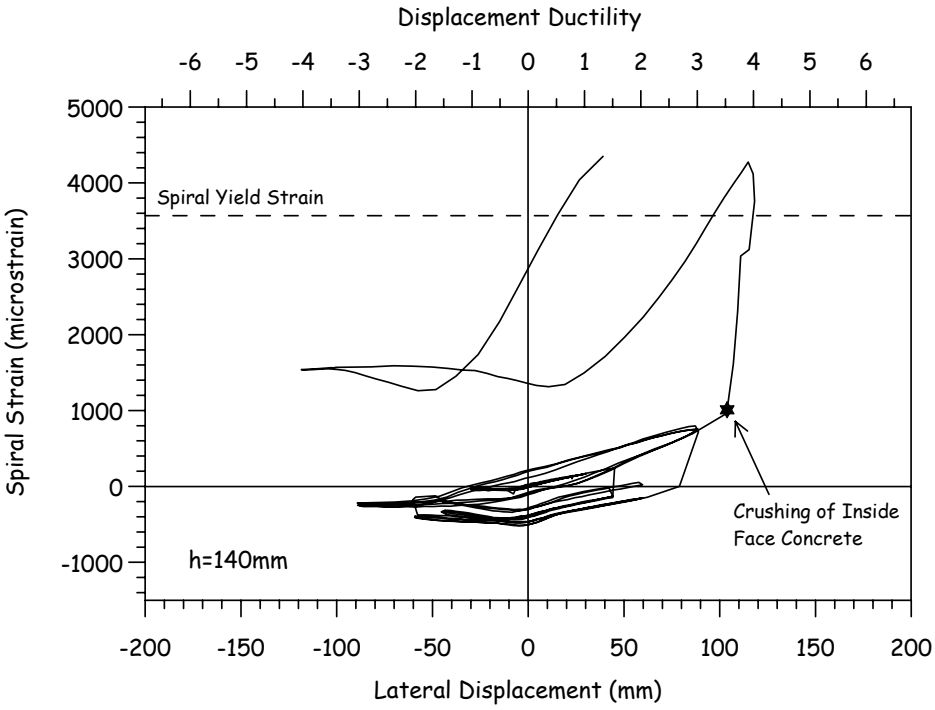

Fig. 3.19 Strain Hysteresis: 140mm Height

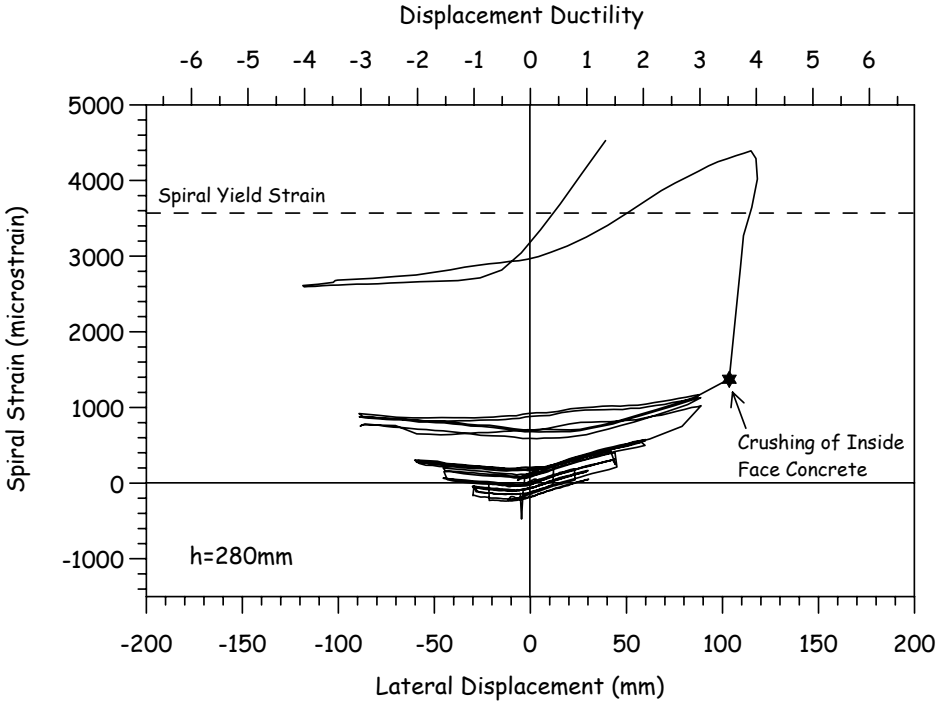

Fig. 3.20 Strain Hysteresis: 280mm Height

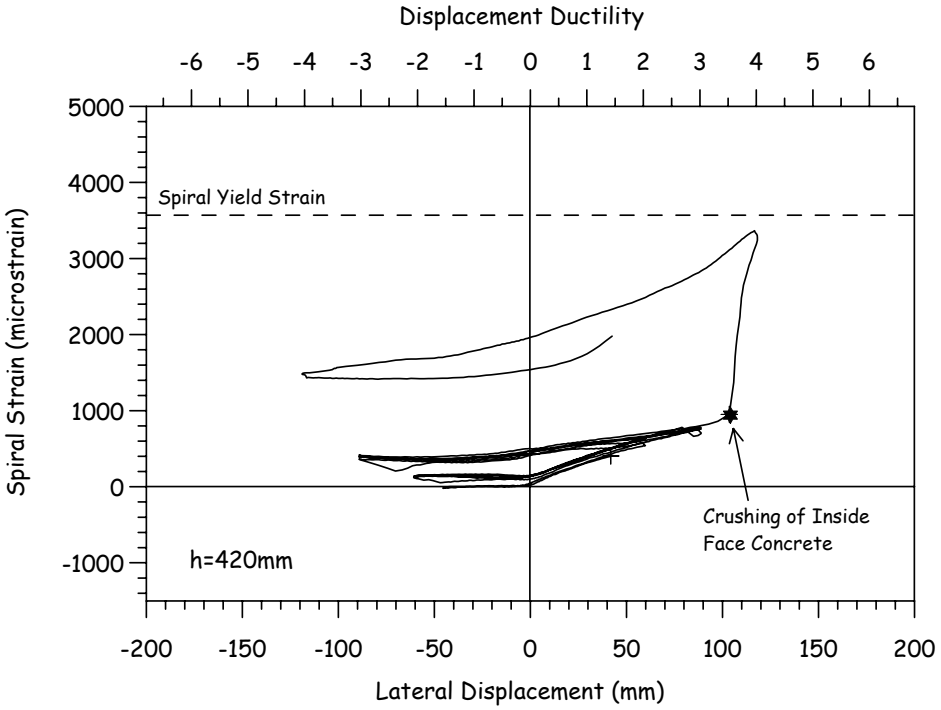

Fig. 3.21 Strain Hysteresis: 420mm Height

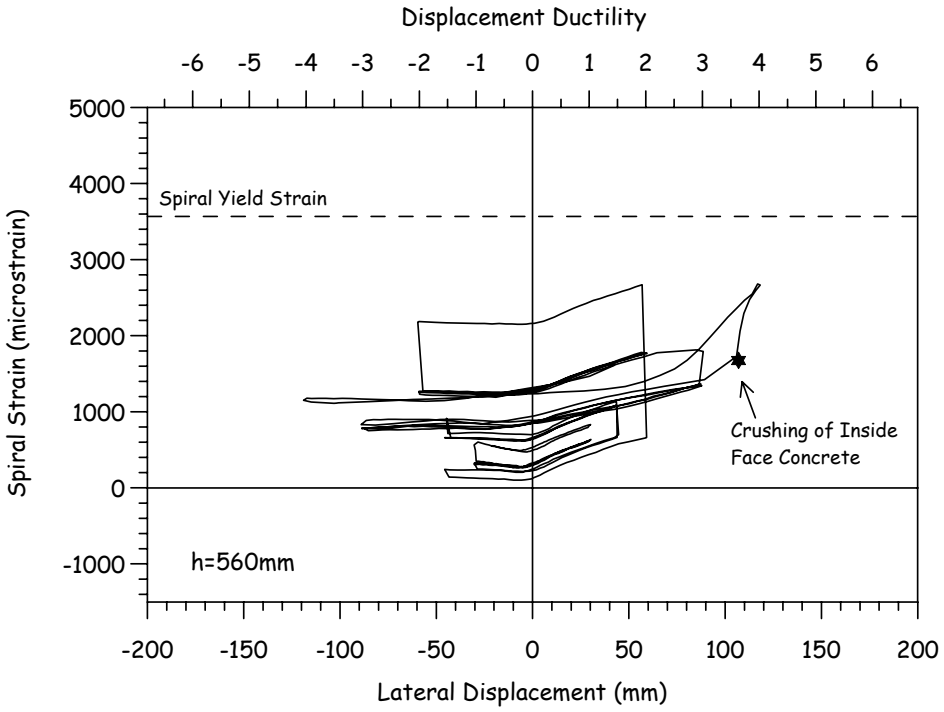

Fig. 3.22 Strain Hysteresis: 560mm Height

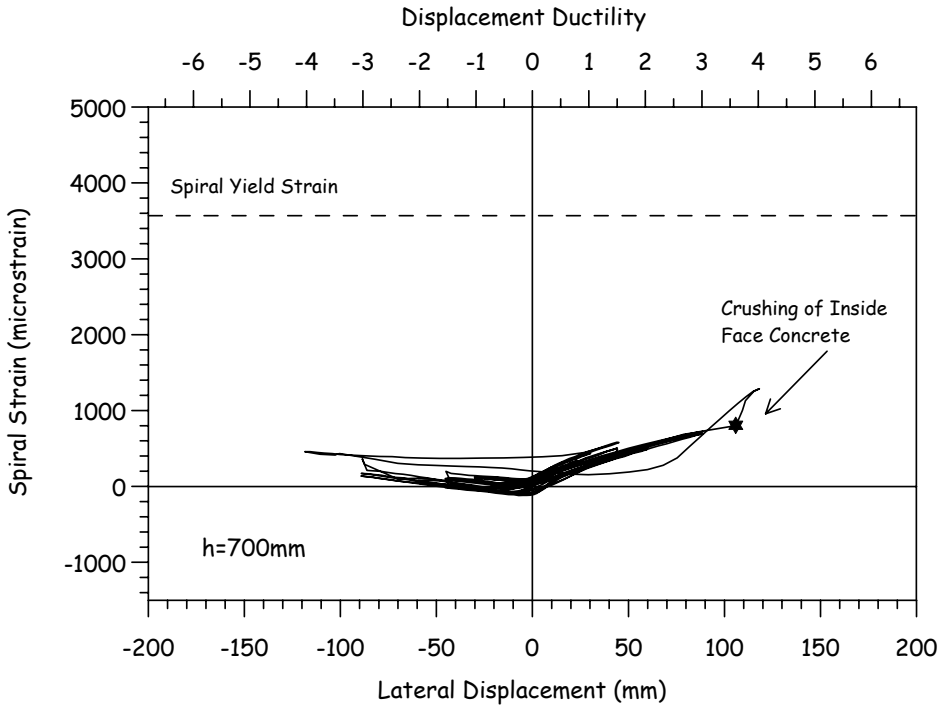

Fig. 3.23 Strain Hysteresis: 700mm Height

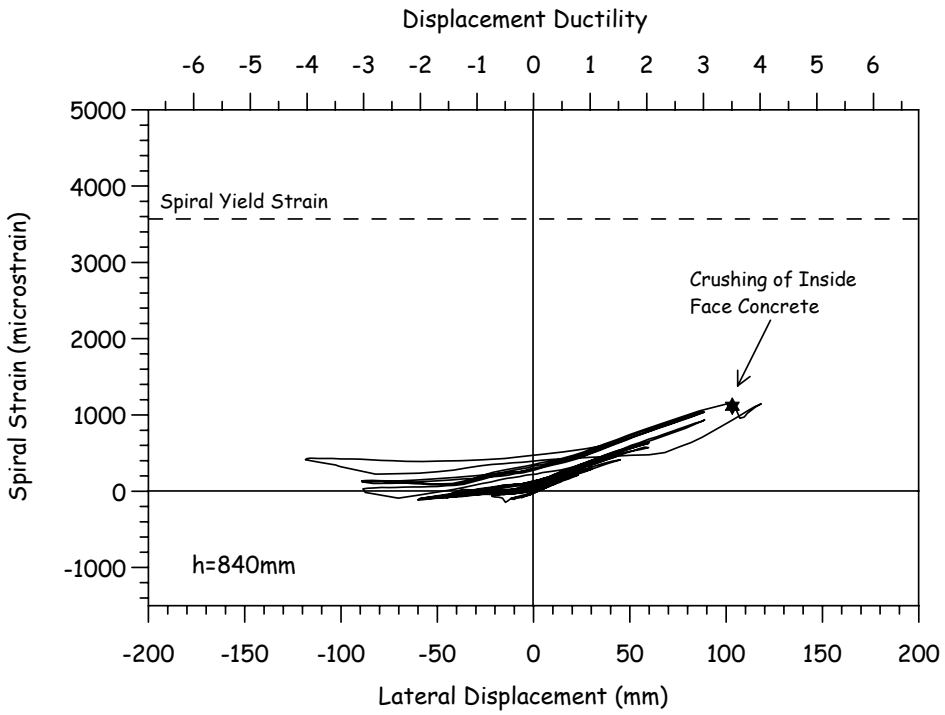

Fig. 3.24 Strain Hysteresis: 840mm Height

3.6 Transverse Strain Profiles in Sections

Transverse steel strain profiles in the plastic end sections at the maximum useful ductility level are shown in Figs. 3.25 to 3.30, where some strain data are not plotted due to failure of gauges before testing. Shear-induced strains measured on east and west faces are around 1500 microstrains up to the height of 1505mm from the column base, indicating that the transverse steel activates for shear resistance evenly in the plastic end region. On the other hand, the confinement-induced strains are between 1000 and 1500 microstrains up to the section of 420mm height and a decrease in the strains is found at the sections of above 700mm height. This result may suggest that the plastic hinge length would be estimated to be between 420mm and 700mm, which, interestingly, agrees with the theoretical plastic hinge length of 522mm, as described in Section 3.3.

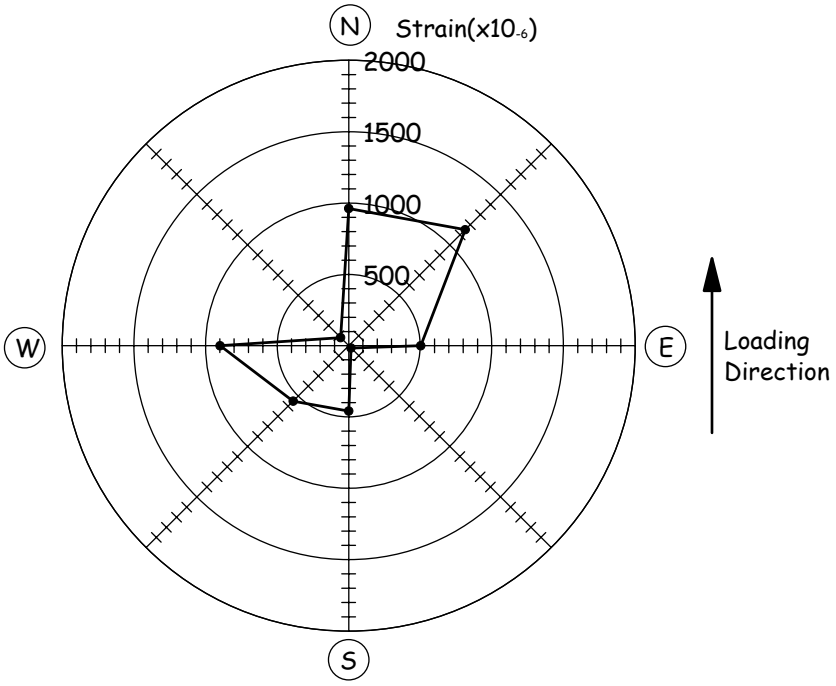

(a) Push Direction

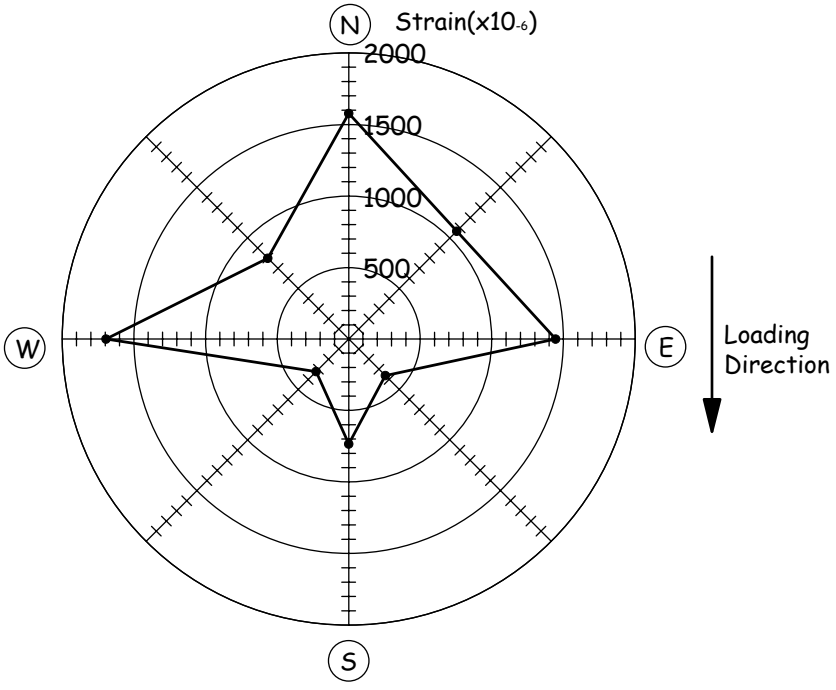

(b) Pull Direction

Fig. 3.25 Lateral Strain Profiles at Section of 140mm Height

$(\mu_{\Delta} = 3.5, -3.3)$

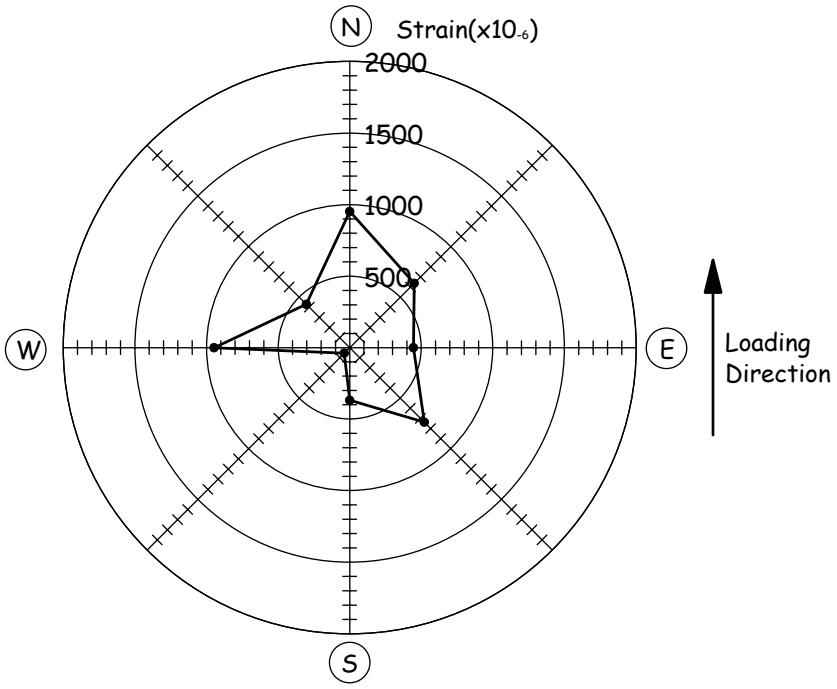

(a) Push Direction

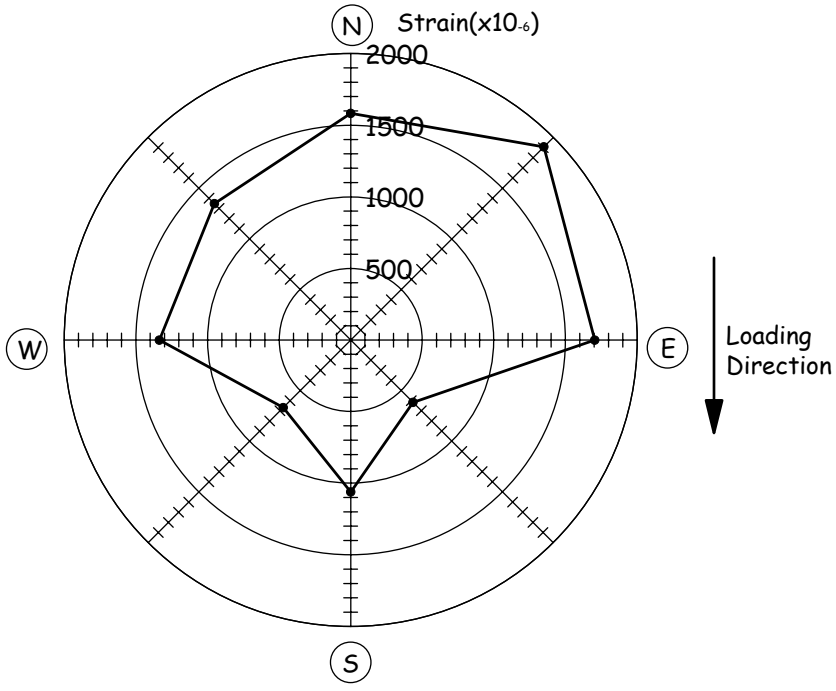

(b) Pull Direction

Fig. 3.26 Lateral Strain Profiles at Section of 420mm Height

$(\mu_{\Delta} = 3.5, -3.3)$

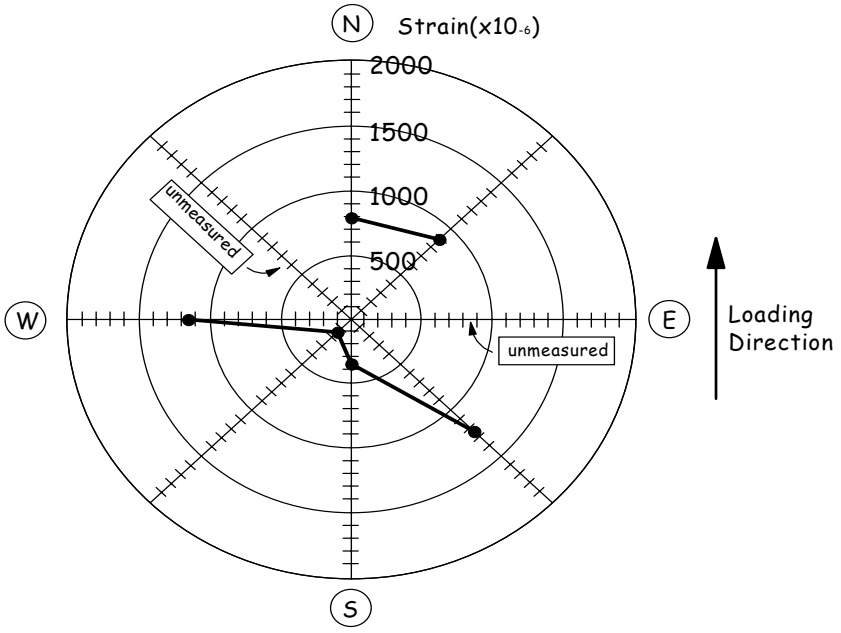

(a) Push Direction

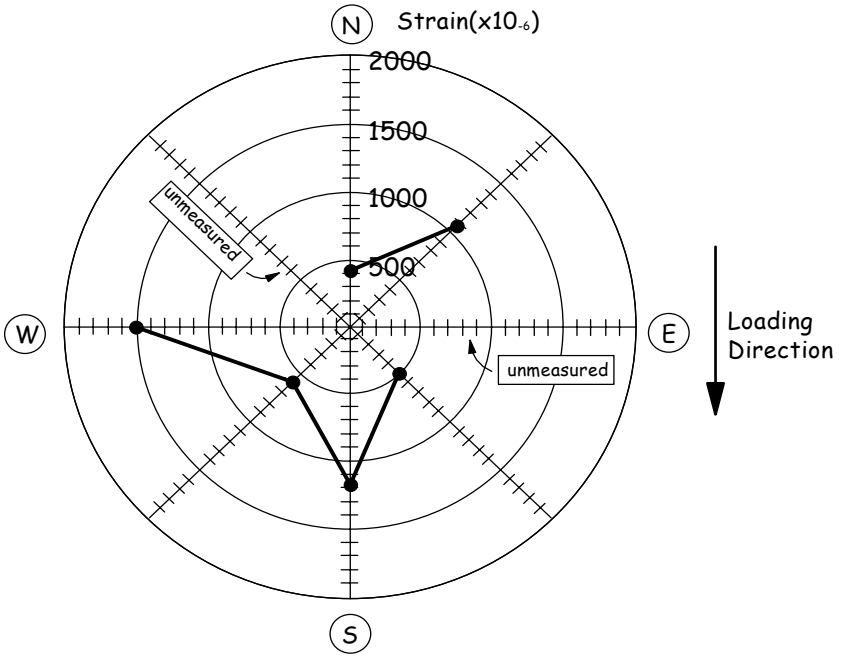

(b) Pull Direction

Fig. 3.27 Lateral Strain Profiles at Section of 700mm Height

$(\mu_{\Delta} = 3.5, -3.3)$

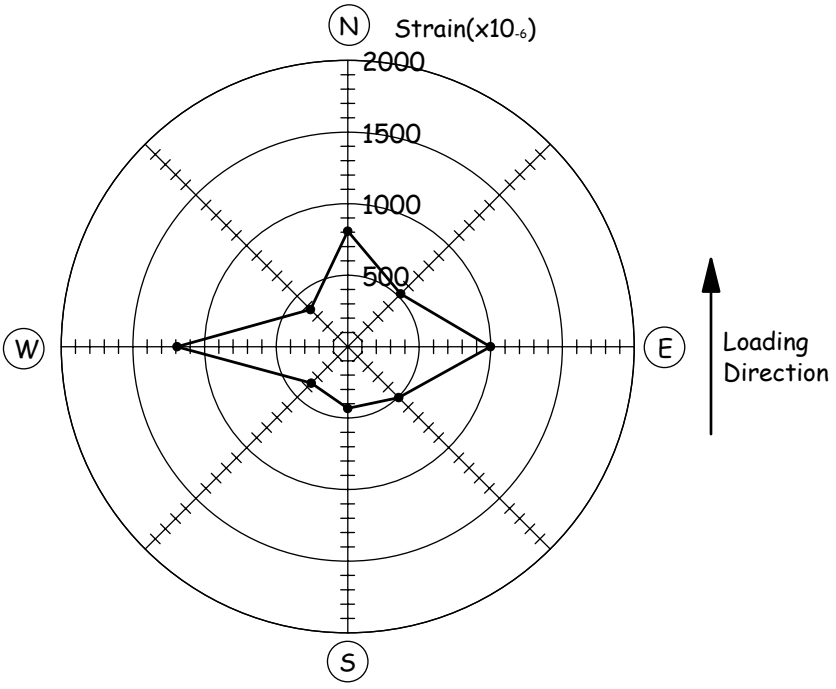

(a) Push Direction

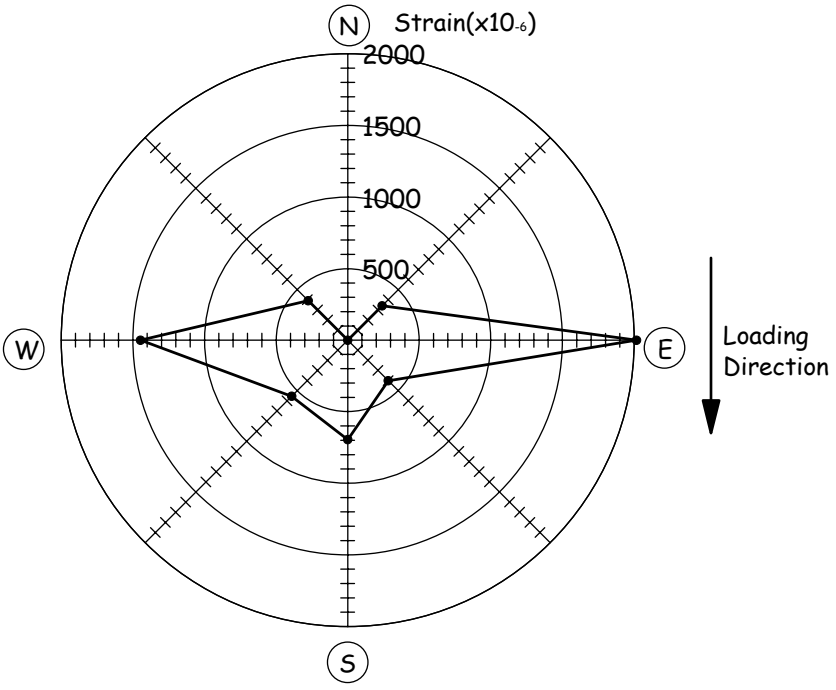

(b) Pull Direction

Fig. 3.28 Lateral Strain Profiles at Section of 980mm Height

$(\mu_{\Delta} = 3.5, -3.3)$

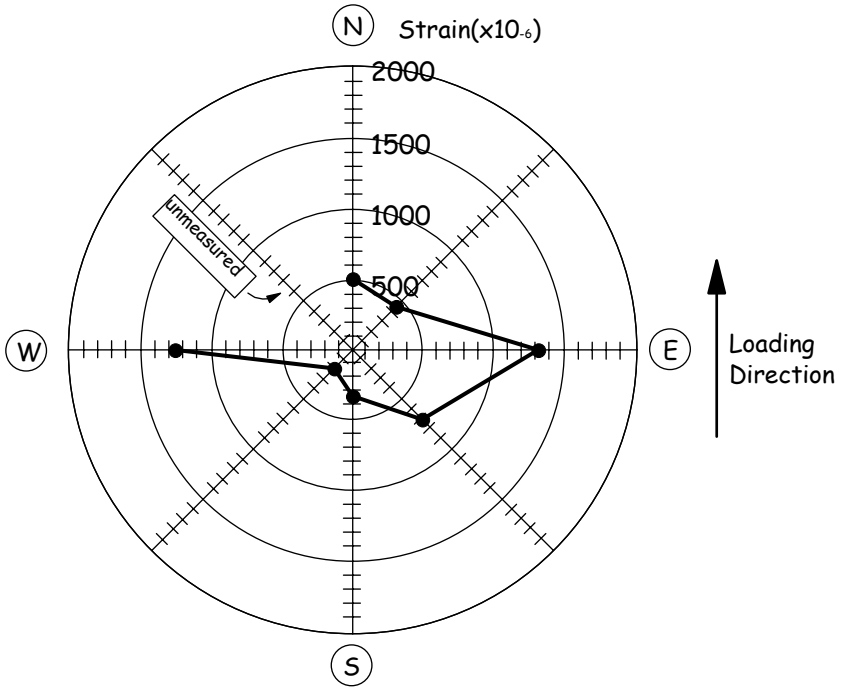

(a) Push Direction

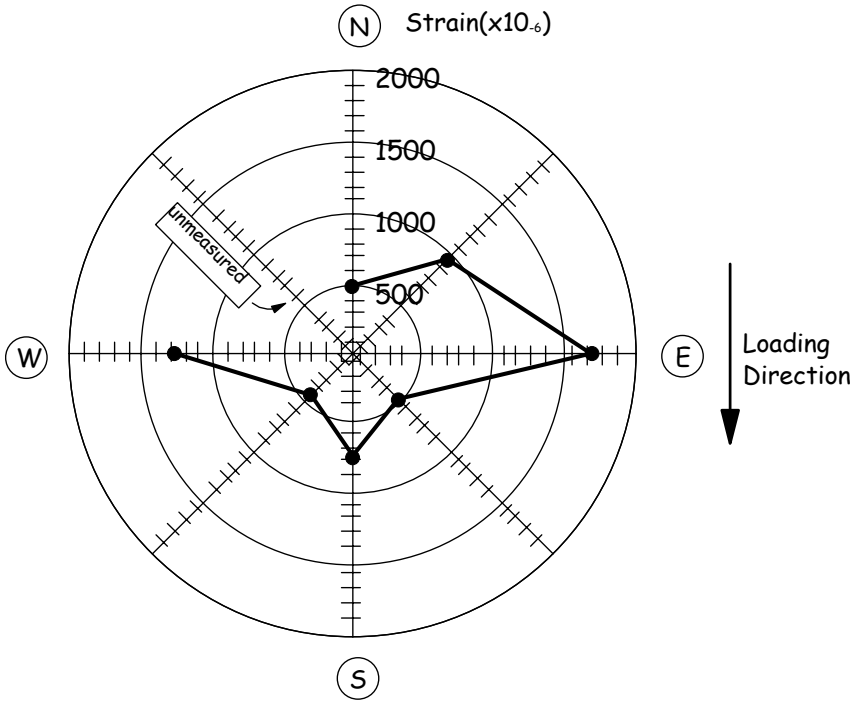

(b) Pull Direction

Fig. 3.29 Lateral Strain Profiles at Section of 1260mm Height

$(\mu_{\Delta} = 3.5, -3.3)$

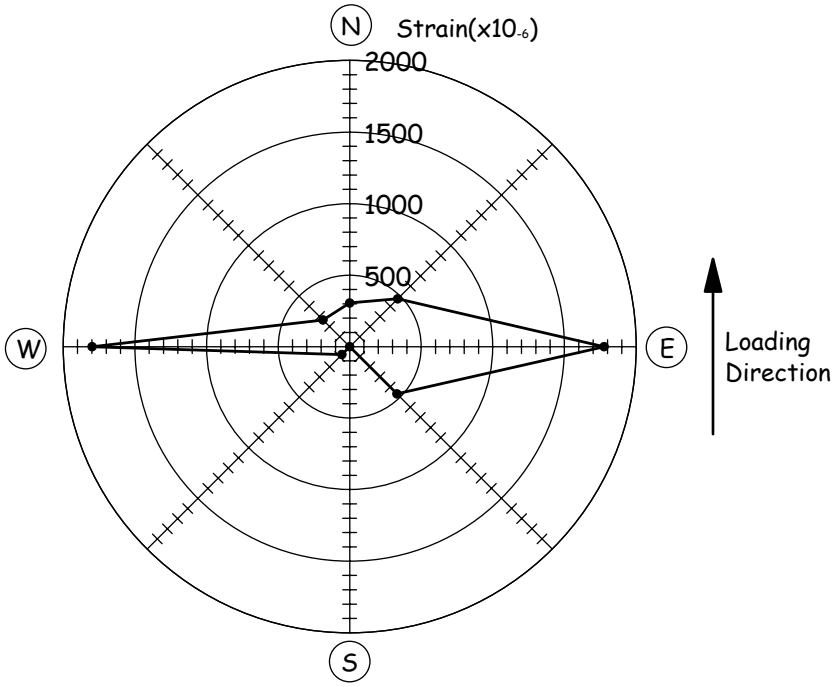

(a) Push Direction

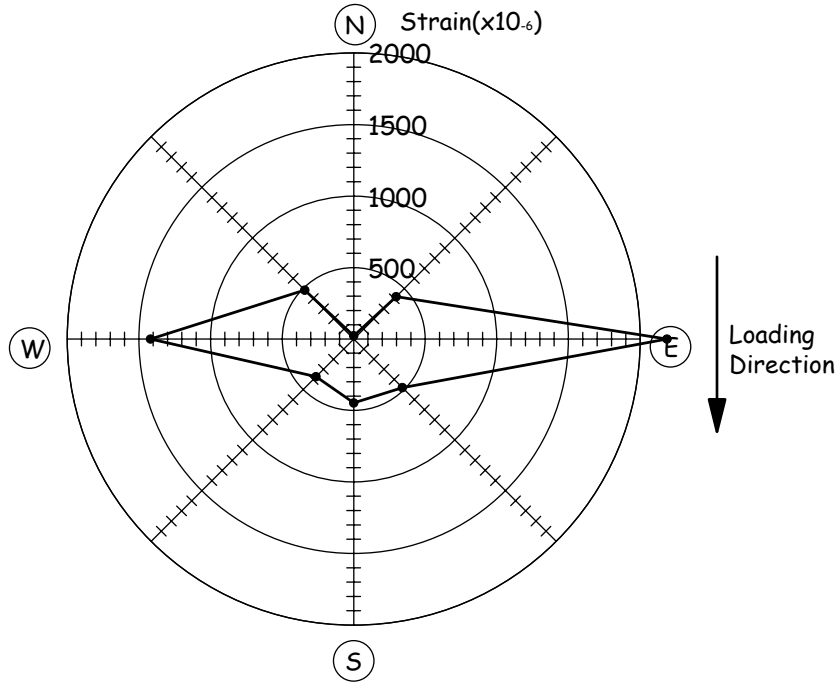

(b) Pull Direction

Fig. 3.30 Lateral Strain Profiles at Section of 1505mm Height

$(\mu_{\Delta} = 3.5, -3.3)$

CHAPTER 4

4 EXPERIMENTAL RESULTS OF TEST UNIT HF2

4.1 Test Observations

General observations made during the test can be summarized as follows. It is noted that the cracks developed on the inside face concrete could not be monitored due to the feeble light unfortunately, however, the major events (crushing of concrete) were recognized through the video camera placed inside.

1) Force control cycles up to 630kN (3/4 of first yield)

The first visible flexural cracks formed at 420kN loading over the bottom 1300mm. At a loading to 630kN, a number of new horizontal cracks were observed up to a height of 2600mm. The cracks widened to less than 0.1mm. The cracks were well-distributed with an average spacing of 70-100mm. Some horizontal cracks extended onto shear faces and inclined about 30 degree.

2) First Yield (840kN)

The horizontal cracks were noted through the whole column height as shown in Fig. 4.1(a). New steep shear cracks (45-55 degree) were developed on east and west faces as depicted in Fig. 4.1(b). The crack width reached at most 0.1mm.

3) Ductility 1.0

Fig. 4.2 shows the horizontal cracks on the north face and shear cracks developed on the east face at the ductility of 1.0. Some vertical splitting cracks were seen at this level. The maximum horizontal crack width was 0.35mm and the biggest shear crack also widened to 0.35mm.

4) Ductility 1.5

The onset of crushing of cover concrete was noted at the column base as proved in Fig. 4.3. No significant damage was observed on inside face concrete through the video camera. On

the first return cycle, minor spalling of the cover concrete was seen locally at the hollow column top section where the loading steel tube was attached through the base plate. This might be caused by the uneven force transmission to the concrete wall. However, the lateral force did not degrade significantly due to this event.

5) Ductility 2.0

In the first push cycle to ductility 2.0, the inside face concrete on the north face was crushed over a height of 500mm from the base as shown in Fig. 4.4 and the lateral force significantly dropped at the displacement of 94.7mm, corresponding to the ductility 1.8. On the other hand, although the onset of minor crushing was recognized on the outside face concrete, no longitudinal reinforcement buckled and no core concrete spalled off to outside at this level. The test observations obviously show that the column failure occurred due to the crushing of the inside face concrete.

Since the axial load would crush the concrete wall at the plastic hinge immediately after crushing of the inside face concrete and the column would be unstable due to the significant loss of the concrete section, the hydraulic pressure for the axial load was shut down after the first push cycle to the ductility 2.0.

After testing and dismounting the loading steel tube, the damage developed inside was observed. Fig. 4.5 shows a panoramic view of the inside damage. The inside face concrete spalled off at the section between 300mm and 600mm height from column base. It should be noted that the inside failure was developed at the similar section to the test unit of HF1.

(a) Horizontal Cracks (North Face)

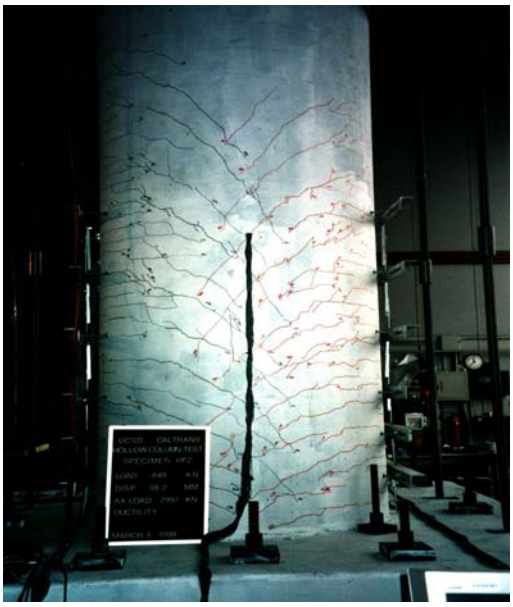

(b) Diagonal Cracks (East Face)

Fig. 4.1 Crack Pattern at First Yield

(a) Horizontal Cracks (North Face)

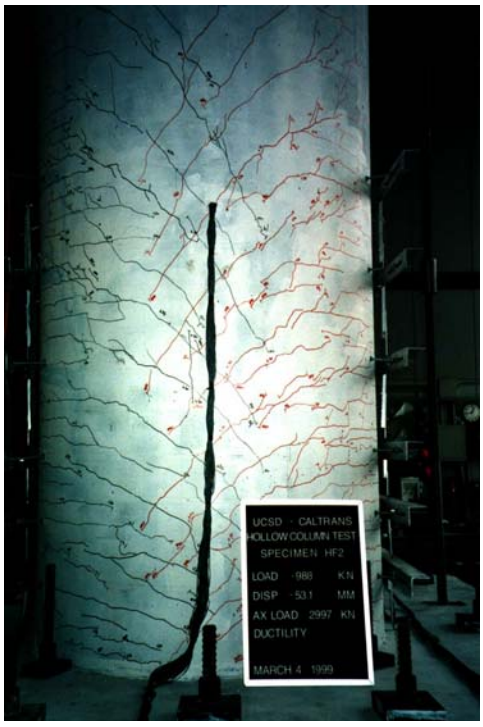

(b) Diagonal Cracks (East Face)

Fig. 4.2 Crack Pattern at Ductility 1.0

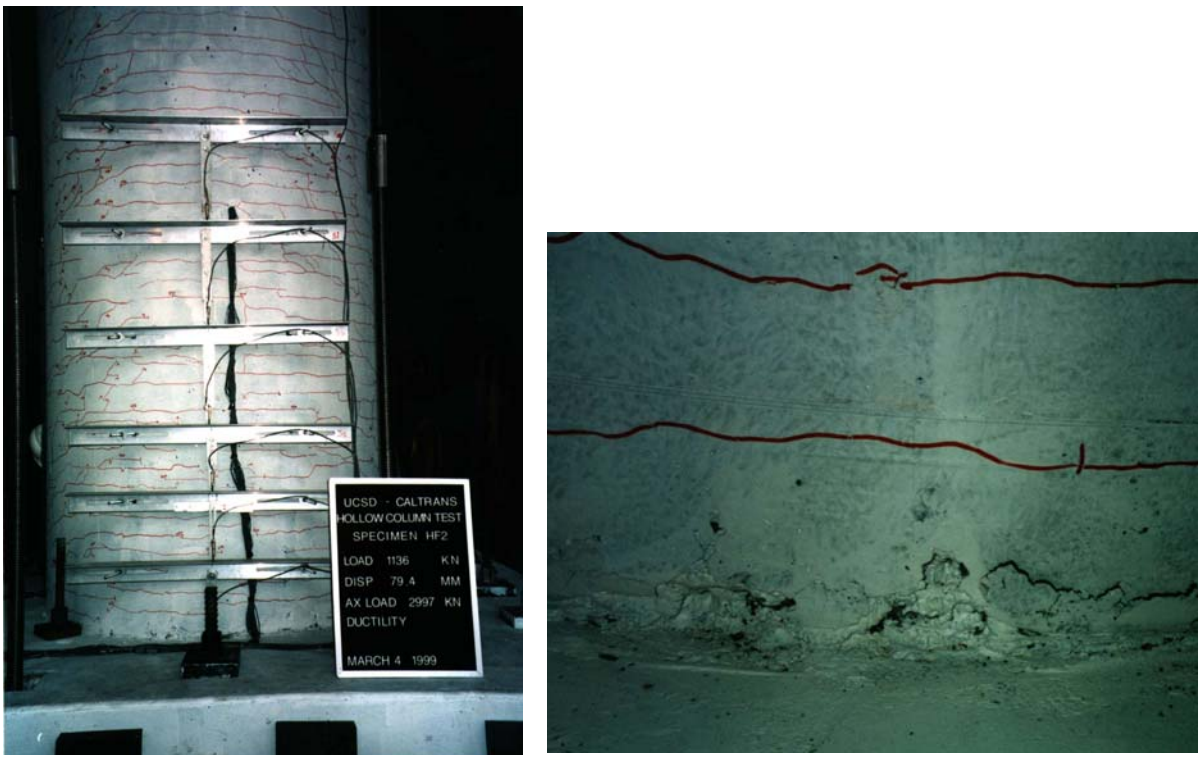

(a) Damage of North Face Concrete (b) Close-up

Fig. 4.3 Onset of Crushing of Cover Concrete at Ductility 1.5

(a) Damage of North Face Concrete (b) Close-up

Fig. 4.4 Failure of Column Base at Ductility 2.0

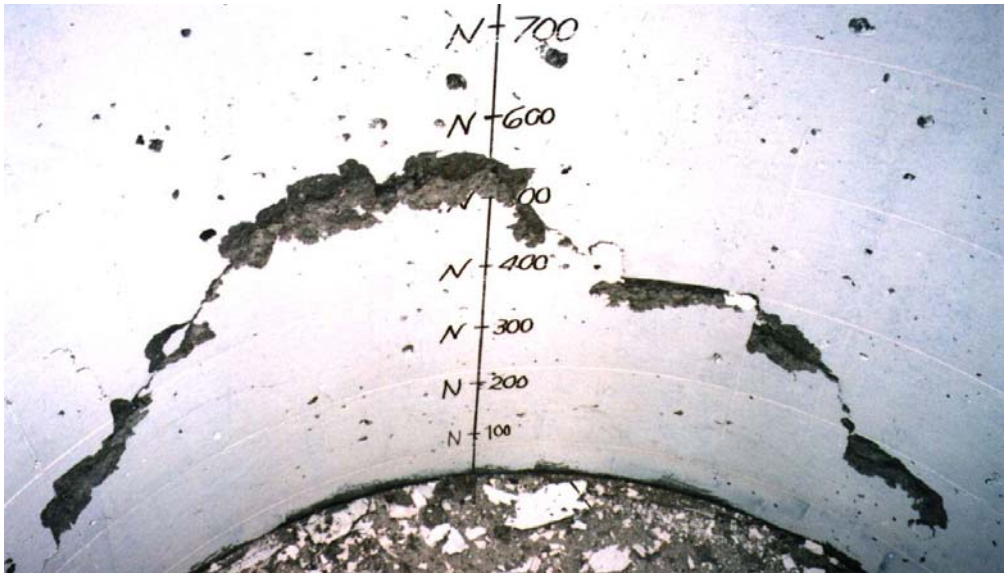

Fig. 4.5 Panoramic View of Inside Face Concrete after Testing (E-N-W)

4.2 Hysteretic Response

The lateral force-displacement hysteretic response of the test unit is shown in Fig. 4.6. It is obviously found that the hysteretic response exhibits a non-ductile behavior as expected and significant degradation was noted at the ductility 2.0, when the inside face concrete was crushed even though the outside face concrete was not damaged seriously. Therefore, it can be said that the failure of the inside face concrete was the key factor causing deterioration of the flexural ductility capacity. Since crushing initiated at a displacement ductility of 1.8, a safe design ductility limit of $\mu_\Delta = 1.2$ can be assessed, ensuring a 50% excess displacement margin. Note that HF2 was about 50% stronger than HF1, and that though the displacement ductility capacity of HF2 was only about 50% of that of HF1, the maximum displacement at onset of inside cover spalling, at 94mm was almost identical to HF1. The reduced ductility capacity of HF2 is thus due primarily to the increased yield displacement.

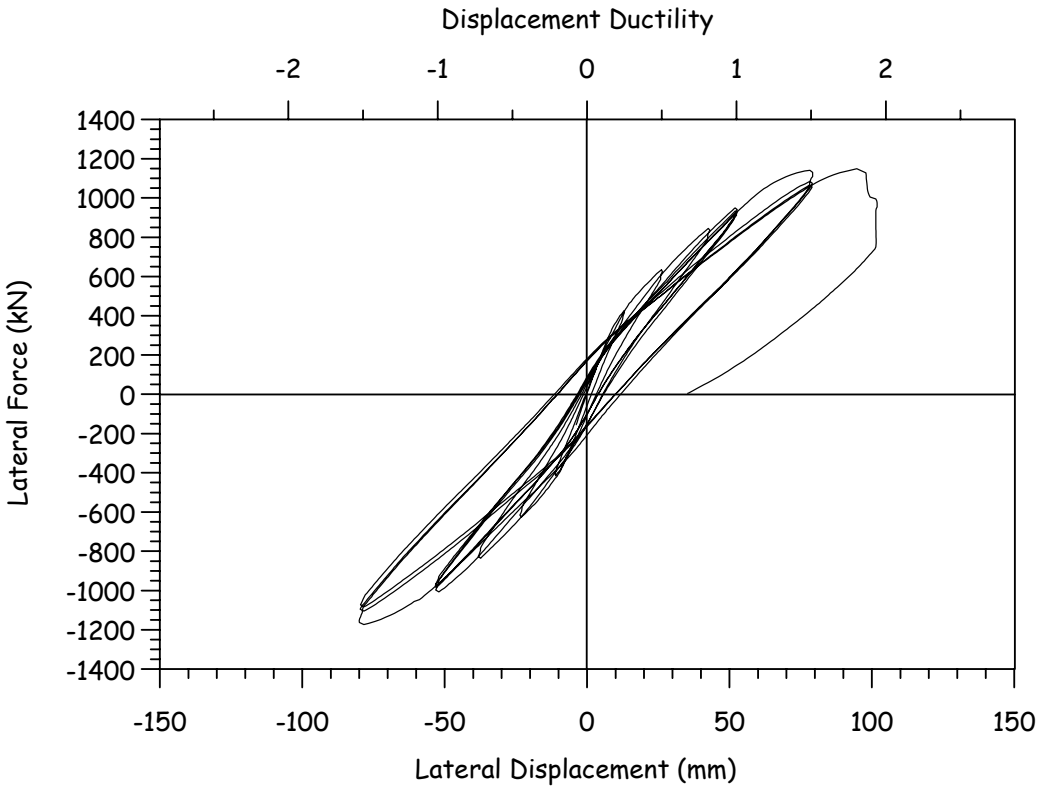

Fig. 4.6 Lateral Force-Displacement Hysteretic Response for Unit HF2

4.3 Curvature Profiles

Figure 4.7 shows curvature profiles up the column height for different stages of testing. Each curvature was calculated by the measured displacements of a pair of LVDT's placed on the north and south faces of the column. In each section, the curvature is reported at the center of the cell and is the average curvature over the cell height. It is noted that the measured curvature at column bottom has included the strain penetration of the longitudinal reinforcement into the footing.

The anticipated plastic hinge length based on 0.08L=522mm, where L is the column height and the rotation at the critical section resulting from strain penetration of the longitudinal reinforcement into the footing is excluded, is also noted in Fig. 4.7. The observed curvature at

the maximum useful ductility of 1.8 in the bottom cell reached nearly 0.016 1/m which was not far from the ultimate curvature measured in the test unit of HF1, while it could be seen that the plastic hinge region is shorter than the anticipated plastic hinge length, as a consequence of the low ductility capacity.

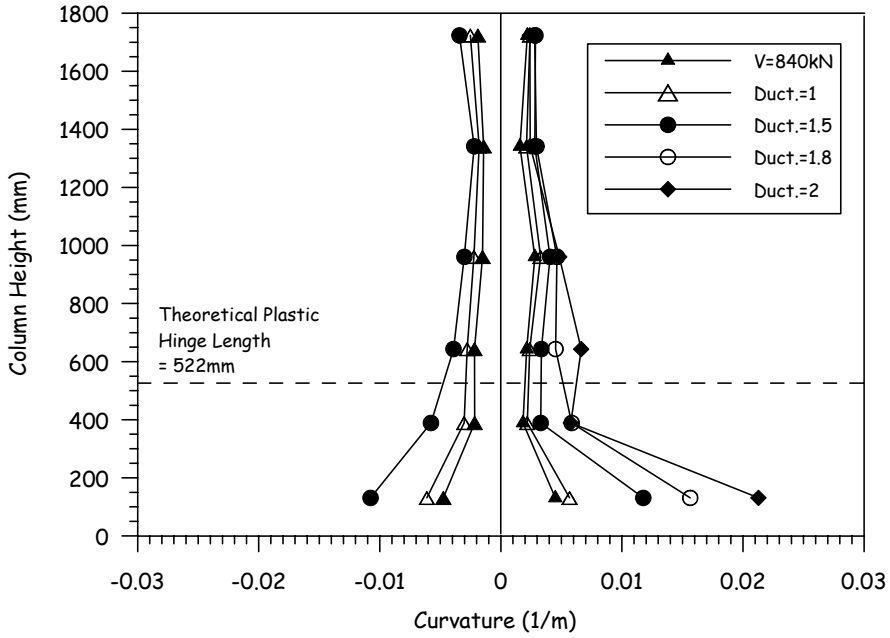

Fig. 4.7 Curvature Profiles

4.4 Longitudinal Strain Profiles

Figure 4.8 shows longitudinal reinforcement strain profiles measured along the extreme tension bars of the column in the plastic hinge region. Some data points were skipped due to the failure of some strain gauges during construction. The significant increase of strains and spread of plasticity occurred up to a height of approximately 900mm from the base at the ductility of 1.0 to 1.5. The strain profiles also show strain penetration to into the footing. Yield strain levels for the tension reinforcement were observed to a depth of 100mm to 200mm from the footing line, and strain penetration extended to about 400mm.

The sectional longitudinal strain profiles at heights of 146mm and 419mm from the column base are depicted in Fig. 4.9 and 4.10, respectively, where the longitudinal strains were directly calculated from vertical LVDT's and strain gauges placed on some column bars. Because the vertical LDVT's give average longitudinal strains over the reference length, the average of some of longitudinal reinforcement strains measured in the reference length were plotted. It could be seen that the plain section remained reasonably plain up to a displacement ductility of 2.0. The neutral axis depth is between 400mm and 500mm up to the ductility 1.8, which agrees well with the theoretical position calculated by the moment-curvature analysis, and was larger than for HF1.

It is interesting in Fig. 4.9(a) that the compressive strain of near inside face concrete at the ductility 1.8 is close to 5000 microstrains, indicating that the inside face concrete was crushed when the compressive strain reached about 5000 microstrains at the column base. As described in previous chapter, test results of the HF1 also showed that the inside face concrete spalled off at the compressive strain of 5000 microstrains. Although the compressive strain of the inside face concrete at crushing depends upon the wall thickness ratio and an amount of longitudinal steel, it could be suggested that the inside face longitudinal compression strain of 0.005 represents an ultimate limit state for curvature ductility of the circular hollow section with the wall thickness ratio (t/D) of around 0.1 and a sufficient amount of transverse steel. For design purposes, a value of 0.0035 could be safely adopted.

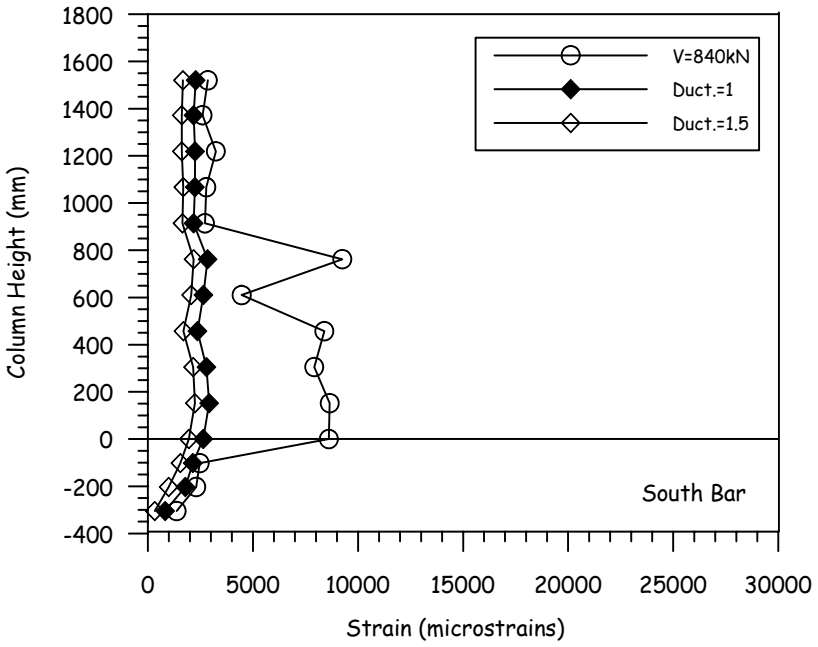

(a) North Bar

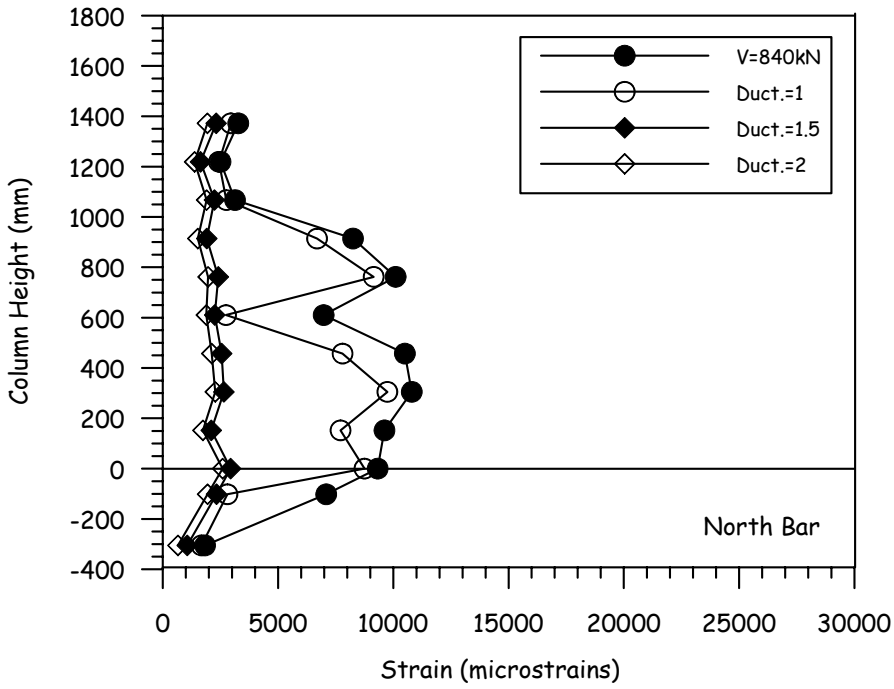

(b) South Bar

Fig. 4.8 Longitudinal Reinforcement Strain Profiles

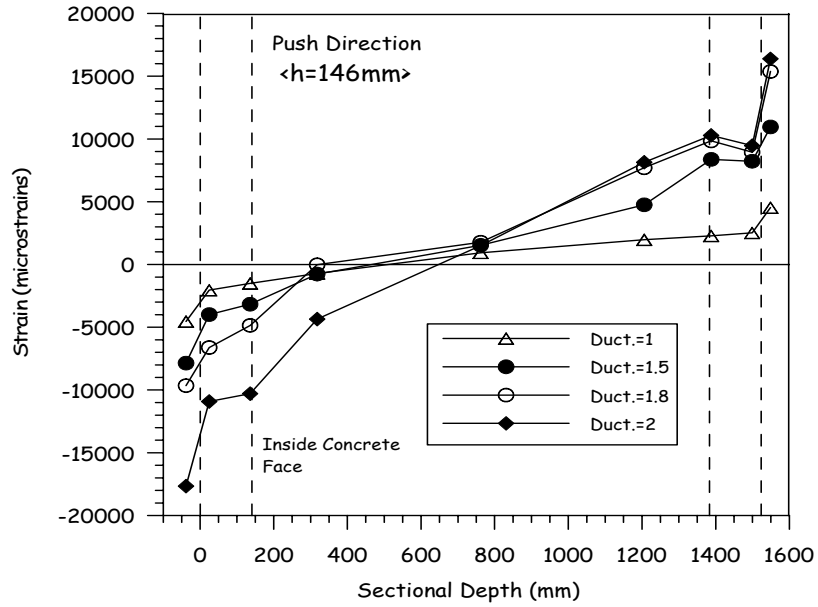

(a) Push Direction

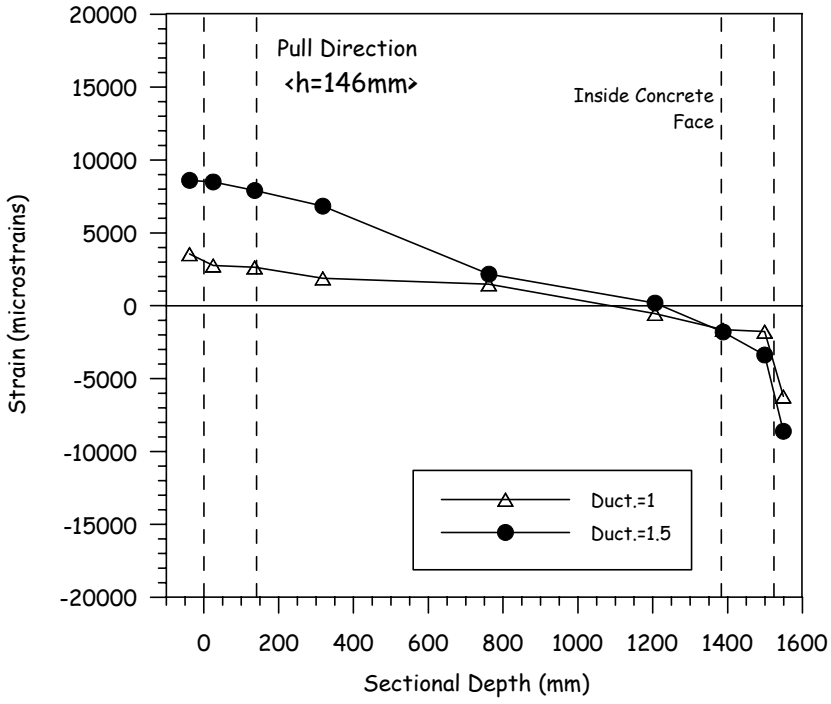

(b) Pull Direction

Fig. 4.9 Longitudinal Strain Profiles at Section of 146mm Height

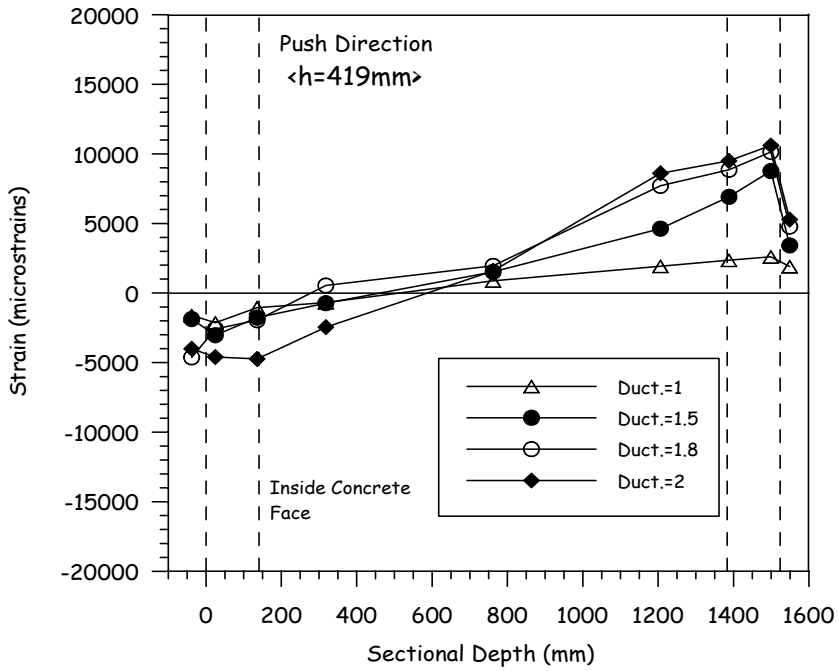

(a) Push Direction

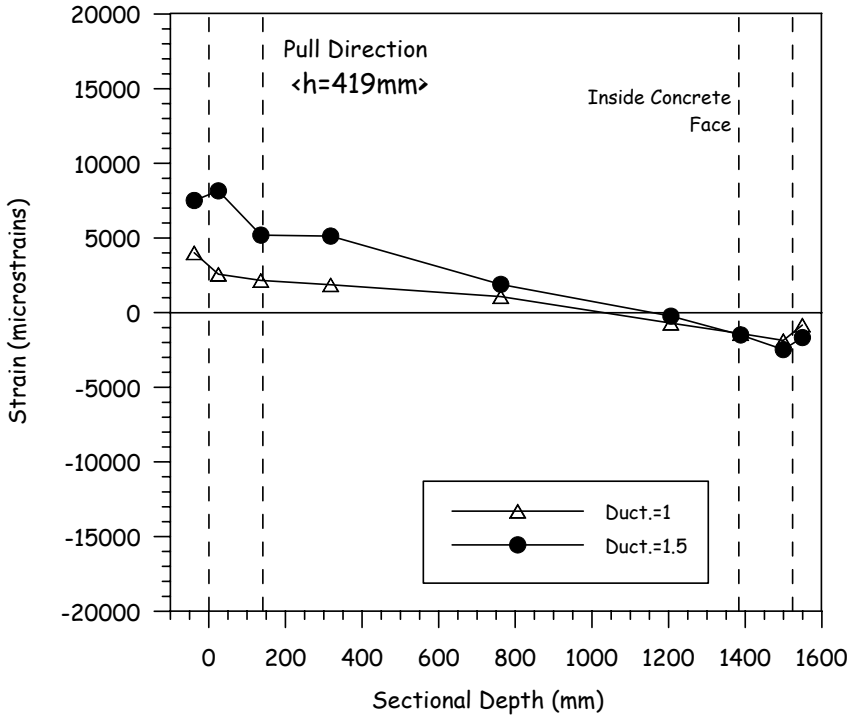

(b) Pull Direction

Fig. 4.10 Longitudinal Strain Profiles at Section of 419mm Height

4.5 Confinement-Induced Transverse Strain at Plastic Hinge Region

The confinement-induced strain profile measured on the north longitudinal bar at the maximum useful ductility of 1.8 is depicted in Fig. 4.11. In the anticipated plastic hinge region (up to 0.08L=522mm), the higher confinement-induced strain was observed in the lower section. It should be noted that the average confinement-induced strain over the anticipated plastic hinge region seems to be nearly 1000 microstrains that is about 30% of the yield strain of the transverse steel.

Fig. 4.12 to 4.18 show the transverse strain hysteresis responses of the north gauges in the plastic hinge region. At a level of 280mm height from the base, the transverse strain has reached 1315 microstrains at the ductility 1.8 and significantly increased immediately after crushing of inside face concrete. Such strain behavior is similar to the previous test unit HF1. It should be noted that the dramatic increase in the transverse steel strain must be induced by the inside surface concrete crushing. Therefore, the full effective lateral pressure that may occur when the spirals are stressed to their yield strength was not induced in the concrete shell before failure of the inside face concrete. Based on the test results from the units of both HF1 and HF2, the strain of 0.001 would represent the effective confinement-induced strain in the hollow section.

On the other hand, the significant increase in the transverse strain after crushing of the inside face concrete was not observed at the sections of 700mm and 840mm height, since the failure of the inside face concrete developed up to the height of 600mm from the footing line.

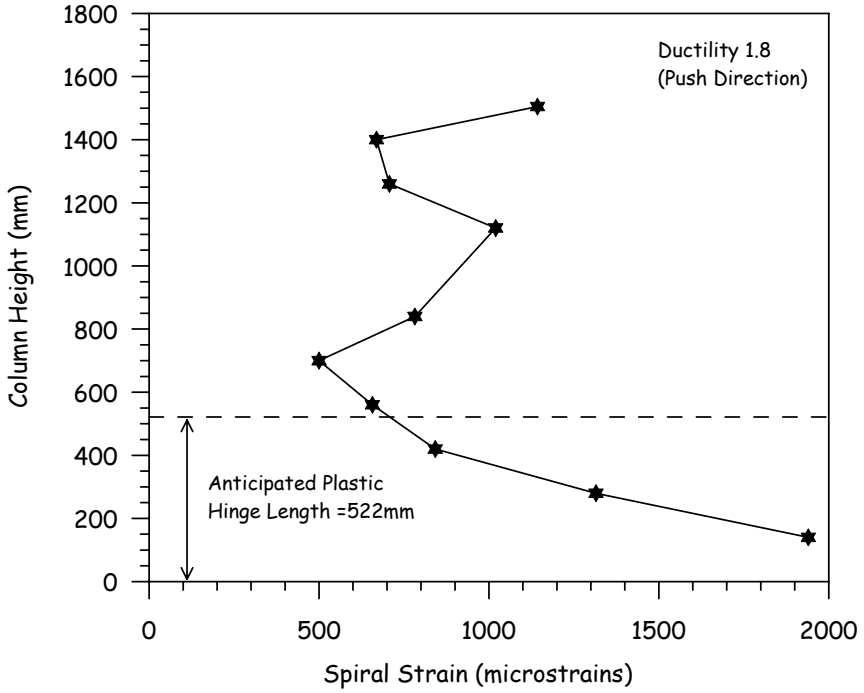

Fig. 4.11 Spiral Strain Profiles (North Face)

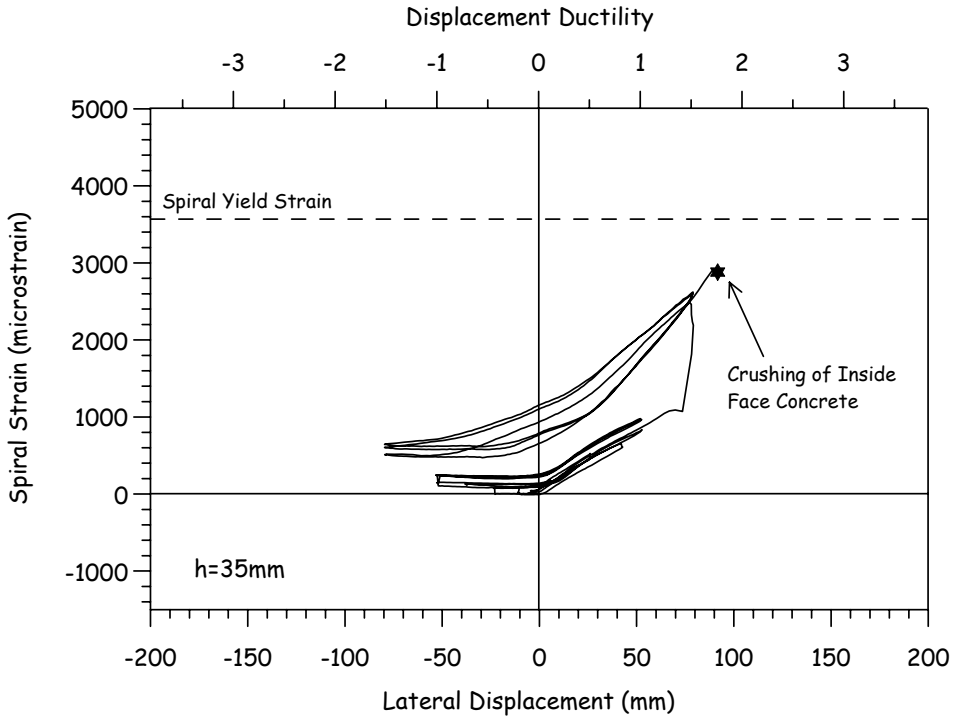

Fig. 4.12. Strain Hysteresis: 35mm Height

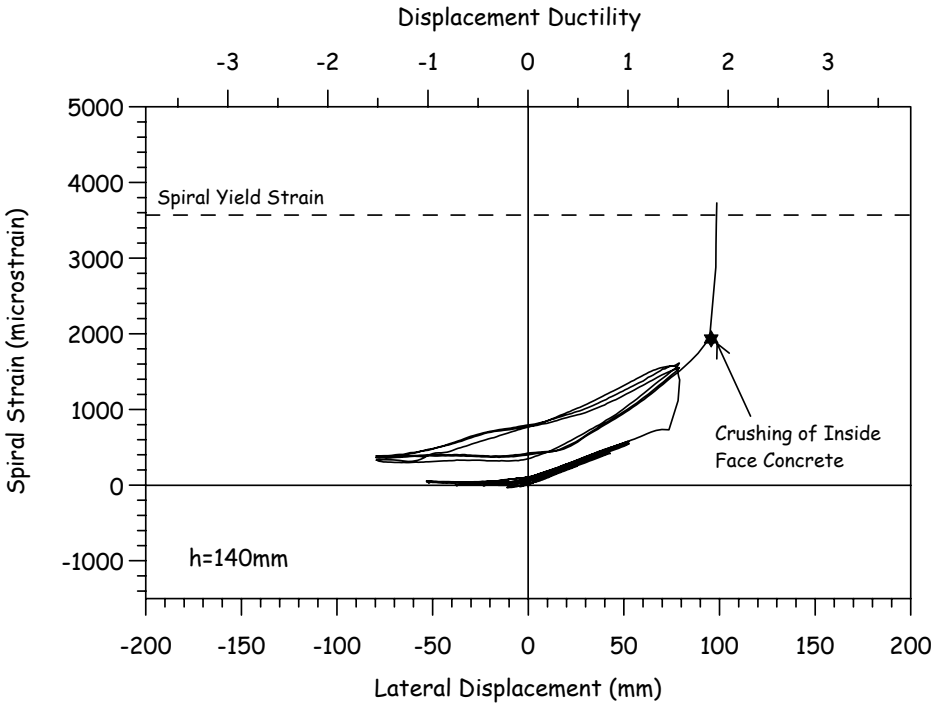

Fig. 4.13 Strain Hysteresis: 140mm Height

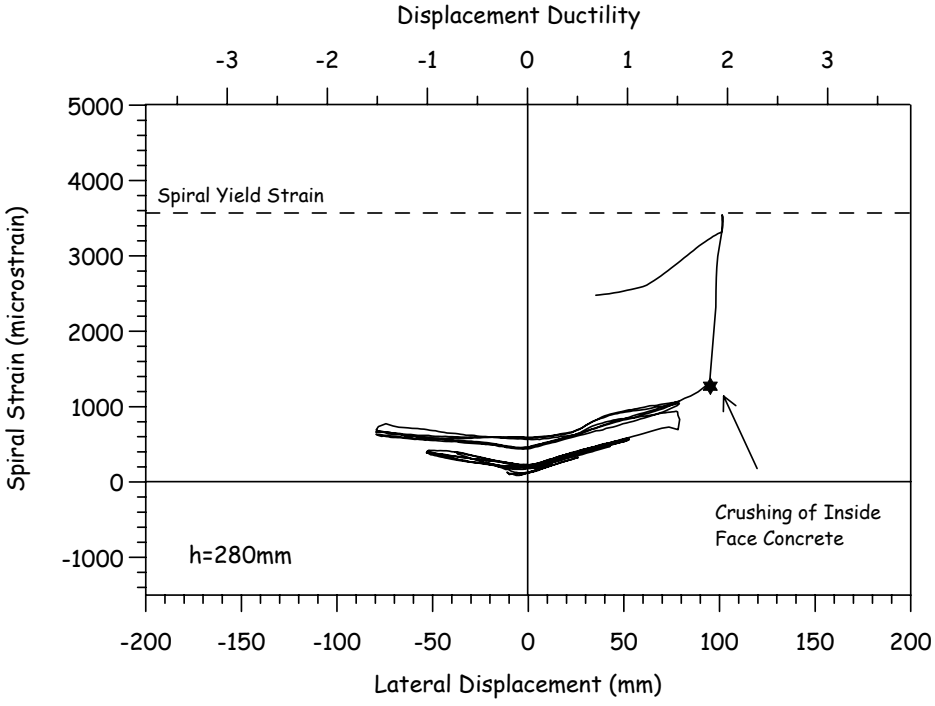

Fig. 4.14 Strain Hysteresis: 280mm Height

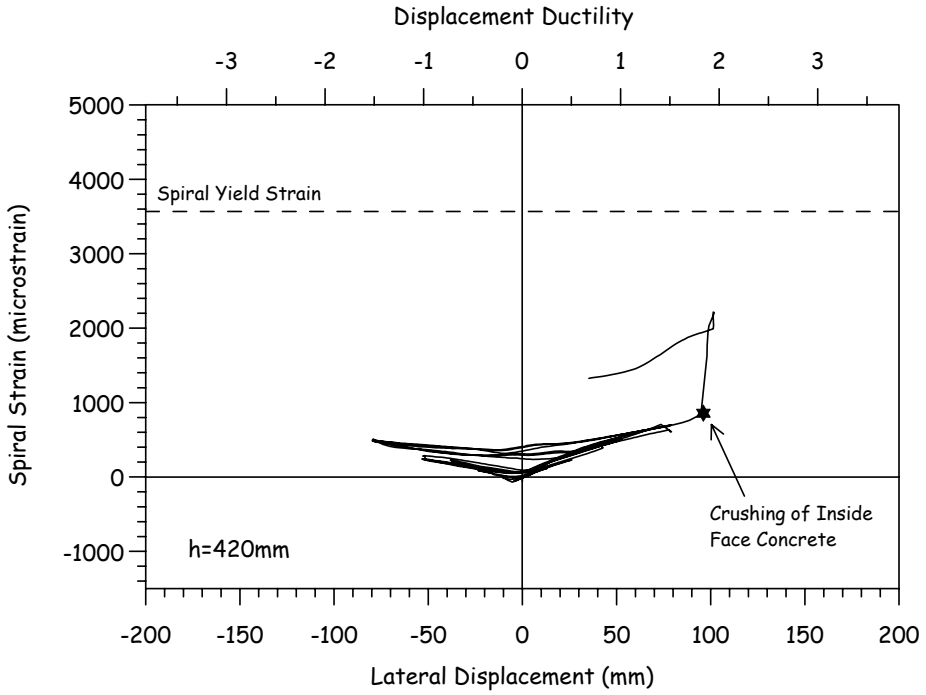

Fig. 4.15 Strain Hysteresis: 420mm Height

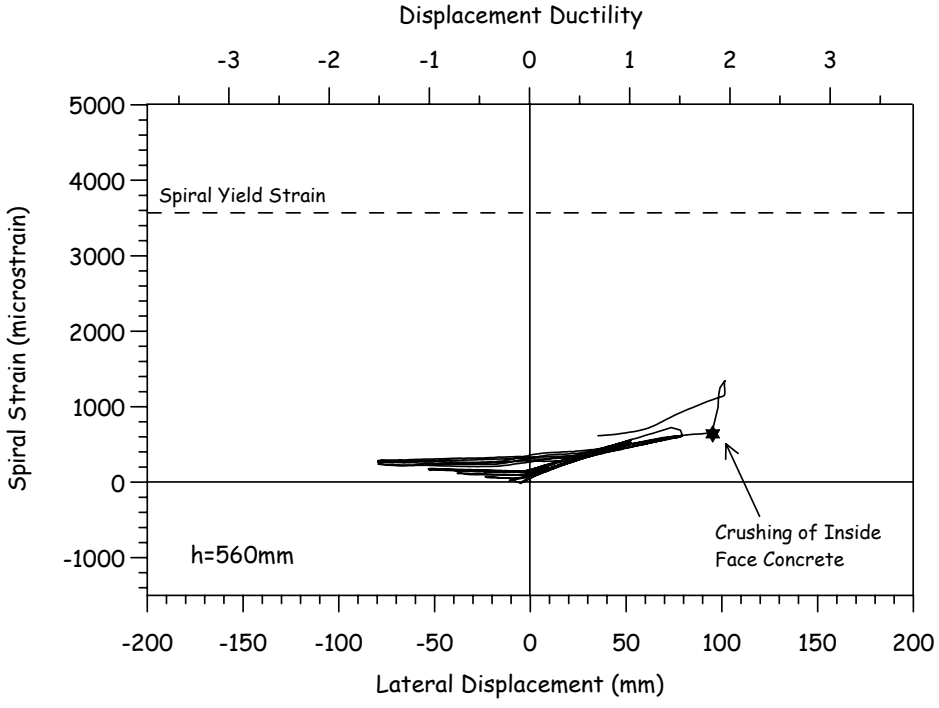

Fig. 4.16 Strain Hysteresis: 560mm Height

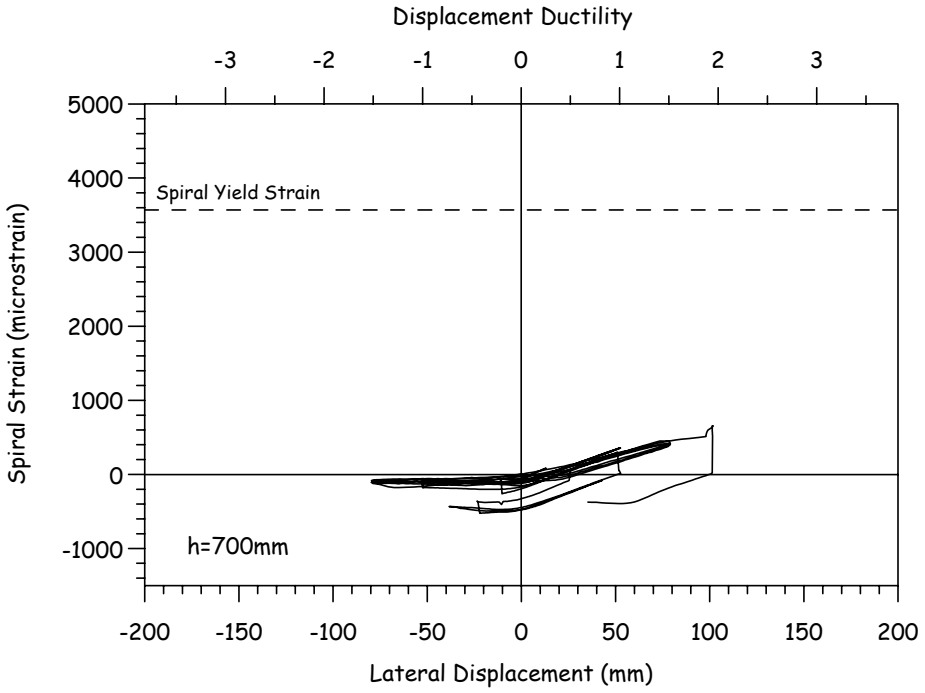

Fig. 4.17 Strain Hysteresis: 700mm Height

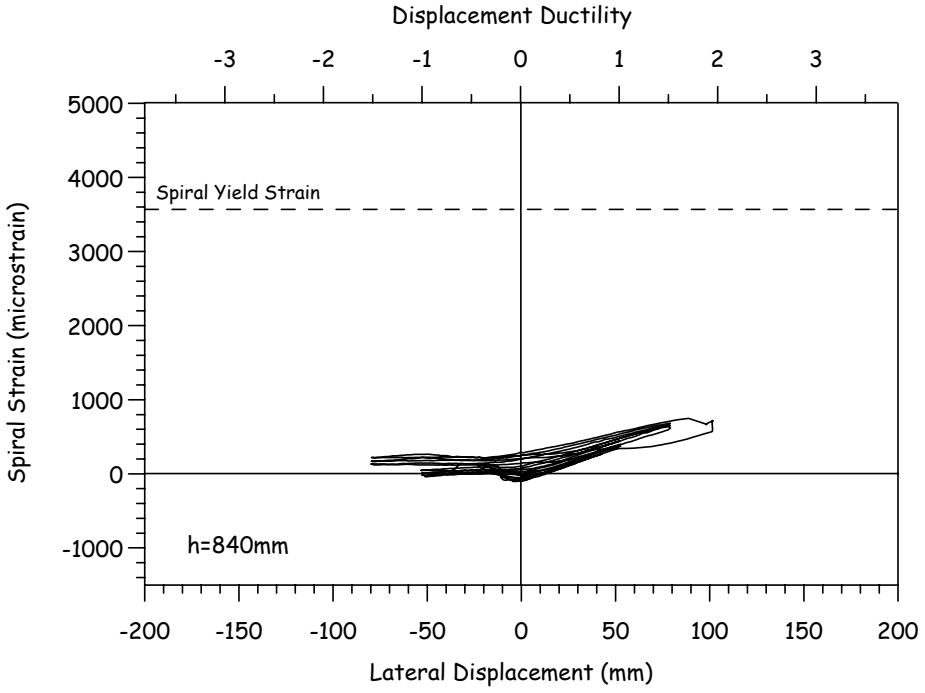

Fig. 4.18 Strain Hysteresis: 840mm Height

4.6 Transverse Strain Profiles in Sections

Figures 4.19 to 4.25 show transverse steel strain profiles in the plastic end sections at the maximum useful ductility, that is, the ductility level of 1.8 in the push direction and of 1.5 in the pull direction. Additional strain gauges were placed on the spiral at the level of 280mm height in order to measure the transverse steel response at the most critical section as exactly as possible. Note that some data are not plotted on the charts due to failure of gauges before testing.

Confinement-induced strains of over 1000 microstrains were observed up to the section of 420mm height, while the transverse steel was strained less significantly on northeast and northwest faces in the push direction and on southeast and southwest faces in the pull direction, which indicates that the confining stress occurred locally. It is also noted that the shear-induced strain dominates the transverse steel response at the section of above 700mm height and exceeded 2000με at many locations. Shear-induced strains were significantly higher than with unit HF1.

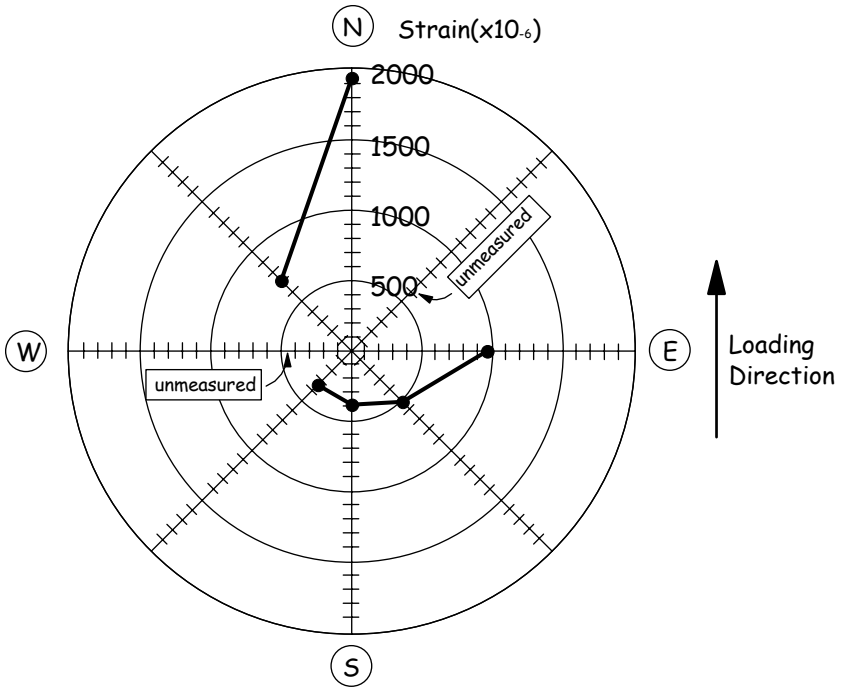

(a) Push Direction

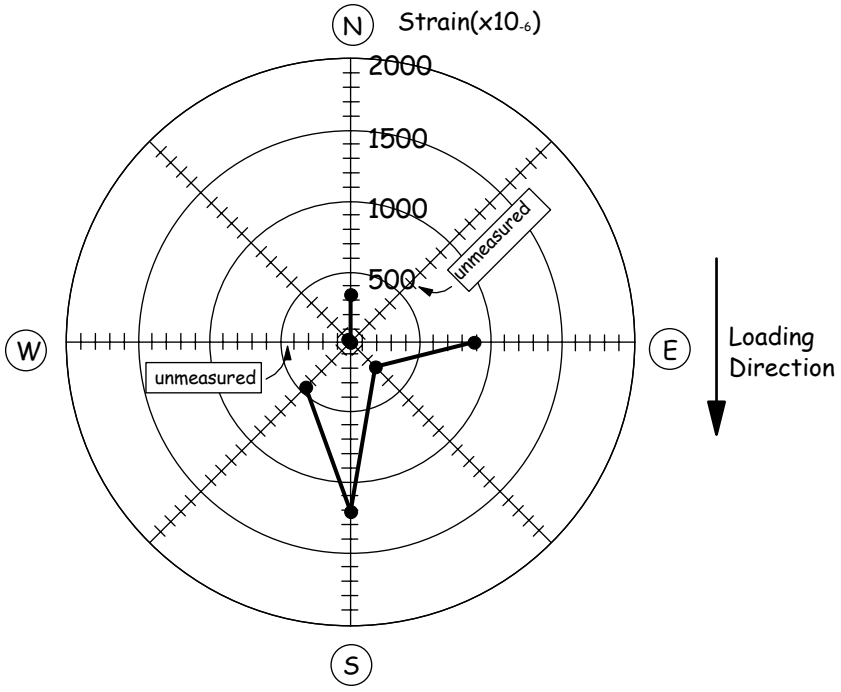

(b) Pull Direction

Fig. 4.19 Lateral Strain Profiles at Section of 140mm Height

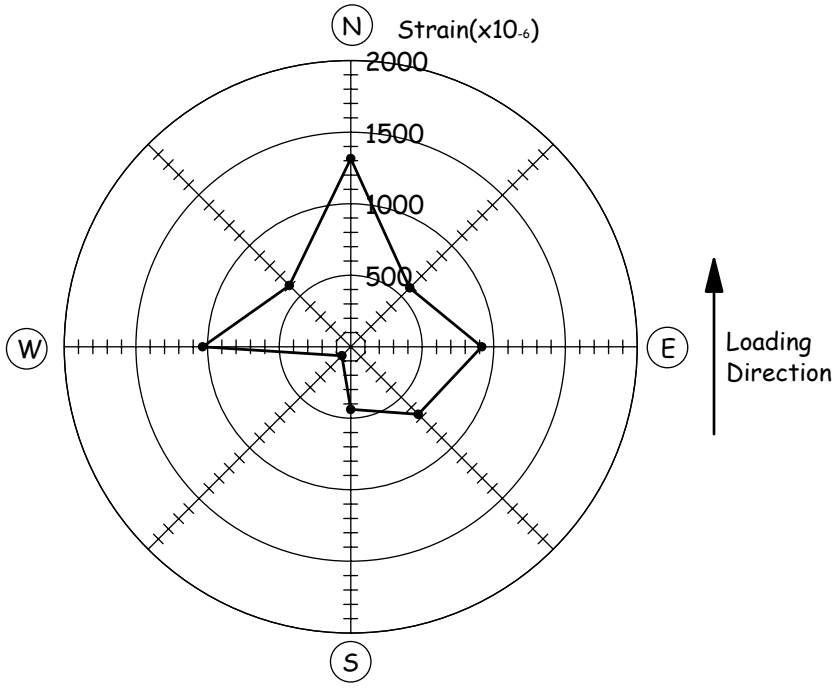

(a) Push Direction

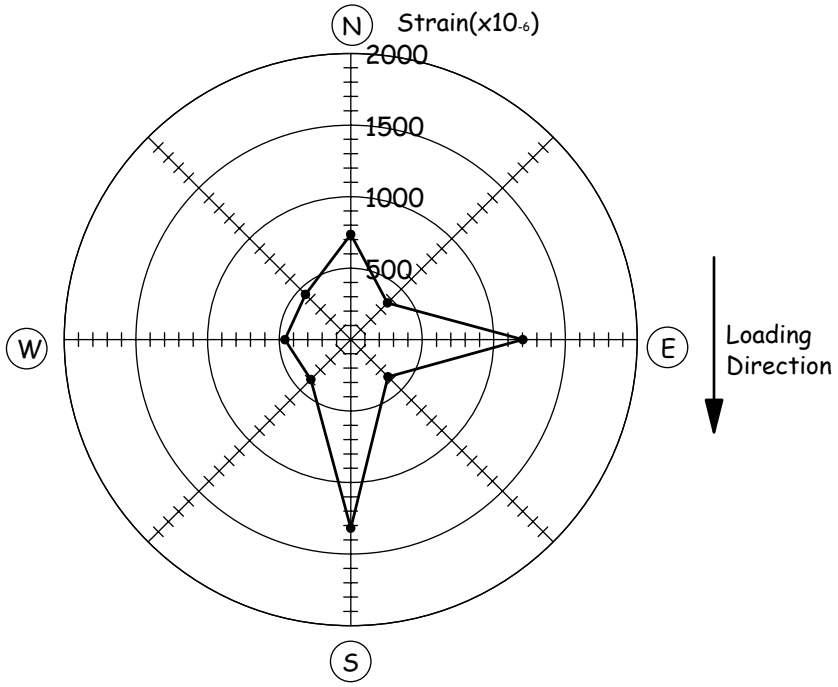

(b) Pull Direction

Fig. 4.20 Lateral Strain Profiles at Section of 280mm Height

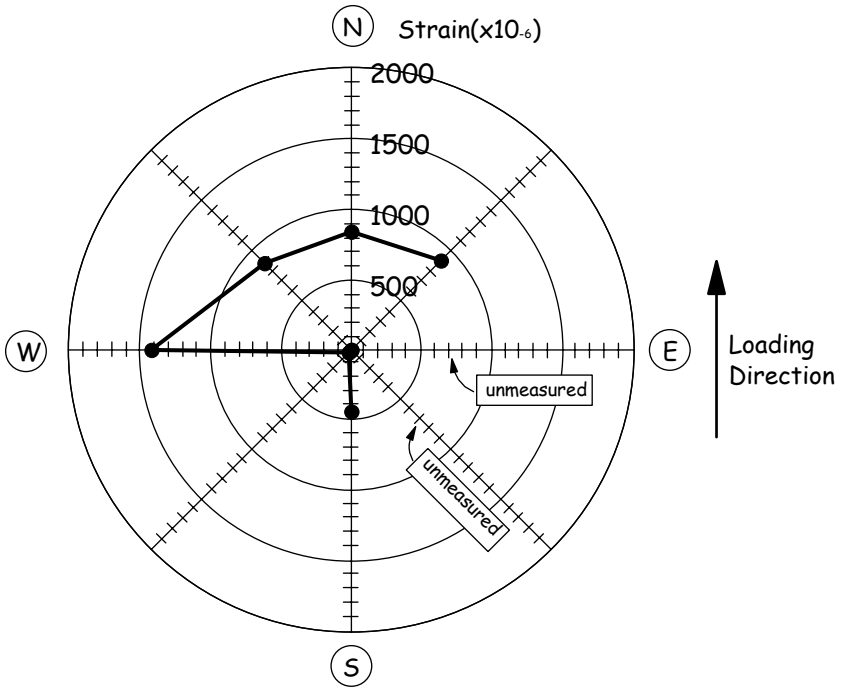

(a) Push Direction

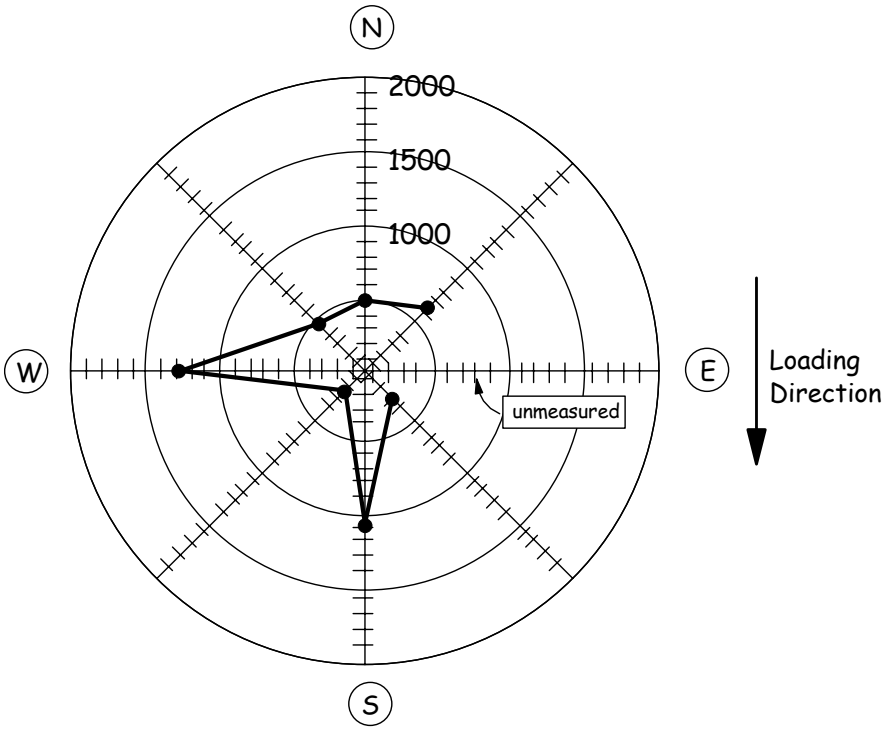

(b) Pull Direction

Fig. 4.21 Lateral Strain Profiles at Section of 420mm Height

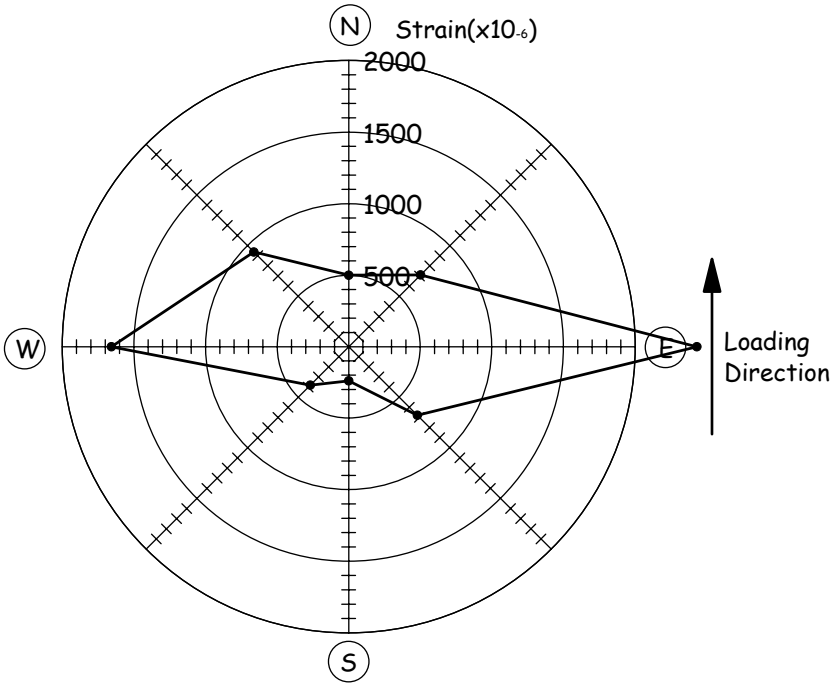

(a) Push Direction

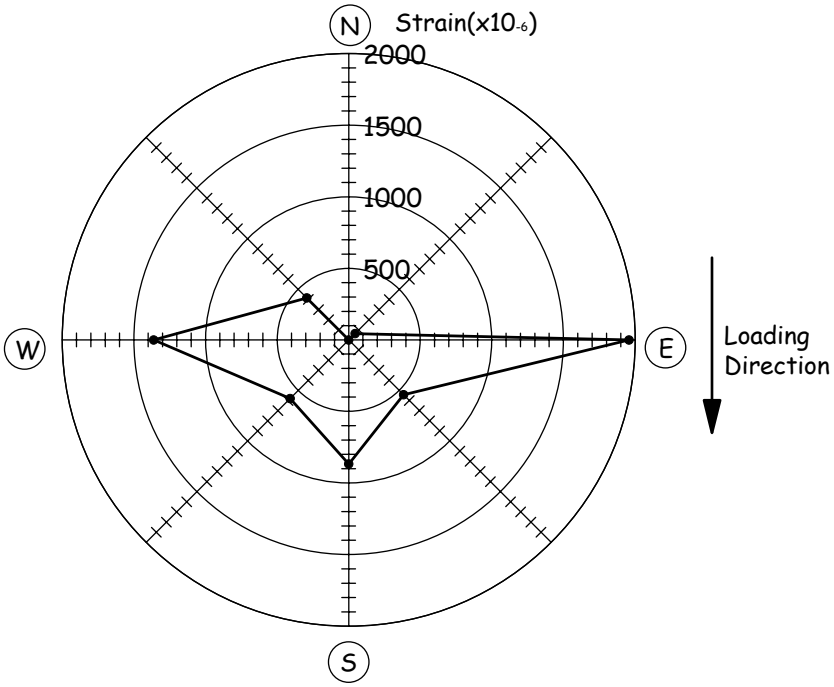

(b) Pull Direction

Fig. 4.22 Lateral Strain Profiles at Section of 700mm Height

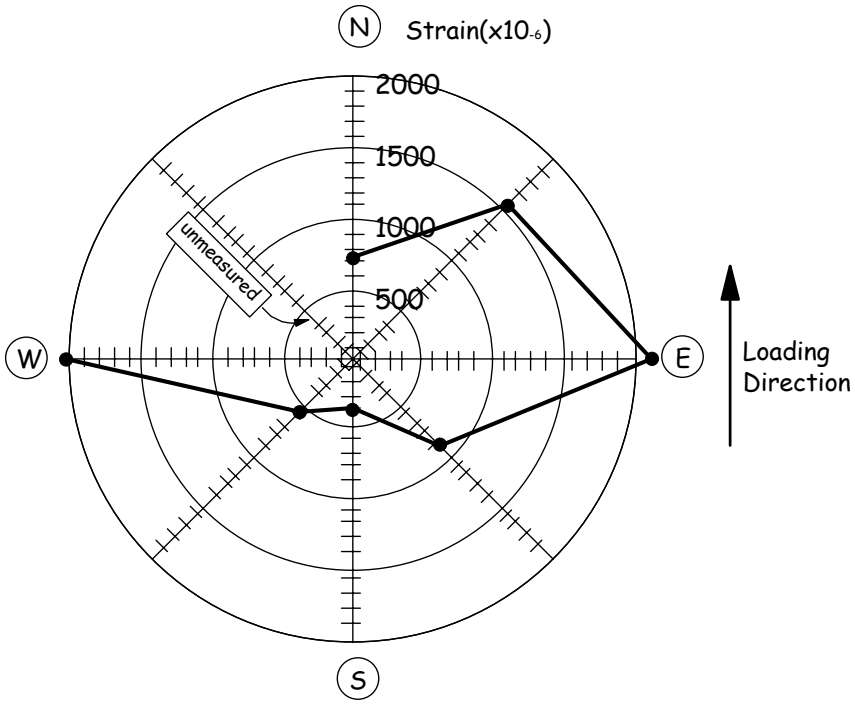

(a) Push Direction

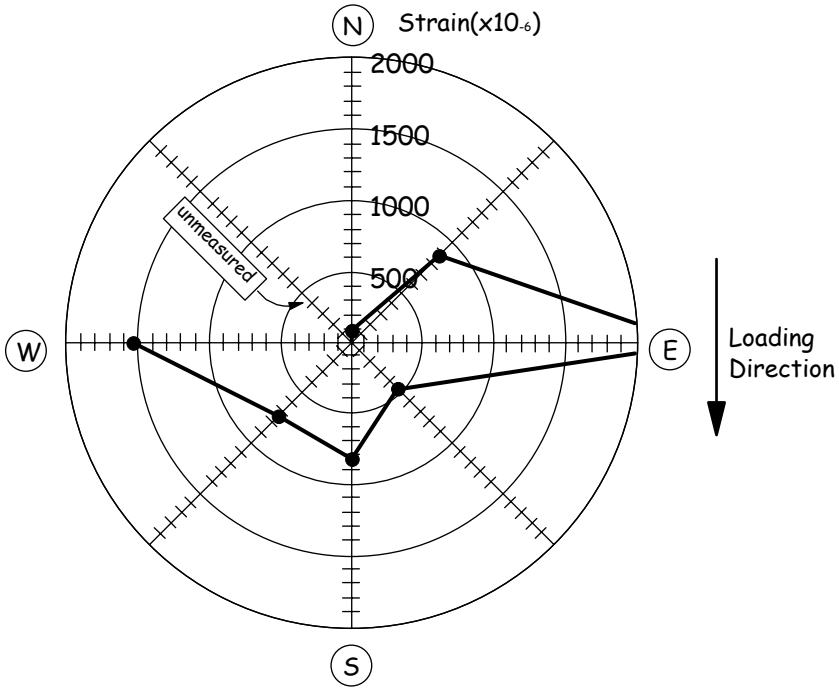

(b) Pull Direction

Fig. 4.23 Lateral Strain Profiles at Section of 980mm Height

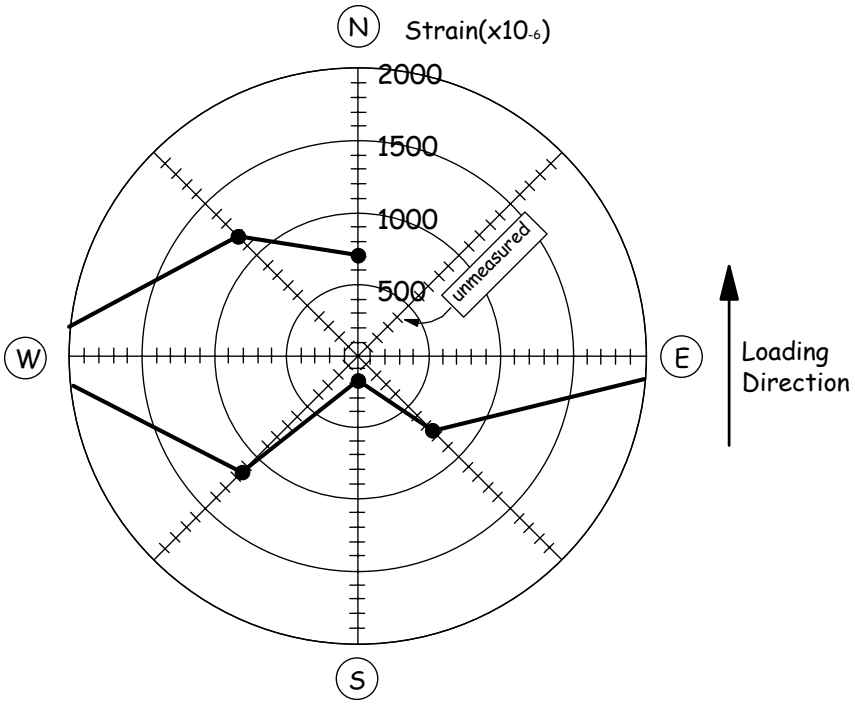

(a) Push Direction

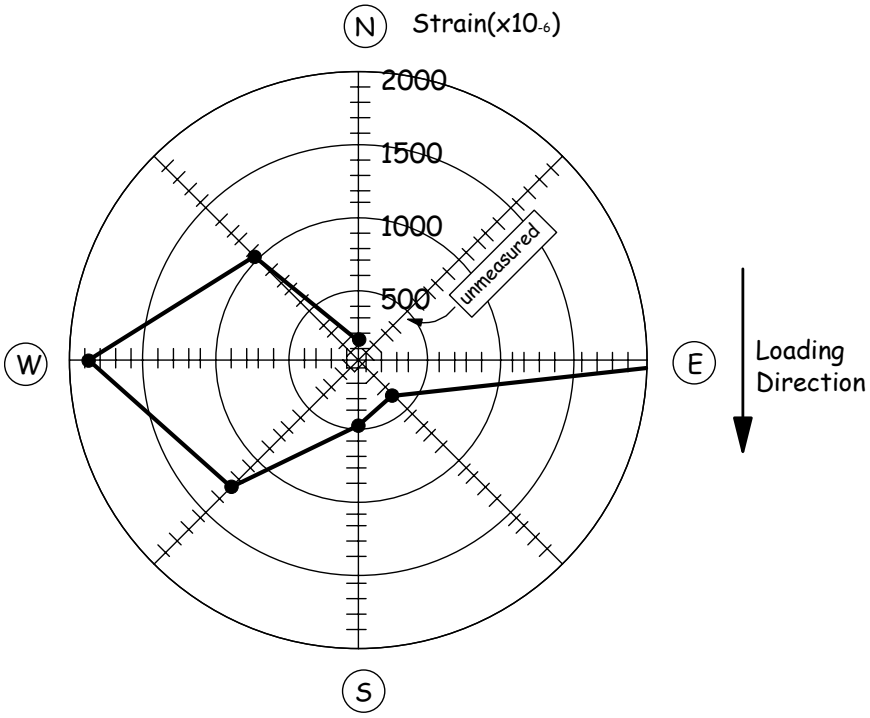

(b) Pull Direction

Fig. 4.24 Lateral Strain Profiles at Section of 1260mm Height

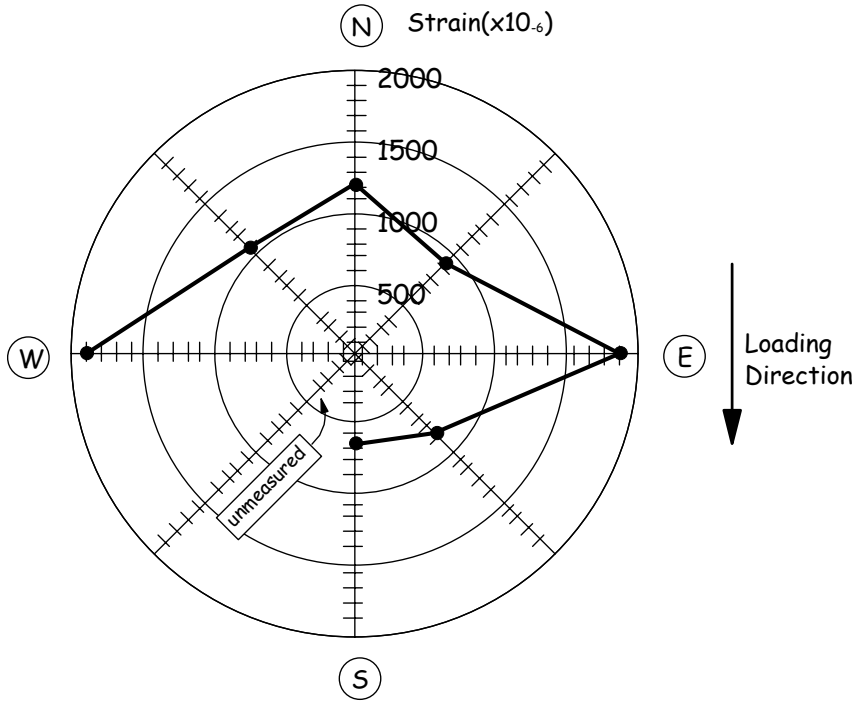

(a) Push Direction

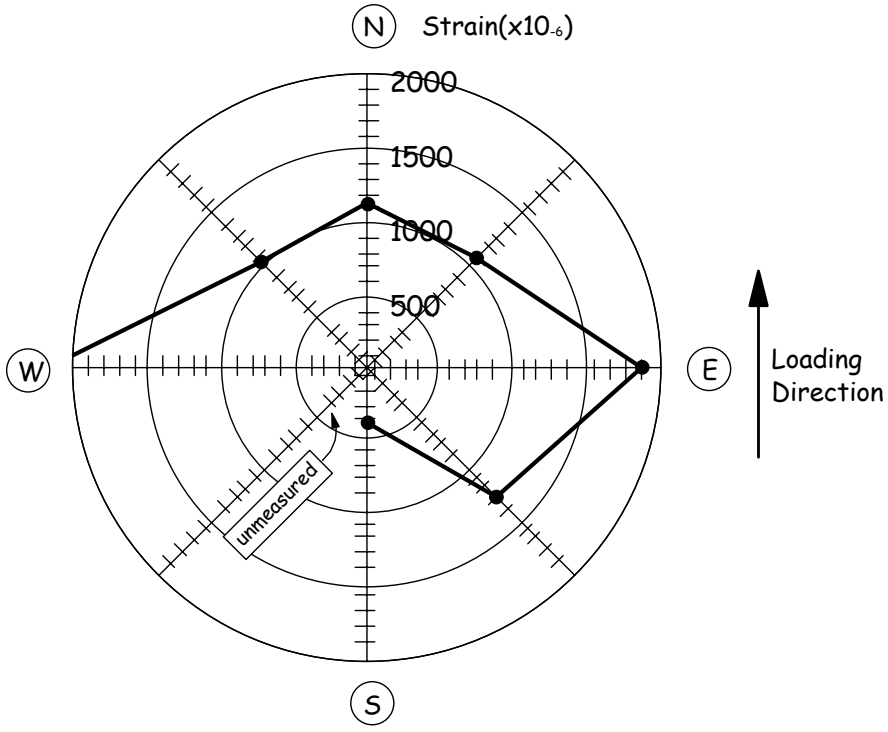

(b) Pull Direction

Fig. 4.25 Lateral Strain Profiles at Section of 1505mm Height

CHAPTER 5

5 ANALYSIS OF HOLLOW COLUMN RESPONSE

5.1 Theoretical Background

The transverse steel placed near the outside face in the plastic hinge region activates in tension when the section performs in a ductile manner in the inelastic range, and the resulting steel stress then applies confinement pressure to the concrete core. It should be noted that the concrete wall in the circular hollow section is subjected to biaxial compression in such situation as illustrated in Fig. 5.1, since the confinement pressure arises primarily in the circumferential direction. As discussed in Chapter 1, radial confining pressure varies from a maximum immediately under the hoop to zero at the inside surface. Since the inside surface is critical for failure, the stress conditions are essentially biaxial. It is known that biaxial compression results in poorer confinement than triaxial compression [1]. Accordingly, this confinement loss should be evaluated in the analytical consideration.

There are some applicable analytical approaches to predict the available flexural ductility of the reinforced concrete columns. In this research, the flexural response was estimated based on a conventional monotonic moment-curvature analysis because it is a simple and convenient approach and has been often employed in the earthquake engineering practice. The effect of the biaxial compression can be estimated through a stress-strain curve of the confined concrete proposed by Mander, Priestley and Park [1]. In the model, the confinement effect is represented by the confined strength ratio f_{cc}'/ f_c', where f_{cc}' is a compressive strength of confined concrete and f_c' is a compressive strength of unconfined concrete. Fig. 5.2 shows a compression strength enhancement of confined sections related to two orthogonal confining stresses. For concrete confined in only one direction (biaxial compression), the left-hand curve noted in Fig. 5.2 can be used to get the confined strength. The circumferential confining stress $f_{12'}$ is written as

$$f_{12'} = k_e \frac{f_h A_b}{t' s} \tag{5.1}$$

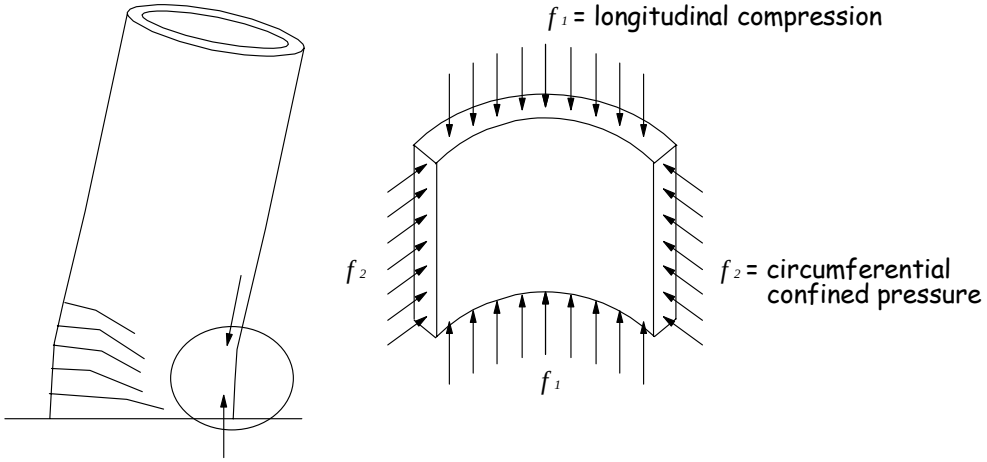

Fig. 5.1 Confinement Mechanism in Circular Hollow Section

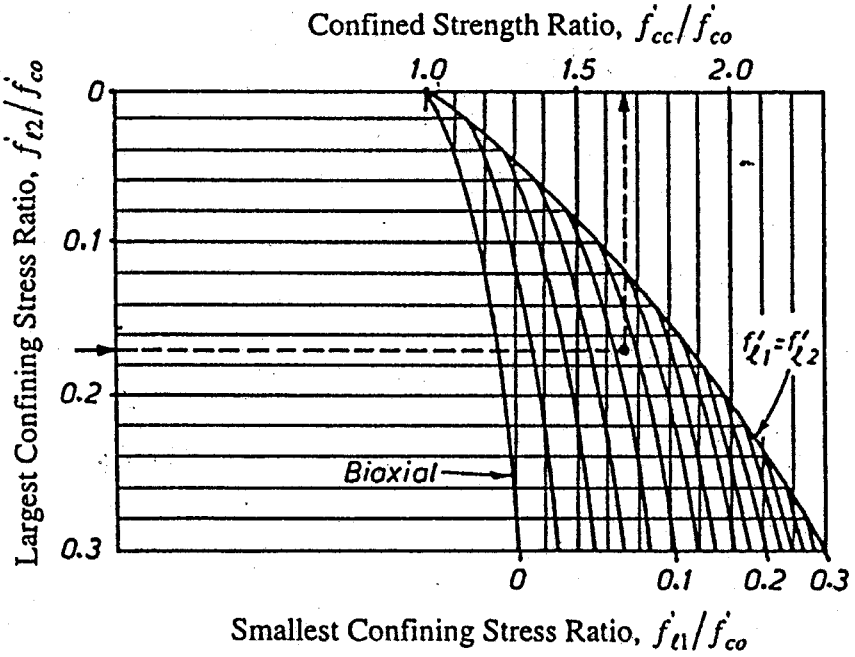

Fig. 5.2 Confinement Effect from Lateral Confining Pressure [1]

where, k_e = a confinement effectiveness coefficient relating the minimum area of the effectively confined core to the nominal core area; f_h = confinement-induced transverse steel stress; A_b = area of transverse steel; t' = concrete wall thickness inside the transverse steel; and s = spacing of transverse steel. An appropriate value of k_e for the hollow section may be taken as 0.6 because it is recommended for wall sections [1]. As described in previous chapters, test results showed that the transverse steel strain induced by confinement was nearly 1000 microstrains averaged over the plastic hinge region before column failure, the confinement-induced transverse steel stress f_h is then calculated as (175000 MPa × 0.001) = 175 MPa. From Eq. (5.1),

$$f_{l2}' = 0.6 \times \frac{175 \times 32}{126 \times 35} = 0.76 MPa$$

is the circumferential confining stress acting effectively to the concrete wall. Using a confining stress ratio of $f_{l2}'/ f_c' = 0.76 / 38 = 0.02$, the confined strength ratio can be read out from Fig. 5.2 as

$$\frac{f_{cc}'}{f_c'} \approx 1.04 \tag{5.2}$$

To simplify an analytical model, an equivalent solid circular section is assumed in terms of the confinement effect. The confined strength ratio in the solid circular section is given by

$$\frac{f_{cc'}}{fc'} = 2.254\sqrt{1 + \frac{7.94\, fi'}{fc'}} - \frac{2\, fi'}{fc'} - 1.254 \tag{5.3}$$

where f_l' is an effective lateral pressure [1]. Equation (5.3) is solved for f_l' with Eq. (5.2) and then one obtains $f_l' = 0.22$ MPa, which indicates that the hollow section in the test unit is equivalent to the solid circular section with the confined core under the lateral pressure of 0.22 MPa. This procedure is illustrated in Fig. 5.3. It should be noted that the equivalent lateral pressure corresponds to nearly 30% of the maximum effective pressure that develops when the transverse steel is stressed to its yield strength. This significant confinement loss is obviously due to the existence of the void section, that is, the premature crushing of inside face concrete.

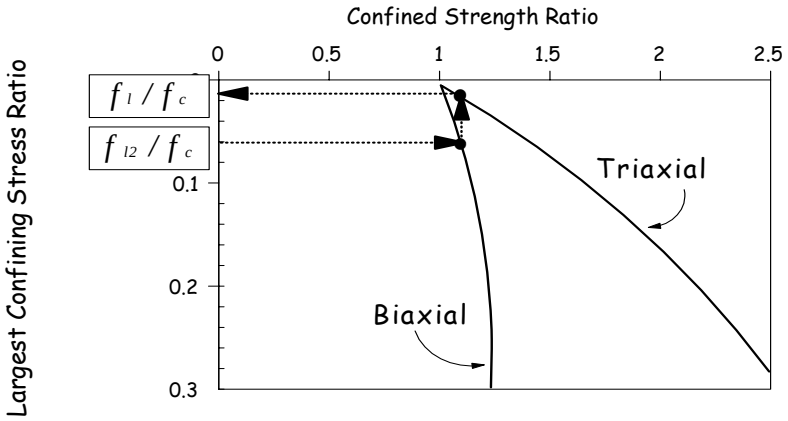

Fig. 5.3 Equivalent Confinement in Solid Circular Section

5.2 Moment-Curvature Analyses

Moment-curvature analyses for the critical sections of the test units were carried out with use of a computer program "CIRMAN4". The program, which is applicable to analysis of hollow section columns, is based on stress-strain curves for concrete and reinforcement proposed by Mander et al. [1]. Confinement effect and strain hardening of longitudinal reinforcement were taken into account through the stress-strain models, which is the same approach as the analyses for the solid circular sections. It should be noted that the lateral confinement pressure is assumed to be 0.22 MPa, as discussed in previous section, to establish the stress-strain curve of confined concrete. Material properties listed in Tables 2.1 and 2.2 were used in the analyses.

Experimental longitudinal strain profiles at the critical sections (h=146mm), measured at the maximum useful ductility, are compared with theoretical responses at ultimate in Fig. 5.4. The theoretical ultimate state is defined herein as the point when the extreme fiber compression strain reaches the ultimate strain of confined concrete or the inside face compression strain reaches 0.005, whichever comes first. As a consequence, analytical results showed that the ultimate state of the HF1 unit was determined by the extreme fiber compression strain, while that of the HF2 (unit was determined by the inside face compression strain. Although experimental responses indicated that the plane sections no longer remain plane at the ultimate stage, neutral axis positions and strain profiles in the compression side agree well with theoretical results in both cases.

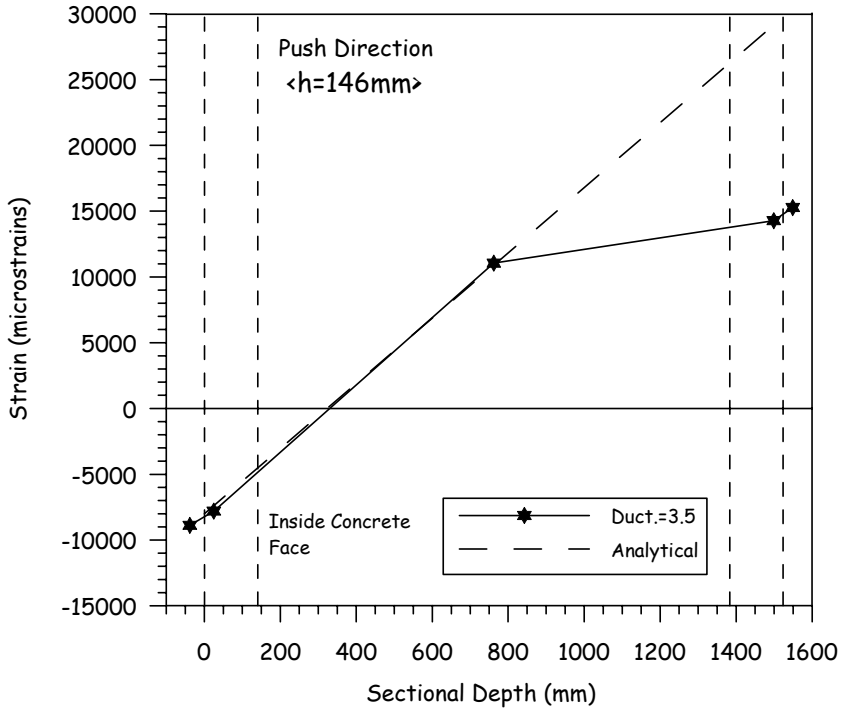

(a) HF1 Unit

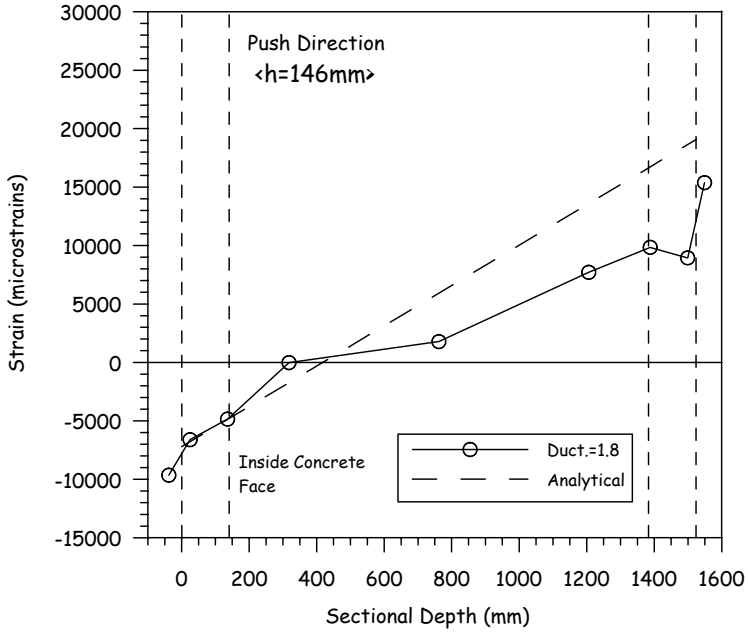

(b) HF2 Unit

Fig. 5.4 Comparison of Strain Profiles at Critical Section with Theoretical Results

5.3 Theoretical Force-Displacement Responses

Theoretical force-displacement relations were evaluated from the moment-curvature responses of the sections, where curvature profiles were idealized as shown in Fig. 5.5. Accordingly, the theoretical structural displacement Δ was calculated from

$$\Delta = \int_0^L \phi \, h \, dh \tag{5.4}$$

where L is a column height and ϕ is the curvature given by Fig. 5.5. The plastic hinge length L_p was based on a standard equation [7] of

$$L_p = 0.08\,L + 0.022\,f_y\,d_{bl} \tag{5.5}$$

where f_y and d_{bl} are yield strength (MPa) and diameter of longitudinal reinforcement, respectively. Equation (5.5) has been developed for solid columns originally, thus its applicability to the hollow columns may be controversial. However, as discussed in Chapters 3 and 4, the curvature profiles and the longitudinal strain profiles show that the plastic hinge length given by Eq. (5.5) seems to provide a reasonable value. Although test data are not sufficient to conclude the applicability of the standard equation of the plastic hinge length, Eq. (5.5) was employed temporarily in the analyses.

As shown in Fig. 5.5, a lateral displacement resulting from curvature in the loading steel tube was added on the elastic-plastic displacement due to the elastic curvature and the plastic rotation in the hollow section. The section curvature at the bottom of the loading steel tube is given by

$$\phi_s = \frac{F_H \left(L - L_0\right)}{E\,I} \tag{5.6}$$

where F_H is a lateral force, L_0 is a hollow column height, and E and I are the elastic modulus and the second moment of area of the loading steel tube, respectively.

The measured envelopes of lateral force-displacement responses are compared with theoretical results in Fig. 5.6. Although the measured lateral force is slightly higher than the theoretical result, the experimental responses of the test units show a good agreement with the theoretical ones. It is also interesting in the analytical result of the HF2 unit that the inside face compression strain exceeded 5000 microstrains before the outside face strain reached the ultimate strain. This predicts that crushing of the inside face concrete occurs before failure of the outside face concrete, which coincided well with the test observation of the HF2 unit.

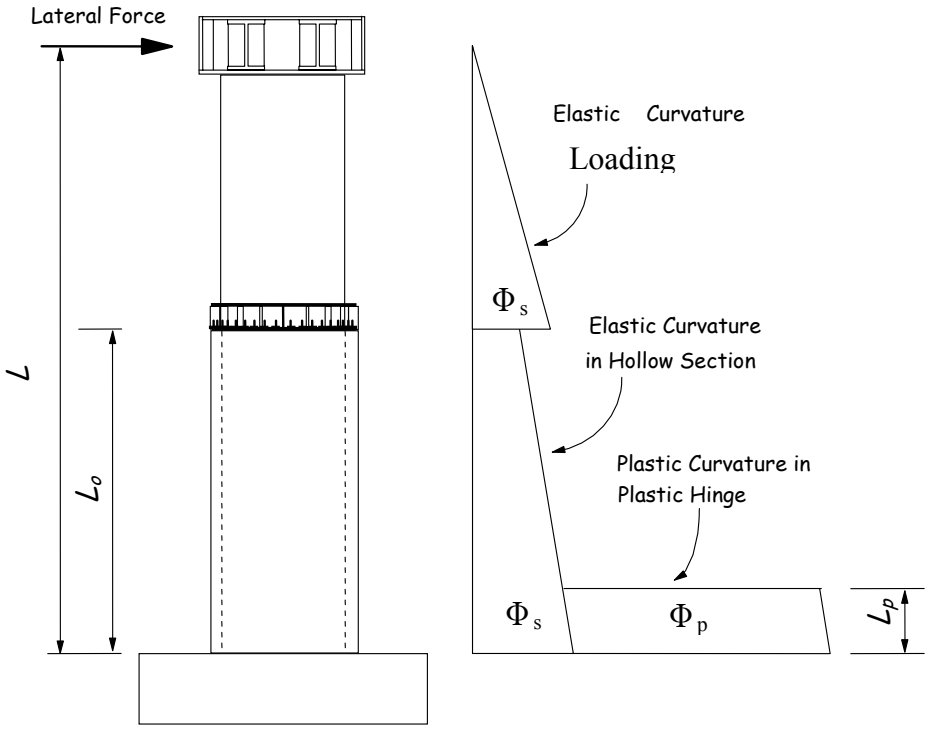

Fig. 5.5 Theoretical Curvature Profiles

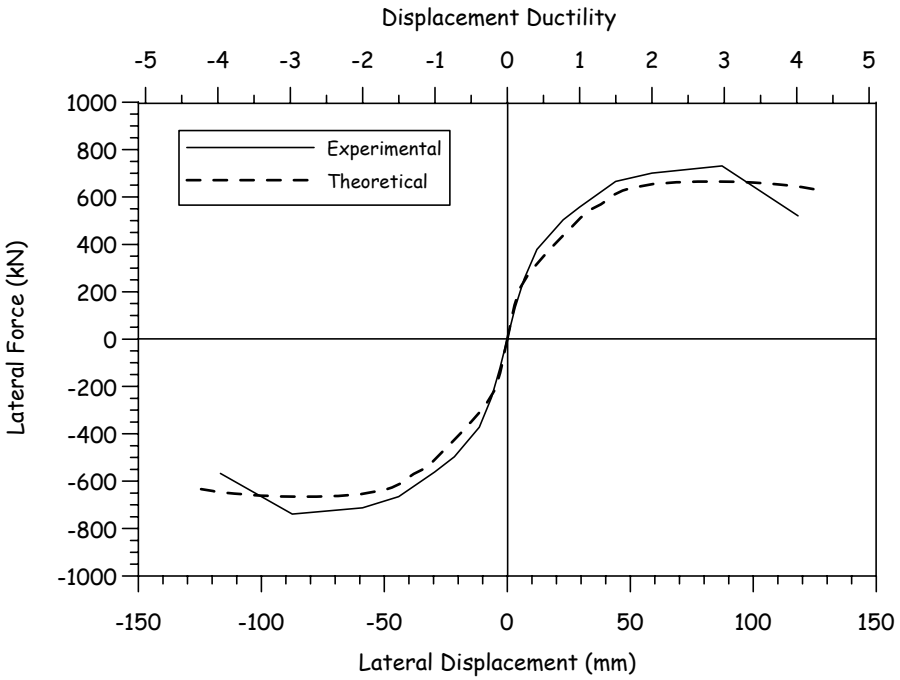

(a) HF1 Unit

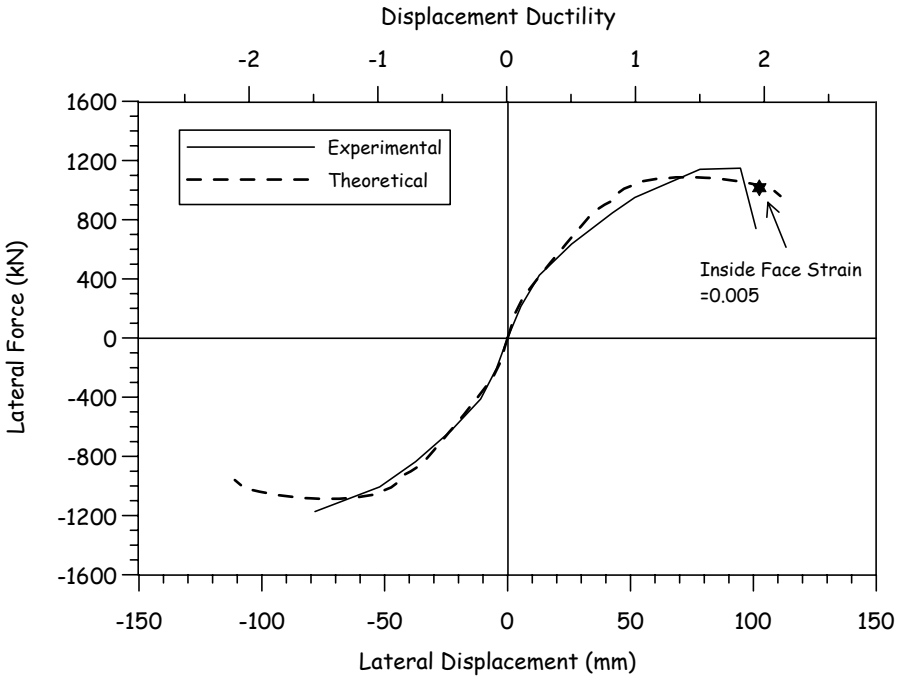

(b) HF2 Unit

Fig. 5.6 Comparison of Measured and Theoretical Lateral Force-Displacement Envelopes

CHAPTER 6

6 CONCLUSIONS AND DESIGN RECOMMENDATIONS

6.1 Conclusions from Tests and Analyses

Two flexural circular hollow columns with one layer of longitudinal and transverse reinforcement were tested under cyclic loading and the flexural performance was investigated based on the test results. The analytical approach methodology to predict the flexural strength and the ductility capacity of the columns was also discussed in this report.

The inside face concrete compression strain is one of the most important parameters to control the ductility capacity of the hollow columns. High axial load, a thin wall or a high longitudinal steel ratio causes the neutral axis to pass through the void section with a deep clearance from the inside face, resulting in high longitudinal compression strain at the inside face. Test results showed that the inside face concrete was crushed when the compression strain reached nearly 0.005 even though a sufficient amount of transverse steel was placed near outside face.

Generally, the transverse steel at the critical section in the solid circular column yields and the full lateral pressure is induced in the core concrete under the triaxial compression when the column behaves in a ductile manner during cyclic lateral loading in the inelastic range. It should be noted, however, that the confinement-induced strain developed on the transverse steel seemed to be nearly 0.001 averaged over the anticipated plastic hinge length and did not exceed its yield strain before column failure. The concrete wall in the circular hollow section is effectively subjected to biaxial compression, which causes the significant reduction in confinement effectiveness and then the premature crushing of inside face concrete. Therefore, the maximum effective lateral pressure should be calculated taking account of the confinement loss. A confinement strain of 0.001 was proposed for the maximum useful transverse steel confinement-induced strain in the critical hollow section based on the test results.

The flexural strength and the ductility capacity of the circular hollow columns were evaluated with use of the conventional moment-curvature analysis for the equivalent solid circular section with the same confinement effectiveness, that is, the same confined strength ratio f_{cc}'/ f_c'. Ultimate compression strain of concrete was defined at both outside and inside faces of the section, to estimate the response at ultimate limit state. It was noted that analytical results coincided well with experimental force-displacement behavior and the analytical approach presented herein could predict the available ductility of the circular hollow columns without inside longitudinal and transverse steel precisely.

6.2 Design Recommendations

- The use of a single layer of reinforcement in hollow circular columns can result in economical designs with limited ductility capacity. It should be noted that the limited ductility capacity will often be adequate since ductility demand of tall piers is generally low.
- For design purposes, the limit to ductility may be considered to occur when the compression strain on the inside surface reaches 0.0035, or the strain at the outer edge of the core reaches the confined crushing strain.
- Confinement effectiveness is reduced as a consequence of biaxial confinement conditions. An equivalent confinement pressure based on Eqns. 5.2 and 5.3, with a maximum strain of 1000με in the confining steel should be used.
- The normal plastic hinge length for solid sections, namely $L_p = 0.08L + 0.022d_bf_y$ (MPa, mm units) may be used to predict displacement capacity of hollow circular columns with adequate accuracy.

REFERENCES

[1] Mander, J. B., Priestley, M. J. N., Park, R., "Theoretical Stress-Strain Model for Confined Concrete," Journal of the Structural Division, ASCE, Vol. 114, No. 8, August 1988, pp. 1804-1826.

[2] Mander, J. B., Priestley, M. J. N., Park, R., "Behavior of Ductile Hollow Reinforced Concrete Columns," Bulletin of the New Zealand National Society for Earthquake Engineering, Vol. 16, No. 4, December 1983, pp. 273-290.

[3] Pinto, A. V., "Pseudodynamic and Shaking Table Tests on R.C. Bridges," ECOEST/ PREC8 Report, No. 5, November 1996.

[4] Zahn, F. A., Park, R., Priestley, M. J. N., "Flexural Strength and Ductility of Circular Hollow Reinforced Concrete Columns Without Confinement on Inside Face," ACI Structural Journal, Vol. 87, No. 2, March-April 1990, pp. 156-166.

[5] Kawashima, K., "Dynamic Strength and Ductility of Hollow Circular Reinforced Concrete Bridge Pier," Civil Engineering Journal, Vol. 34, No. 10, October 1992, pp. 34-39 (in Japanese).

[6] Ranzo, G., Priestley, M. J. N., "Seismic Performance Of Circular Hollow Columns Subjected To High Shear," Structural Systems Research Project, Report SSRP-2001/01, University of California, San Diego, March 2001.

[7] Priestley, M. J. N., Seible F., Calvi G. M., "Seismic Design and Retrofit of Bridges," Wiley-Interscience.

[8] Seible F., Priestley, M. J. N., Latham C. T., Silva P., "Full-scale Bridge Column/ Superstructure Connection Tests under Simulated Longitudinal Seismic Loads," Structural Systems Research Project, Report SSRP-94/14, University of California, San Diego, June 1994.